Experimental Study and Numerical Modelling of Soil-Roots Hydro-Mechanical Interactions

Alessandro Fraccica

UNIVERSITAT POLITÈCNICA DE CATALUNYA

Doctoral Thesis

Experimental Study and Numerical Modelling of Soil-Roots Hydro-Mechanical Interactions

Author:

Alessandro Fraccica

Directors:

Enrique Edgar Romero Morales

Thierry Fourcaud

Doctoral programme: Geotechnical Engineering

Department of Civil and Environmental Engineering

December 2019

THÈSE POUR OBTENIR LE GRADE DE DOCTEUR
DE L'UNIVERSITÉ DE MONTPELLIER

En Ecologie fonctionelle

École doctorale GAIA

Unité de recherche AMAP

En partenariat international avec Universitat Politècnica de Catalunya, SPAIN

Experimental Study and Numerical Modelling of Soil-Roots Hydro-Mechanical Interactions

Présentée par Alessandro FRACCICA
Le 09 Décembre 2019

Sous la direction de Thierry FOURCAUD
et Enrique Edgar ROMERO MORALES

Devant le jury composé de

Loïc BRANCHERIAU, Directeur de recherche, Université de Montpellier	Examinateur
Cristina JOMMI, Full professor, TU Delft – Politecnico di Milano	Rapporteur/Examinateur
Evelyne KOLB, Maître de conférences, Sorbonne Université	Examinateur
Alberto LEDESMA VILLALBA, Full professor, Universitat Politècnica de Catalunya	Examinateur
Slobodan MICKOVSKI, Full professor, Glasgow Caledonian University	Rapporteur/Examinateur

UNIVERSITÉ DE MONTPELLIER

Abstract

The thesis is aimed at characterising the multi-scale and hydro-mechanical behaviour of lightly compacted silty sand penetrated by a bermudagrass (*Cynodon dactilon*). The study will allow better assessing the impact of vegetation on this compacted soil that has been used in an experimental and fully instrumented embankment.

The literature agrees that roots are enhancing soil shear strength properties, while contrasting results have been found in terms of soil hydraulic behaviour. Moreover, there is a lack of information on how roots affect soil microstructure and its consequences at the macroscopic scale (soil hydraulic behaviour, volume change and shear strength properties).

A protocol for soil compaction and roots growth was followed for preparing all the samples. The soil was lightly compacted, wetted under unconfined conditions to favour plant growth, and then dried to different hydraulic states. The same soil, plant and seeding density used in the monitored embankment were adopted for laboratory experiments. Several techniques were exploited to characterise roots geometrical and mechanical features.

Large cell triaxial and direct shear tests were performed under saturated and partially saturated conditions. Different stress-strain responses were observed in the vegetated soil at different hydraulic states, due to different roots failure mechanisms and to the combination of water availability and suction within the soil. Results were interpreted with several constitutive stress expressions for partially saturated soils to consider these state and stress variables. Compression deformations on shearing observed on rooted samples were systematically larger than fallow ones. Roots slightly affected the friction angle but generated an increase in soil cohesion. These observations were confirmed by direct tensile tests performed with a new apparatus at different roots growth stages and hydraulic states. With the results obtained in this thesis, a constitutive expression was

proposed to predict the increase in cohesion knowing the properties of roots and the soil hydraulic state.

Concerning the hydraulic behaviour, roots induced a systematic increase in soil water-saturated permeability. Water retention properties were also affected, with a decrease in the retention capacity as roots volume increased. Micro-CT tomography and mercury intrusion porosimetry were carried out at different soil hydraulic states on samples including plant individuals to obtain information about changes in soil microstructure. Reconstructed information from the two techniques showed that roots were generally increasing macropores (larger than 100 μm) due to fissuring and soil-root interface phenomena while reducing smaller pores (below 5 μm) due to mucilage clogging. The volume of macropores generated by roots, in saturated conditions, furtherly increased upon drying due to concurrent soil and root shrinkage. The alterations generated by roots growth on the soil structure allowed explaining not only the different soil hydraulic responses but also the soil volume change behaviour. A good agreement between the volume of fissures and the volume of roots was found and allowed calibrating and validating a model able to predict the soil water retention properties and permeability values based on the microstructural changes observed.

Results coming from the hydro-mechanical characterization carried out within the thesis were used to simulate the effect of different periods of plants growth on the hydro-mechanical behaviour of the monitored embankment during a rainfall event. The vegetated slopes remained stable throughout the simulation, even when completely saturated, thanks to the mechanical reinforcement of the roots. Nevertheless, the higher permeability within the vegetated soil had a negative consequence, which was evidenced by a drastic drop in the slope stability safety factor at the early stages of the hydraulic event.

Resumen

La tesis tiene como objetivo caracterizar el comportamiento hidromecánico de una arena limosa compactada y con raíces (*Cynodon dactilon*). El estudio ha permitido evaluar el impacto de la vegetación en este suelo, que ha sido utilizado en un terraplén experimental.

El estado de arte indica que las raíces mejoran las propiedades de resistencia al corte de un suelo, mientras que hay resultados contrastantes en términos del comportamiento hidráulico. Además, se carece de información sobre cómo las raíces afectan a la microestructura del suelo y sus consecuencias a escala macroscópica.

Se siguió un protocolo para la compactación del suelo y el crecimiento de las raíces para la preparación de todas las muestras estudiadas. El suelo se compactó ligeramente, se humedeció en condiciones no confinadas para favorecer el crecimiento de la planta, y luego se secó a diferentes estados hidráulicos. Se utilizaron varias técnicas para caracterizar las propiedades geométricas y mecánicas de las raíces.

Se realizaron ensayos de corte directo, edométricos y triaxiales con equipos de grandes dimensiones. Se observaron diferentes respuestas de tensión-deformación en el suelo con vegetación debido a los diferentes mecanismos de rotura de las raíces y a la combinación de humedad y de succión en el suelo. Los resultados se interpretaron con leyes constitutivas en términos de tensiones efectivas para suelos parcialmente saturados. En las muestras con raíces se observaron sistemáticamente deformaciones mayores de compresión durante el desarrollo del corte. Las raíces afectaron ligeramente el ángulo de fricción y desarrollaron un aumento en la cohesión del suelo. Estas observaciones también se confirmaron mediante ensayos de tracción mediante un nuevo equipo, que se realizaron a diferentes estados de crecimiento de las raíces. Se propuso una expresión constitutiva para predecir el aumento de la cohesión en función de las propiedades de las raíces y el estado hidráulico del suelo.

En cuanto al comportamiento hidráulico, las raíces inducen un aumento de la permeabilidad saturada del suelo y una disminución en la capacidad de retención al agua a medida que aumenta el volumen de las raíces en el suelo. Se realizaron ensayos de micro-tomografía de rayos X y de porosimetría de intrusión de mercurio sobre muestras con raíces. La información reconstruida de las dos técnicas ha indicado que las raíces han inducido el aumento de los poros de más de 100 μm debido a la generación de fisuras y a fenómenos de interfase suelo-raíz, a la vez que han ocluido los poros más pequeños (menores de 5 μm) debido a la producción de mucílago. Las fisuras también se han abierto por la retracción simultánea del suelo y de las raíces durante el secado. Estas alteraciones inducidas sobre la microestructura han permitido explicar mejor los cambios en las propiedades hidráulicas y de cambio de volumen del suelo. Se ha encontrado una relación entre el volumen de fisuras y el volumen de raíces, lo que ha permitido desarrollar y calibrar un modelo capaz de predecir las propiedades de retención al agua y los valores de permeabilidad del suelo.

Los resultados experimentales se han utilizado para simular el efecto que tiene los diferentes crecimientos de las plantas sobre el comportamiento hidromecánico del terraplén instrumentado durante un episodio de lluvia. Los taludes con raíces se mantuvieron estables a lo largo de la simulación, incluso cuando estaban completamente saturados, gracias al refuerzo mecánico de las raíces. Sin embargo, la mayor permeabilidad del suelo vegetado tuvo una consecuencia negativa, que se evidenció con una drástica caída en el factor de seguridad del talud en las primeras etapas del episodio de lluvia.

Resumé

La thèse vise à caractériser le comportement multi-échelles et hydro-mécanique du sable silteux pénétré par des racines de *Cynodon dactilon*. L'étude permettra d'évaluer l'impact de la végétation sur ce sol compacté utilisé dans un remblai expérimental en extérieur.

La littérature s'accorde à dire que les racines améliorent les propriétés de résistance au cisaillement du sol, tandis que des résultats contrastés ont été obtenus en ce qui concerne leur effet sur le comportement hydraulique. De plus il existe peu d'information sur la façon dont les racines affectent la microstructure du sol et leurs conséquences à l'échelle macroscopique.

Un protocole de compactage du sol et de croissance de racines a été suivi pour la préparation de tous les échantillons testés. Le sol a été légèrement compacté, mouillé pour favoriser la croissance des plantes, puis séché jusqu'à différents états hydrauliques. Les plantes et la densité d'ensemencement ont été les mêmes que ceux utilisés dans le remblai. Plusieurs techniques ont été exploitées pour évaluer les caractéristiques géométriques et mécaniques des racines.

Des essais de cisaillement triaxial et direct ont été effectués avec des équipements de grande dimension dans des conditions saturées et partiellement saturées. Différentes réponses de contrainte-déformation ont été observées pour le sol végétalisé à différents états hydrauliques, en raison de différents mécanismes de rupture des racines. Les résultats ont été interprétés à l'aide de plusieurs lois de comportement pour les sols partiellement saturés afin de tenir compte des variables d'état et de stress. Des déformations de compression plus importantes lors du cisaillement ont été observées sur des échantillons avec racines. Les racines ont généré une augmentation de la cohésion du sol. Ces observations ont été confirmées par des essais de traction directe effectués à différents stades de croissance des racines. Une loi de comportement a été

proposée pour prédire l'augmentation de la cohésion en connaissant les propriétés des racines et l'état hydraulique du sol.

En ce qui concerne le comportement hydraulique, les racines ont induit une augmentation de la perméabilité saturée en eau du sol et une diminution de la capacité de rétention à mesure que le volume des racines augmentait. La tomographie microCT et la porosimétrie par intrusion de mercure ont été effectuées à différents états hydrauliques du sol sur des échantillons avec racines pour obtenir des informations sur les changements de la microstructure du sol. L'information reconstruite à partir des deux techniques a montré que les racines augmentaient généralement les macropores (plus de 100 micromètres) en raison de phénomènes de fissuration et des interfaces sol-racine tout en réduisant les pores plus petits (moins de 5 micromètres) en raison du colmatage dû au mucilage. L'ouverture des fissures a été augmentée par le retrait simultané du sol et des racines lors du séchage. Les altérations générées par la croissance des racines sur la structure du sol ont permis d'expliquer les différentes réponses hydrauliques du sol et aussi son changement de volume. Un bon accord entre le volume des fissures et le volume des racines a été trouvé et a permis de calibrer et de valider un modèle capable de prédire les propriétés de rétention d'eau et les valeurs de perméabilité du sol à partir des changements microstructurels observés.

Les résultats ont été utilisés pour simuler l'effet de différentes périodes de croissance des plantes sur le comportement hydro-mécanique du remblai lors d'une chute de pluie. Les pentes végétalisées sont restées stables tout au long de la simulation, même complètement saturées, grâce au renforcement mécanique des racines. Néanmoins, la perméabilité plus élevée dans le sol végétalisé a eu une conséquence négative, qui a été mise en évidence par une baisse drastique du facteur de sécurité de stabilité de la pente aux premiers stades de l'événement hydraulique.

Acknowledgments

I want to express my thankfulness to my thesis directors, Enrique Romero and Thierry Fourcaud, for the great chance they gave me to collaborate with them on this fascinating project.

I thank Enrique, for patiently guiding me through the proactive and exciting world of UPC's geotechnical laboratory, for listening to and discussing ideas anywhere or during a walk, to strengthen my knowledge on soil mechanics and all equipment made and to be invented for carrying out experiments. I thank him also to always give me support (*No pasa nada, tranquilo!*), to get me involved in his countless projects and presentations, and for making me indirectly learn and love Spanish (*Ya me dirás!*).

I thank Thierry for encouraging me to give the best of myself, even at a distance, to inspire me with his enthusiasm in the discovery and deepening of phenomena involving the growth and development of plants, to give me valuable observations on the work done and on the ideas to develop to meet the thesis objectives. I thank him also for his patience in “waiting for me” and for his welcome in Montpellier, for his greetings at the end of the day and for his humour (*Ton article est nul! Non, je rigole!*).

It was an honour to collaborate and discuss ideas and results with all the members of SMuCPhy Project: Raul Oorthuis, Marcel Hurlimann, Antonio Lloret, Jean Vaunat, Jose Moya and Càrol Puig-Polo. I have been given the opportunity to experience in the field what has been observed in the laboratory, to have other points of view on my results, to have support and awareness of the applicability of my thesis work.

A special mention should be made to my office colleagues: Agustín Cuadrado, Stefano Collico, Lluís Monforte and Erdem Toprak. All hard-working people, who don't waste time looking at what's outside the window.

It was a pleasure to interact with the other researchers and staff in the TERRE Project. The critical eye of numerous international experts in the geotechnical field, together

with the friendship of the other doctoral students has made this experience unforgettable.

I thank all my colleagues and friends at the UPC for the short but intense moments of break and for sharing their ideas and knowledge: Oriol, Arisleidy, Núria, Rodrigo, Luis, Clara, Fernando, Alejandra, Michela, Riccardo, Gaia, Ferran, Ningning, Gerard, Fabiola, Christina, Miky, Lu, Laura, Jattna, Jackson, Saeed, David. I also thank Luis Gandarillas, with whom I've had the opportunity to collaborate on lab tests included in this thesis and Vito Tagarelli, with whom there have been many fruitful discussions

I thank my friends and colleagues in AMAP, for their time to discuss about funny and useful stuff about plants, trips, food, culture, bureaucracy: Sofia, Roberta, Lorenzo, Jean-François, Hervé, Mao, Nora, Nathalie, Miléna, Nicolas, Gilles, Ghislain.

I acknowledge the precious work of the technicians, from Barcelona and Montpellier's lab: Rodrigo Gómez, José Alvarez, Tomás Perez, Mercedes Sondon, Markos Dueñas, Stéphane Fourtier.

Both in Barcelona and Montpellier, I've met a lot of people who haven't made me feel alone: Christian, Marc, Jack, James, Joan, Pol, Pau, David, John, Gerard, Claudia, Jordi, Nico, Lucia, Bea, Valeria, Francesca, Fadel, Giulio, Mattia, Sara, Carolina, Steve, Martina. Thanks for the laughter, the adventures, the football games and the evenings spent together: they were my energy to continue working on this thesis.

I want to thank my family at this point, for having always been close to me, even at a distance, with a video call, a message. For all the "welcome back" and "goodbye" received in these years. For soccer matches organized by the brothers or the best dishes prepared by grandmothers or mother when I came home.

Finally, I want to thank my girlfriend Lucy, for giving me support and understanding my moods even via messages, for enduring my absences and postponed returns because of complicated work periods or tests to do.

To the reviewers of this thesis: Slobodan Mickovski and Cristina Jommi: my gratefulness for improving a lot the quality of this thesis.

All mentioned people contributed to keep my mood up, to carry out a job that sometimes requires a huge psychological effort.

Table of contents

1. Introduction and objectives

This thesis has received support by the European Commission via the Marie Skłodowska-Curie Innovative Training Networks (ITN-ETN) project TERRE 'Training Engineers and Researchers to Rethink geotechnical Engineering for a low carbon future' (H2020-MSCA-ITN-2015-675762).

1.1 Background

Global warming and the approach of many countries towards ways of environmentally sustainable development are bringing new challenges to engineers. In the field of geotechnical engineering, for example, global warming and climate change are contributing to increase landslides and erosion phenomena, stemming from isolated and very intense rainfall events followed by long periods of drought (Alonso et al. (2003); Alvioli et al. (2018); Cui et al. (2013); Vardon (2014)). A possible environmentally sustainable solution from a geotechnical viewpoint is to counteract these phenomena, which may cause significant socio-economic losses, by studying the effects of roots of special plants on the global soil hydro-mechanical behaviour.

To date, most of the earthworks (railway and motorway embankments, canals, flooding protection structures) already built for engineering purposes, are currently vegetated: sometimes plants were left to grow spontaneously, some others they are sown intentionally by specialised companies (Naturalea; Prati armati ®). Although detailed manuals on the use of in situ vegetation have been produced (Sauli et al. (2005); Coppin and Richards (1990)) there are no specific regulations that guide consulting companies and contractors in the process of construction, maintenance and prediction of the overall response of the work when interacting with atmosphere and vegetation. As a result, the (positive and negative) effects of vegetation are often neglected at the design stage of these works because they are difficult to predict. In this sense, scientific research is required to adopt protocols, advanced methodologies and to produce databases and

models that allow characterizing and interpreting the effects of roots on soil geotechnical properties necessary for design, for both ultimate and serviceability limit states.

Many experimental studies on soil-root interactions agree on the fact that plants are enhancing soil mechanical properties (e.g., shear strength). Nevertheless, protocols observed in literature for preparing and testing samples are often deeply different and conflicting with each other. So far, the most commonly used technique to quantify roots reinforcement of soil is the direct shear test (Gonzalez-Ollauri and Mickovski (2017); Ghestem et al. (2014); Yildiz et al. (2018); Veylon et al. (2015); Mickovski et al. (2009)). Large shear boxes are commonly adopted for laboratory and in-situ investigations, to test representative element volumes of vegetated soils. In most investigations, these tests are carried out under conditions of total soil saturation and observing the effects of different types of plants and different root spatial distribution on soil response in terms of shear stress evolution and displacements. These studies have given an insight into the characteristics of the roots that most influenced the response of the soil (roots tensile strength, diameter size, root length and area density). The main limitation of this equipment arises from the small horizontal displacements often allowed: this causes roots partial extension and therefore, partial exploitation of their tensile strength. Moreover, large equipment often needs to be deeply adapted to test vegetated soil under its corresponding low confinement stress level (typical of shallow ground depths). Few investigations focused on the combined effects of suction and roots on soil hydro-mechanical behaviour: partial saturation may affect the mechanical characteristics of roots and soil structure and consequently influence reinforcement's efficiency. Indeed, Gonzalez-Ollauri and Mickovski (2017) performed tests at different hydraulic states and observed a very small increase in shear strength for a vegetated soil at high value of suction, compared to bare soil at the same condition. In mechanical tests described in the literature, roots effects on volumetric deformations upon shearing , upon loading and suction changes have been generally neglected, resulting in a considerable lack of knowledge. Moreover, there is still not a clear insight on how soil hydro-mechanical response observed at the phenomenological scale could be linked to soil micro-structural changes generated by roots growth, even if some

recent studies point in that direction (Fraccica et al. (2019); Scholl et al. (2014); Koebernick et al. (2017); Anselmucci et al. (2019); Kolb et al. (2012)).

Concerning soil hydraulic response, investigations carried out on vegetated soils presented different and counterposed results. Saturated soil permeability was enhanced by roots (Smethurst et al. (2012); Vergani and Graf (2016); Scholl et al. (2014)), whereas plant effects on soil's water retention capacity were found to vary according to the type of soil, its dry density on compaction, the type of roots and the chemical interactions between soil and plants (Ng et al. (2014); Pagano et al. (2019); Ni et al. (2019); Ohu et al. (1987); Karup et al. (2017); Read et al. (2003)). In this regard, geotechnical and agronomic investigations seem to focus on different phenomena involved in the problem: mechanic aspects (fissuring, void ratio increase, clogging of pores) for the former, and chemical effects (organic matter/mucilage production) for the latter. Both fields of study bring interesting results to the study of the hydraulic effects of plants on soil. What is missing is a framework that can integrate different points of view and couple all relevant observed phenomena.

All the above aspects must be considered together when simulating the behaviour of geotechnical earthworks, especially if it is vegetated. Indeed, we know from the principles of geotechnics that the hydraulic state of soil has a great influence on its mechanical behaviour (Romero and Vaunat (2000); Vanapalli et al. (1996); Fredlund and Rahardjo (1993); Alonso et al. (1990); Terzaghi (1936); Skempton (1954); Bishop (1954)). We also know that the condition of total saturation is the most critical, all other variables being equal, in most of geotechnical problems. Nevertheless, for a geotechnical work subject to ground-atmosphere interactions, it is important to consider the transition from partially to totally saturated soil.

1.2 Aim and objectives

The aim of the thesis is to achieve an advance in the state-of-the-art knowledge of the hydro-mechanical behaviour of vegetated and partially saturated compacted soils within an experimental framework and with analyses at different scales (microstructural and phenomenological). Protocols and results will be produced in the thesis, in such a way as to be a useful tool for engineers and scientists in the assessment of slope stability with vegetated soil subjected to ground-atmosphere interactions, as well as in projects

involving the use of materials in which roots may grow. Laboratory tests will be designed to identify the potential positive and negative aspects of the use of plants in geotechnical engineering problems.
The thesis work has been organised in such a way as to achieve the following objectives:

- Execution of a hydro-mechanical testing program on partially saturated soils with roots (large size triaxial, direct shear and oedometer cells; water retention tests; permeability; direct tensile tests).
- Study of the effect of different roots quantities and plants growing periods on soil response at different scales.
- Experimental characterization of roots main features that should be included in constitutive laws for predicting their reinforcement in partially saturated soils.
- Implementation of root morphological and mechanical traits into constitutive models to predict vegetated soil's water retention and shear strength.
- Use of the experimental data to simulate the hydro-mechanical response of a fallow and a vegetated soil slope subject to changes in water content.

1.3 Thesis content

The thesis has been organised in an introduction, four main chapters and conclusions. Main chapters have been prepared in the form of scientific articles.
In the **Introduction**, a general state of the art about techniques and results obtained during different investigations on soil-roots interactions and from different scientific fields are presented. From the literature review, the objectives of the thesis will be defined, aiming at:

- performing a comparative analysis between the results obtained within this thesis, on roots effects on soil hydro-mechanical behaviour at the phenomenological scale, and observations coming from other authors;
- carrying out a gap analysis in a vegetated soil's geotechnical characterization and to assess them;

- assessing the causes of the results obtained in the thesis by evaluating phenomena occurring at soil micro-scale that were partially or completely unexplored/unquantified;
- understanding which are the most important plant features, from an engineering point of view, to consider when assessing soil hydro-mechanical response after their growth;
- implementing plant characteristics in well-established constitutive laws for bare soil, to predict its response when vegetated;
- bringing a new point of view to the numerical modelling of a possible engineering application, based on the laboratory results obtained.

In **Chapter 2,** a multi-scale experimental program and its results are presented on the hydraulic behaviour of a vegetated compacted soil. Standard geotechnical tests were carried out with repetitions to assess the global hydraulic response. Furthermore, two advanced and complementary techniques were adopted to investigate the causes of the aforementioned global behaviour and to correlate them to the presence of roots. Two main effects of plants on soil structure were observed: fissures generation and pores clogging. Roots geometrical features linked to these effects were carefully characterized and cross-validated through different techniques. The quantification of these two phenomena helped to interpret laboratory results obtained in this Chapter and in the following ones, as well as to justify choices made in the building of a numerical model for the simulation of an earth embankment covered with vegetation.

In **Chapter 3,** information was gathered from results obtained at soil-microscale presented in the previous Chapter. A good correlation was found between some root traits and the volume of fissures generated by plant development. This correlation was used to implement a constitutive model for double-porosity soils to predict changes in soil water retention and permeability due to root penetration in the matrix. The model was then validated by predicting retention and hydraulic conductivity measurements presented in Chapter 2.

In **Chapter 4,** different techniques were adopted to assess shear strength and volume change behaviour of a vegetated soil at different hydraulic states. Different plant

growing periods were defined to investigate their effects on soil response. Results were interpreted using constitutive laws for partially saturated soils with a strongly coupled hydro-mechanical response. A net increase in soil shear strength was observed as the number of roots in soil was rising. However, some aspects of the general mechanical response of the vegetated soil revealed a clear dependence on root-generated changes in soil structure.

In **Chapter 5,** results coming from the whole geotechnical characterization presented in the thesis were used to simulate the response of a full-scale embankment vegetated by plants at different growth stages. A wetting stage was imposed to the earthwork, starting from a condition of partial saturation. Slope minimum safety factor was then evaluated after different wetting steps and up to complete soil saturation. As expected, vegetated slopes were safe throughout the simulation, whereas failure was predicted in the bare slope. Nevertheless, the vegetated soil hydraulic behaviour observed in the laboratory has manifested its negative effect on the stability of the vegetated slopes, along the first stages of the simulation.

Finally, **Chapter 6** contains the main conclusions of the work carried out, as well as future research proposals.

1.4 Workshops and conference presentations:

The thesis has resulted in several contributions to different international conferences and workshops:

- Fraccica A., Romero E. and Fourcaud T. 2019. Multi-scale effects on the hydraulic behaviour of a root-permeated and compacted soil. IS-GLASGOW 2019, Glasgow 26-28/06/2019. E3S Web of Conferences, 92, 12014.
- Fraccica A., Romero E. and Fourcaud T. 2019. Hydro-mechanical response of bare and root-permeated soil slopes to rainfall: from a multi-scale laboratory research to modelling. MUSLOC, Barcelona 19-20/09/2019.
- Fraccica A., Romero E. and Fourcaud T. 2019. Multi-scale observations on a root-permeated compacted soil at different hydraulic states. ALERT Workshop, Aussois 01/10/2019.

- Fraccica A., Romero E., Fourcaud T., Sondon M. and Gandarillas L. 2020. Tensile strength of a vegetated and partially saturated soil. Paper accepted E-UNSAT 2020.

1.5 Publications in ranked scientific journals

- Oorthuis R., Hurlimann M., Fraccica A., Lloret A., Moya J., Puig-Polo C. and Vaunat J. 2018. Monitoring of a full-scale embankment experiment regarding soil-vegetation-atmosphere interactions. Water, 10 (6) 688.
- Fraccica A., Romero E. and Fourcaud T. Effects of plant root growth on soil microstructure and hydro-mechanical behaviour. Géotechnique. In preparation.
- Fraccica A., Romero E. and Fourcaud, T. Hydro-mechanical framework to study roots effects on compacted silty soil. Géotechnique Letters. In preparation.
- Fraccica A., Romero E. and Fourcaud, T. On the shear and tensile strength properties of partially saturated and vegetated soil. Geomechanics for Energy and the Environment. In preparation.

2. Effects of plant growth on soil microstructure and hydro-mechanical behaviour

2.1 Abstract

Many studies on soil-root interactions agree on the fact that plants are enhancing soil mechanical properties (e.g., shear strength). Concerning the hydraulic aspects, observations performed on different and unrelated phenomena and scales are evidencing counterposed results. The macroscopic features of vegetated soils (water retention, permeability) are rarely linked to soil-root interactions at the microscale which, in addition, have only been described qualitatively.

The current study is aimed at assessing the alterations induced by roots on soil hydro-mechanical behaviour and microstructure, at different and hydraulic states. Laboratory experiments were carried out on compacted silty sand seeded with *Cynodon dactilon* (Bermudagrass). Net changes were observed comparing bare and vegetated soil's response in terms of water-saturated soil permeability, water retention and soil shrinkage upon drying. Due to the difficulty in the phenomenological interpretation, the study was complemented with X-ray microtomography and mercury intrusion porosimetry to quantify soil fabric changes at the soil-roots interface and at the clay aggregate scale.

The effects of roots on the soil multi-modal pore size distribution were significant and caused by multi-physics phenomena: fissures generation and widening during soil and roots shrinkage, voids clogging and soil aggregation due to mucilage production. The characterization of these phenomena was used to explain and predict quantitatively the vegetated soil behaviour observed at the macro-scale.

2.2 Introduction

Many investigations have focused on the effect of plants on the hydraulic properties of soils. Smethurst et al. (2012) found an increase of permeability within clay embankments due to plants; Ng et al. (2014) showed that clayey soils compacted at different dry densities have contrasting water retention behavioural features when permeated by roots, while Pagano et al. (2019) did not observe relevant effects of plants in a high porosity silty soil. Indeed, the soil dry density and water content, as well as the stress state, are imposing constraints on roots diameters, volumes, length and their ability of opening fissures and/or clogging pores (Kolb et al. (2017)). Vergani and Graf (2016) showed that vegetation generally increased the saturated permeability during the whole growing stage (from 1 to 8 months). Ng et al. (2016) proposed a model dependent on a root geometrical parameter (root volume ratio R_v) to consider pores clogging and its hydraulic consequences on soil, while Ni et al. (2019) analysed the impact of plants growth and decay on the overall soil hydraulic behaviour. Ng et al. (2019) observed that also plant spacing might affect root growth and soil hydraulic behaviour.

The above-mentioned authors performed observations at the specimen and slope scale. Some of them empirically correlated macroscopic evidences (air-entry value - permeability change) to roots geometrical traits and soil initial compaction state by realistic but undemonstrated theories (void ratio alteration, soil fissuring etc.). In fact, there are few studies on roots effects at the pore-scale: among them, the effects of roots on the pore size distributions of a fine-grained soil by an inverse estimation while Koebernick et al. (2017) performed high-resolution X-ray micro-tomography on a loose silty sand, focusing on a single soil-root interface. The latter estimated a general decrease in porosities between 5 and 300 μm due to a compaction process triggered by roots diameter enlargement against the soil interface, and a minor porosity generation due to root hairs (root protuberances with a few microns diameter). Nevertheless, the investigated range of porosity was too narrow, and information was missing at the root system scale and at the aggregation level. X-ray micro-tomography was also used by Soriano et al. (2017) and Anselmucci et al. (2019). The former built porosity distributions in a soil with fibres, finding an increase of void volume close to them. The latter computed sand grains kinematics due to plant growth, showing important

displacements in roots vicinity. Forces exerted due to root growth were measured by Kolb et al. (2012) as function of the crossed gap between two photo-elastic grains.

Agronomic literature is focusing on chemical interactions between roots and soils fabric, which are indirectly affecting soil macroscopic hydraulic behaviour (Ohu et al. (1987); Watt et al. (2006); Hinsinger et al. (2009); Moradi et al. (2011); Karup et al. (2017)). Indeed, polymeric substances produced by roots (mucilage) modify significantly the chemo-physical properties of the soil by reducing the water surface tension, clogging pores and forming and stabilizing aggregates (Read et al. (2003); Carminati et al. (2010)). The reduction of the water surface tension or the generation of a water repellent surface inside a soil may generate a decrease of its retention capacity (Beckett et al. (2016)). Mucilage facilitates water and nutrients uptake from the surfaces of the soil aggregates (Tinker and Nye (2000)) and keeps root tips strongly bound to solid grains as the soil dries out (Watt et al. (1994)). Finally, Carminati et al. (2013) and Liu et al. (2015) observed roots shrinkage upon drying causing gaps opening at the root-soil interface. These microscopic phenomena are often qualitatively described or analysed in a decoupled way with the macro-scale behaviour and soil properties. Considering all this knowledge, the present study aims at investigating jointly the chemical-hydro-mechanical effects that roots have at different scales on soil and the influence that soil hydro-mechanical states (changes in void ratio and suction) have on microstructure and plants physiology.

2.3 Soil properties and initial state

The tested silty sand was retrieved in the Llobregat river's delta (Barcelona, Spain). Its grain-size distribution is presented in Figure 1, jointly with the curve obtained for the same material after sieving at 4.76 mm. As part of a hydro-mechanical characterization campaign, this study involved sieving the material at 4.76 mm (ASTM E11 (2017)) to respect the ratios between sample diameter and maximum grain size indicated in the ASTM standards (ASTM D2435-M (2011); ASTM D7181 (2011)). The soil has been classified as silty sand according to the USCS. Further details on soil main physical properties are presented in Table 1.

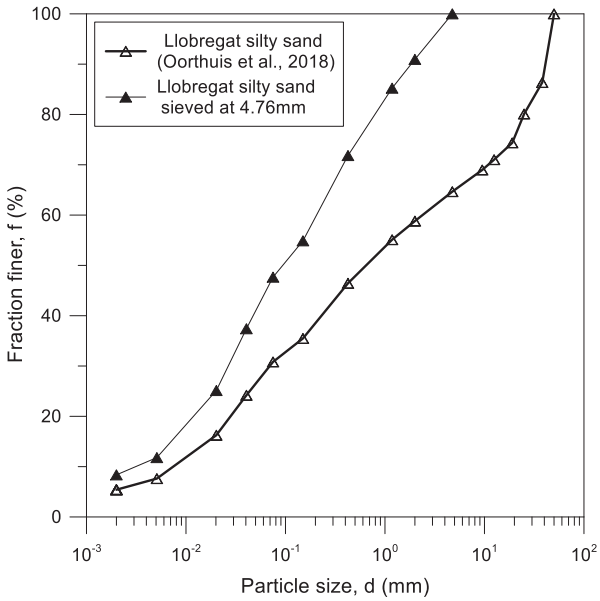

*Figure 1 Particle-size distribution for the soil tested in the present study (sieved Llobregat silty sand) and as-retrieved (*Oorthuis et al. (2018)*).*

Table 1 Main soil physical properties and as-compacted state.

Soil properties / as-compacted state	Value
Soil fraction < 2 mm (%)	58.8[b]
Soil fraction < 75 μm (%)	30.8[b]
Soil fraction < 2 μm (%)	5.4[b]
Liquid limit (%)	29.5-34.4[a]
Plasticity index (%)	9.6-13.5[a]
Density of solids, ρ_s (Mg/m^3)	2.65-2.70[a]
Gravimetric water content, w (%)	15[+b]
Water ratio, $e_w = \rho_s w/\rho_w$ (-)	0.40[+b]
Void ratio, e (-)	0.67[+b]
Matric suction, s (kPa)	40[+b]
Max compaction vertical stress, $\sigma_{v,0}$ (kPa)	100[+b]

[a] Oorthuis et al. (2018) [b] Fraccica et al. (2019) [+] *As-compacted state*

Soil was statically compacted in PVC cylindrical pots (150 mm in diameter, 70 mm high) by a hydraulic press, at a displacement rate equal to 0.5 mm/min. The as-compacted state is indicated by point *A* in Figure 2. The as-compacted state and the maximum vertical stress reached on compaction are also summarised in Table 1. After compaction, 8 pots were seeded with *Cynodon dactilon* (plant spacing: 30 mm, seeding

density: 34 g/m^2), a plant already investigated by several authors for geotechnical purposes (Chen et al. (2015); Garg et al. (2015); Leung, Garg, Coo, et al. (2015); Fraccica et al. (2019)). All the pots were watered under unconfined condition to a water content w = 21% and a matric suction around s = 1 kPa to allow plants development (point B in Figure 2). Matric suction was monitored by a ceramic tip tensiometer (T5x, UMS, München, Germany). The potential soil volume change on wetting was checked by a calliper (precision 0.02 mm) but not detected. Roots growth lasted 3 months, until they reached the bottom of the pots (70 mm below the soil surface). After roots establishment, specimens were subjected to air-drying, at null vertical stress, in a controlled temperature/relative humidity room (T = 20 ± 1° C, RH = 50%). Measurements were done when reaching intermediate points between *B* and *C* in Figure 2. Bare soil samples were prepared following the same path.

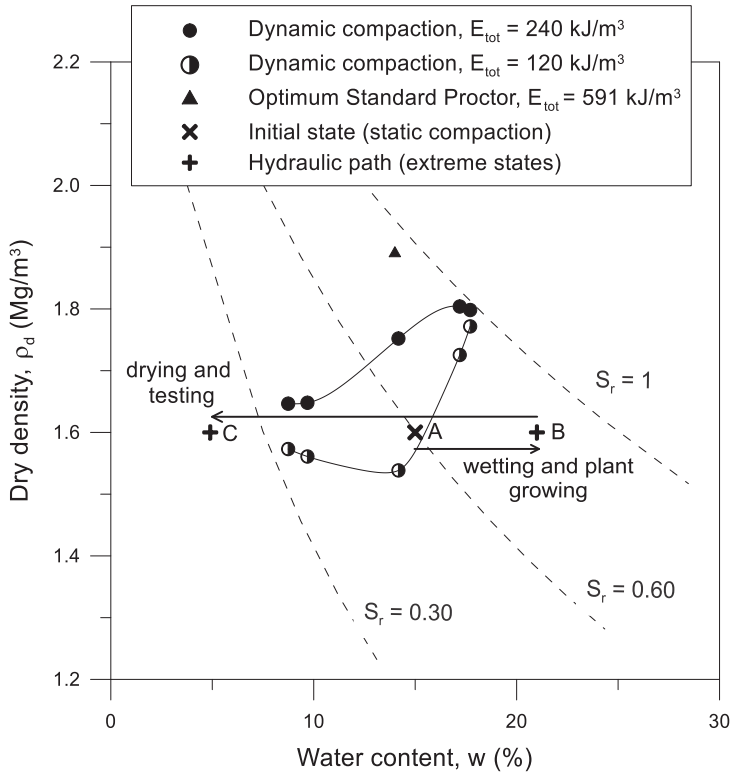

Figure 2 As-compacted state for tested samples (point A), and low-energy compaction curves. Hydraulic paths followed after compaction: wetting (from A to B), plant growing and drying (from B towards C) prior to test.

2.4 Roots volume and structural features

2.4.1 X-ray microtomography

The volume of roots is, for this study, a fundamental parameter to understand the hydro-mechanical behaviour of a vegetated soil, in which the size and the volume of pores play a significant role. Thus, it was necessary to evaluate this structural root trait by destructive and non-destructive techniques, during and after other geotechnical tests. Moreover, roots volume will be used to compute the resulting void ratio $e = V_{voids}/V_{solid}$ within the soil according to the scheme showed in Figure3a. and as: this assumption leads to considering roots neither as solid phase nor gaseous/liquid phase.

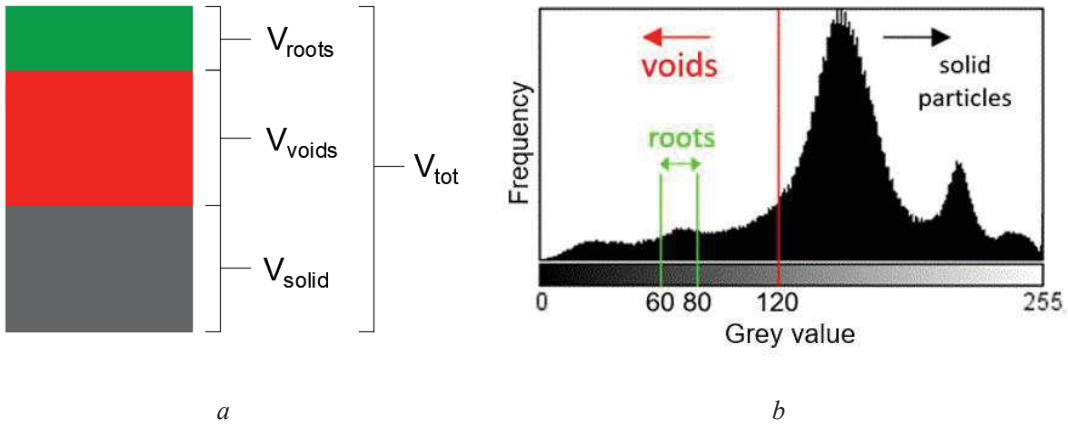

a *b*

Figure 3 a) Scheme of the volumes considered in the root-permeated soil (re-adapted from Wood et al. (2016)*). Volume of voids includes gas and liquid phases. b) 8 bit stack histogram by X-ray microtomography of the region of interest, with threshold values considered to distinguish the desired volumes.*

X-ray microtomography scans were carried out on two bare and five vegetated soil samples (Figure 4), each one containing an individual of *Cynodon dactilon*. The samples were extracted from pots when the soil was at different states (Table 2). They were scanned by X-ray micro-tomography (MicroCT V|Tome|X s 240, GE Sensing & Inspection Technologies GmbH, Germany).

Table 2 Testing state for X-ray micro-CT and mercury intrusion porosimetry samples

Soil initial state	VEG 1	VEG 2	VEG 3	VEG 4	VEG 5	BARE 1	BARE 2
Gravimetric water content, w (%)	12	5	13	22	18	12	23.5
Water ratio, $e_w = \rho_s w/\rho_w$ (-)	0.32	0.13	0.36	0.60	0.47	0.33	0.63
Matric suction, s (kPa)	120	1000	40	0.5	3	110	0.3

Cone-beam CT scans at 170 kVp / 250 mA were used to reconstruct 2024x2024 pixels, 16 bits image stacks with an isometric voxel size equal to 36 µm. A calibration of bulk density *vs* grey values of air and aluminium allowed determining a density resolution of 0.030 Mg/m^3.

Image processing was done by *ImageJ* (Fiji) (Schindelin et al. (2012)). For the treatment, stacks were scaled to an 8 bits format. A region of interest (*ROI*) was defined within the specimen as the 85% of its total volume, to avoid samples irregularity. From the grey value histogram (Figure 3b) of the original image stack (Figure 4a) it was possible to identify the grey intensity peak mainly corresponding to the roots and to isolate them by a threshold between 60 and 80 (Figure 4b). These values were confirmed by calculating the CT grey value according to the equation:

$$CT_{grey\,val.} = 1000\left[1 + \left(\frac{\mu_t - \mu_w}{\mu_w}\right)\right] \quad (1)$$

Parameters μ_w and μ_t are, respectively, the linear attenuation coefficients of the water and of the matter of which the roots are composed (water, cellulose and lignin). These coefficients were found on the XCOM database managed by The National Institute of Standards and Technology (NIST) (Berger et al. (2010)). The CT values were calculated by the attenuation coefficients also for air and typical soil minerals, for comparison purpose (Table 3).

Table 3 Linear attenuation coefficients for the average energy used in the X-ray tomography, CT grey values calculated for 12-bits and 8-bits scales

Material	Linear Attenuation Coefficient at 170 kVp (mm^{-1})	$CT_{grey\ val.}$ (-) (12-bit scale)	$CT_{grey\ val.}$ (-) (8-bit scale)
Air	$1.63*10^{-3}$ (*)	1.08	0.07
Water	1.51 (*)	1000.00	62.26
Cellulose	2.03 (*)	1324.50	82.46
Lignin	1.80 (*)	1192.05	74.21
Kaolinite	3.03 (*)	2006.62	124.92
Calcite	4.02 (*)	2662.25	165.74
Quartz	3.72 (*)	2463.58	153.37

(*) Berger et al. (2010)

The binarized stack was treated with the *Local Thickness* plugin (Figure 4c) (Dougherty (2007)) to remove noise and pores' borders with thickness below 4 pixels (Figure 4d). Finally, roots volume was estimated in *ImageJ* by the plugin *MorphoLibJ* (Legland et al. (2016)).

2.4.2 Pycnometry and WinRHIZO scans

After the laboratory tests described furtherly (Sections 2.5.1 to 2.5.3), soil was washed away to retrieve the plants individuals. Roots were placed in a pycnometer (Figure 5a), already filled with 100 mL of distilled water. The system was vibrated for 30 min to let the air bubbles come up and then, the water raised beyond the control line, due to roots immersion, was extracted with a pipette with a capacity of 0.01 mL and was assumed as roots volume.

After pycnometry, the same roots were scanned and analysed with the commercial software WinRHIZO (Regent Instruments Inc., Quebec, Canada). The software can capture and binarize images (Figure 5b) to evaluate root diameters (as projected area per length) and total length.

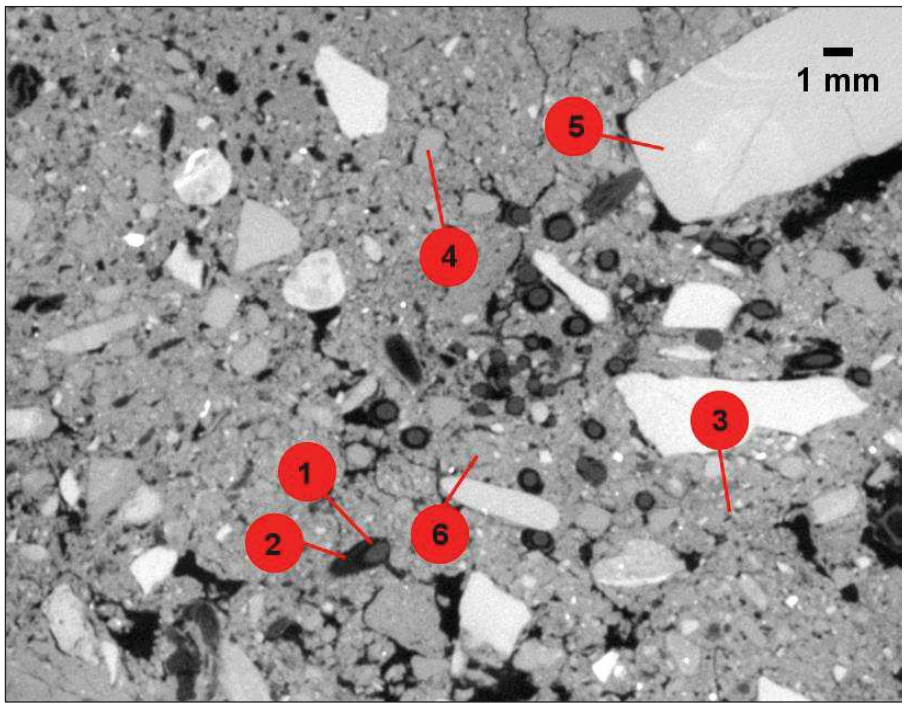

a

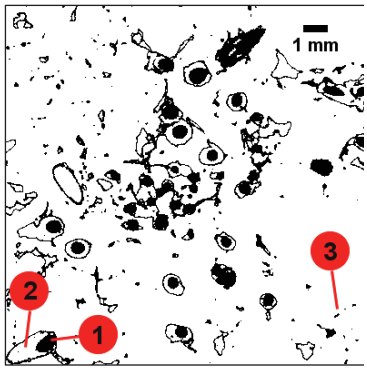

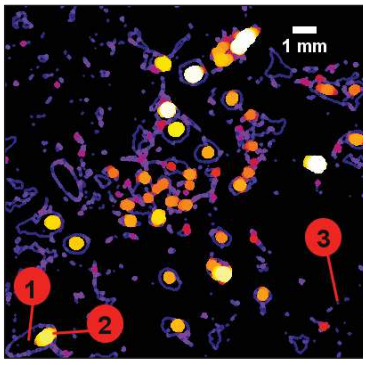

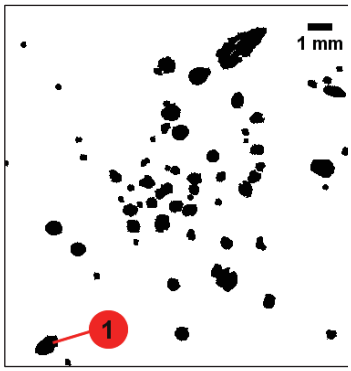

b *c* *d*

Figure 4 a) Region of interest (ROI) considered within the image stack to assess roots volume and pore-size distributions. b) Image threshold between 60 and 80 to isolate roots: fissures and pores boundaries are still visible. c) Local thickness assessment to filter the roots map. d) Roots phase completely isolated from other soil phases.

Given the root length (L_i) for each root diameter class (D_i), the total root volume (V) is then estimated by summing up the partial values (V_i), according to the formula:

$$V = \sum_i V_i = \sum_i \pi \frac{D_i^2}{4} L_i \qquad (2)$$

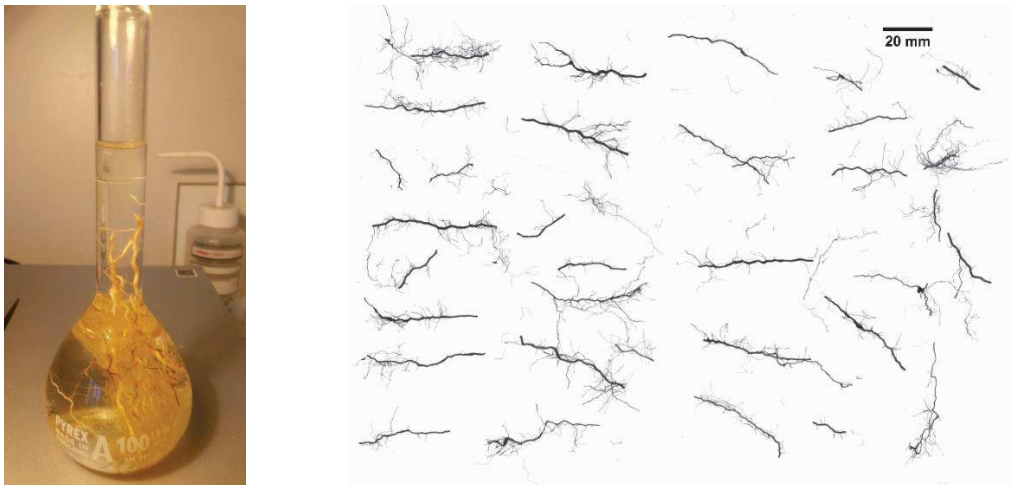

a *b*

Figure 5 a) Roots volume assessment by pycnometry. b) WinRHIZO acquired image.

2.4.3 Comparison of results

All roots volume estimations, for each tested specimen, are summarised in Table 4. X-ray scans were not performed on large samples that were used for water retention measurements, soil water saturated permeability and oedometer tests.

For each sample, the root volume ratio ($R_v = V_{roots}/V_{tot}$) was computed (Table 4). This ratio was calculated with the roots volume values given by the different techniques already explained (X-ray micro-tomography/WinRhizo/pycnometry). By subtracting the root volume ratio obtained by pycnometry from the one obtained by X-ray micro-tomography, it was possible to estimate the potential absolute error in porosity made by considering a certain number of *roots* as *pores* while choosing the threshold value. The potential relative error done in terms of porosity was instead given by the ratio between the absolute error and the initial porosity at which the samples were prepared ($n_o \approx 0.49$). In Figure 6a, a comparison of the root volume values obtained by the three techniques is presented, showing good statistical correlations between measurements. In Figure 6b, for the same samples, "potential" relative errors are presented as a function of the water ratio ($e_w = \rho_s w/\rho_w$ (-), with ρ_s=2.65 Mg/m^3, ρ_w=1.00 Mg/m^3, water content w (-)). The relative error is decreasing as the water ratio is increasing: this means that differences observed should be attributed to roots volume shrinkage, as observed by Carminati et al. (2013); Liu et al. (2015). The higher and the lower values of root volume ratio found

with X-rays were 0.010 and 0.003. Root volume ratio evaluated by pycnometry, for large samples, ranged between 0.006 and 0.014.

Root volume ratio profiles with depth were also computed from X-ray images (Figure 7), confirming the average values showed in Table 4.

Differences in root volume values given by the different techniques may be attributed to the different hydraulic conditions at which measurements were done. Indeed, X-ray microtomography were performed while soil and roots were partially saturated, then they may have undergone shrinkage. Pycnometry, instead, was done submerged in water, which may let the roots swell due to liquid absorption. Finally, WinRHIZO, evaluates the total roots volume assuming a perfectly circular root section and considering the total root length per each root diameter class. Different authors that made comparisons between WinRHIZO and pycnometry measurements observed that the software tends to overestimate root diameters and then, root volumes (Wang and Zhang (2009); Pornaro et al. (2017); Rose (2017); Pang et al. (2011)). WinRHIZO revealed also the root tips density (the number of tips per unit volume of soil), a parameter linked to chemical interactions: its average value for the analysed samples was 0.057 tips/mm^3 (σ^2 = 0.01).

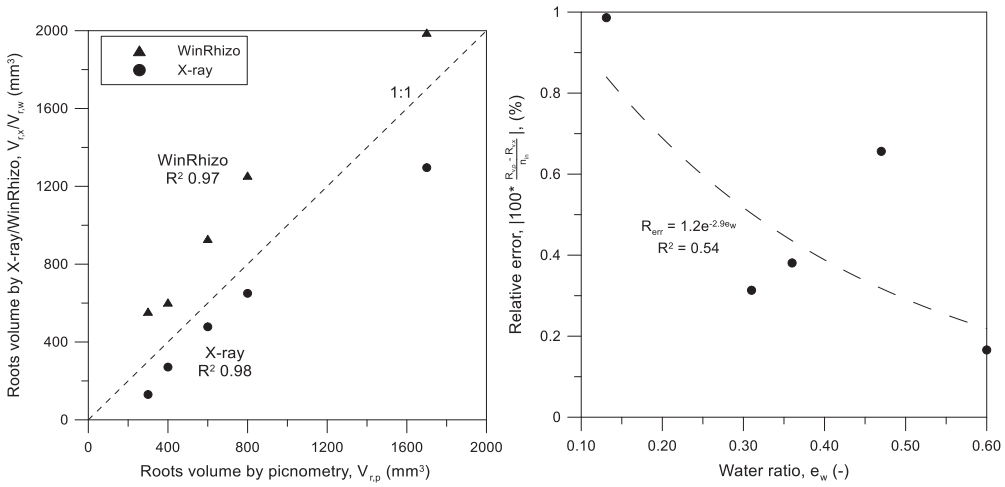

Figure 6 Comparison of values of roots volume obtained from the different techniques and b) potential relative error in porosity between measurements done with X-ray micro-tomography and picnometry.

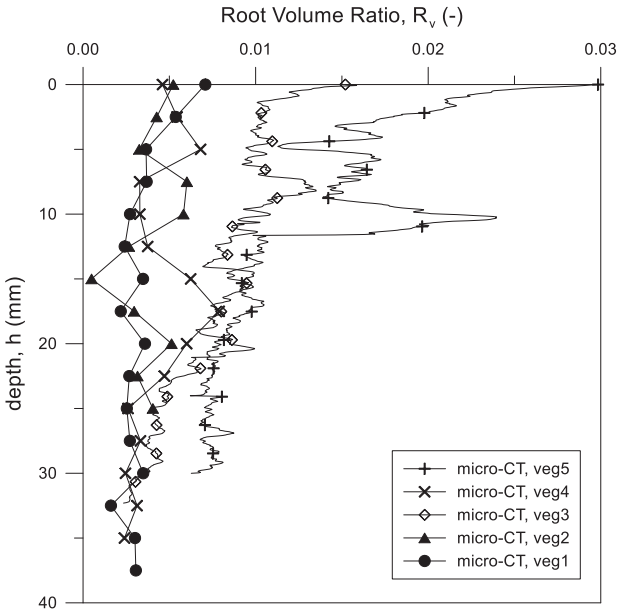

Figure 7 Root volume ratio vs depth, evaluated by X-ray micro-tomography.

Table 4 Soil samples' volume, roots volume comparison for X-ray microtomography, picnometry and WinRHIZO. Estimated root volume ratios.

	Pots for water retention measurements			**Permeameter**	**Pot for Oedometer test**	**Samples for Pore-size distribution assessment**				
Sample name	17	13	6	Perm1R	Oed1R	Veg1	Veg2	Veg3	Veg4	Veg5
Soil bulk vol. (mm^3)	$1.24 \cdot 10^6$	$1.24 \cdot 10^6$	$1.24 \cdot 10^6$	$1.47 \cdot 10^6$	$1.24 \cdot 10^6$	$8.36 \cdot 10^4$	$3.50 \cdot 10^4$	$8.00 \cdot 10^4$	$1.49 \cdot 10^5$	$1.25 \cdot 10^5$
Initial porosity, n_{in} (-)	0.49	0.49	0.49	0.49	0.49	0.49	0.49	0.49	0.49	0.49
Roots - X-ray microtomography (mm^3)	n.a.	n.a.	n.a.	n.a.	n.a.	271	130	650	478	1296
Roots - Picnometry (mm^3)	18510	7430	9900	8540	18910	410	340	800	630	1700
Roots - WinRHIZO (mm^3)	19790	8660	12370	10140	20370	600	560	1260	930	1990
R_v (X-ray) (-)	n.a.	n.a.	n.a.	n.a.	n.a.	0.003	0.004	0.008	0.003	0.010
Root Volume Ratio (Pycnometry) (-)	0.014	0.006	0.008	0.006	0.009	0.005	0.009	0.010	0.004	0.014
Root Volume Ratio (WinRHIZO) (-)	0.015	0.008	0.010	0.007	0.010	0.007	0.016	0.016	0.006	0.016
"Potential" absolute error in porosity $\lvert R_v(\text{X-ray}) - R_v(\text{Pycnometry})\rvert$ (-)	n.a.	n.a.	n.a.	n.a.	n.a.	0.002	0.005	0.002	0.001	0.003
"Potential" relative error in porosity $100*(\lvert R_v(\text{X-ray}) - R_v(\text{Pycnometry})\rvert)/n_{in}$ (%)	n.a.	n.a.	n.a.	n.a.	n.a.	0.31	0.99	0.38	0.17	0.75

2.5 Plant effects at the macroscale

2.5.1 Water retention properties

Three root-permeated samples and one bare sample were used to determine the soil water retention curves. Matric and total suctions were assessed respectively by a ceramic tip laboratory tensiometer, up to 0.20 MPa, and a chilled mirror dew point hygrometer (WP4, Decagon Devices, Pullman, WA, USA), from 0.50 MPa on. After each drying phase during 30 min, soil samples were placed for 24 hours in glass desiccators (Figure 8a-b) with natural light, to allow suction and water content equalisation. Specimens with roots were left in the darkness for at least 2 hours to induce stomatal closure (Snyder et al. (2003)) and to completely stop the plant's transpiration process (Howard et al. (2009)). Transpiration is in fact inducing hydraulic gradients within the matrix (Aylmore (1993)). After this period, the tensiometer was placed into the specimens up to a depth equal to their half height (35 mm).

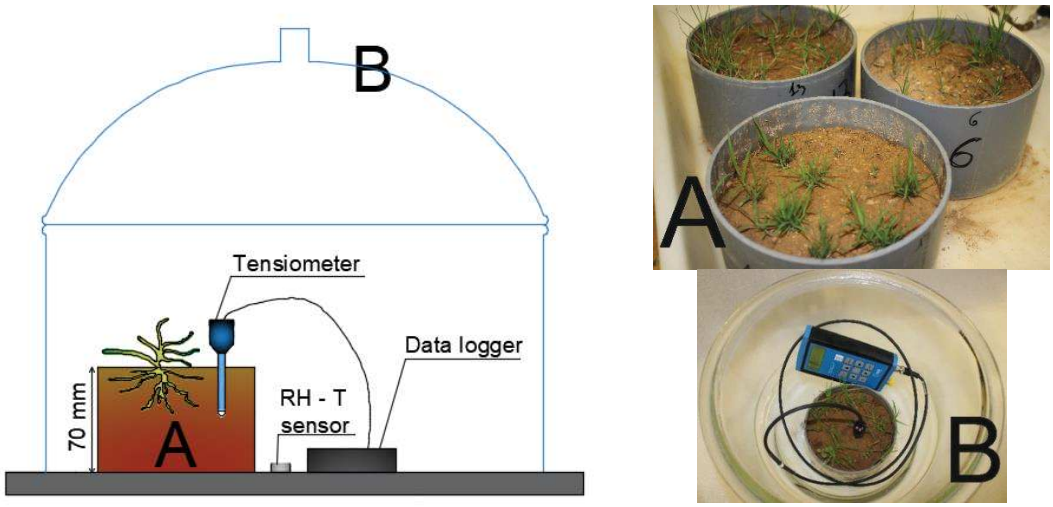

a *b*

Figure 8 a) Schematic of the glass desiccator used for retention measurements. b) Replicates used for suction measurements(A) and tensiometer placed within the specimen (B).

Water content during tensiometer measurements was evaluated by oven-drying (ASTM D2216 (2019)): two soil samples of 30 g each were extracted using a spatula, one from the upper and one from the lower surface of the pots. Visual inspection before placing

the samples in the oven made it possible to prevent the presence of roots inside them. This was done because the water contained in roots is not belonging anymore to soil pores (Boldrin et al. (2018); Garrigues et al. (2006); Prieto et al. (2012)). When the maximum measurable suction for tensiometer was reached, soil samples were trimmed out from the bottom part of the pots and installed in the abovementioned hygrometer, which is providing a measurement of the total suction. Results are presented in terms of water ratio ($e_w = \rho_s w / \rho_w = S_r e$) because they are easily comparable with void ratio variations, since the two variables coincide when $S_r = 1$. Matric and total suctions were plotted in the same graph: indeed, according to Nam et al. (2009), osmotic effects are negligible in this kind of soil.

Data was fitted using the model of Romero and Vaunat (2000), based on a modified form of the van Genuchten (1980) expression:

$$S_r = C(s)\left(\frac{1}{1+(\alpha s)^n}\right)^m \quad ; \quad C(s) = 1 - \frac{ln\left[1+\frac{s}{a}\right]}{\ln(2)} \tag{3}$$

where s is suction (MPa), S_r is the degree of saturation (-), C(s) is a function used for adjusting the curve in the higher suction range. Parameter $1/\alpha$ is linked to the air entry value, n to the slope of the curve and m to the residual degree of saturation. Parameter a is considered as the maximum suction for $S_r = 0$. Calibrated parameters are summarised in Table 5.

Table 5 Parameters calibrated for soil water retention measurements.

	α (MPa^{-1})	**n**	**m**	**a (MPa)**
Bare soil, $e = 0.67$	0.53	0.28	1.77	200
Root-permeated soil, $e = 0.67$	0.15	0.19	2.38	200
Bare soil, $e = 0.74$	0.38	0.20	2.00	200
Bare soil, $e = 0.49$	2.6	0.63	0.67	200

Bare soil retention properties are represented in Figure 9: the plot compares the main drying curve obtained for soil compacted at different values of void ratio and maximum vertical stress (see legend). This parallel study was conducted to represent the influence of the initial void ratio on soil retention properties, since some authors linked roots growth within the soil to a void ratio variation (Ng et al. (2016); Ni et al. (2019)). The more compacted soils presented a higher air-entry value and a higher retention capacity.

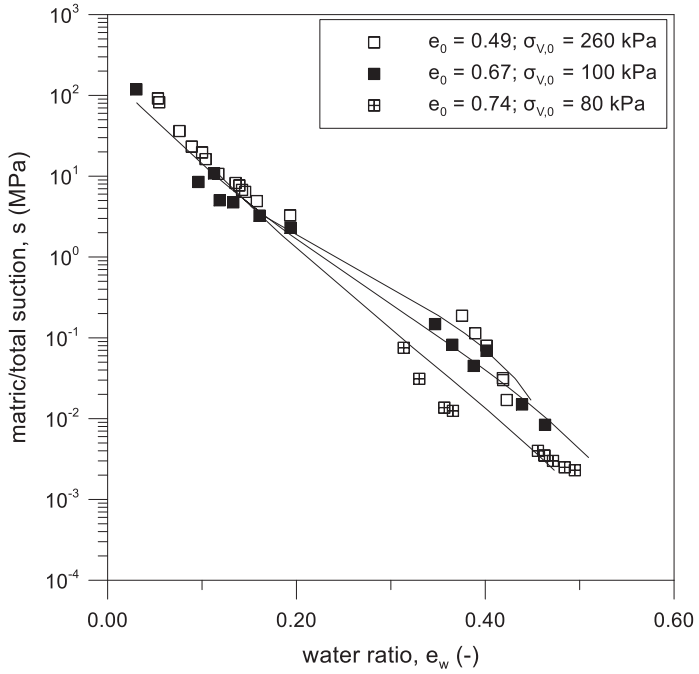

Figure 9 Soil water retention curves, obtained staring from different compaction states, for the bare soil under study

This study mainly focuses on the properties of a soil compacted at a void ratio equal to $e \approx 0.67$. A comparison of the measurements obtained and of the fitted drying curves for bare and vegetated samples is presented in Figure 10. The 14 water retention measurements carried out in the fallow soil were in good correlation with the respective fitted curve ($R^2 = 0.99$), whereas correlation decreased ($R^2 = 0.80$) for the case of vegetated soil. Indeed, this attempt to model the 44 water retention measurements jointly in the vegetated soil, leads to a low coefficient of determination because measurements belong to soil pots in which different values of root volume ratio were observed. This last parameter, representing roots morphology, has been observed to have an influence on soil hydraulic response (i.e. water retention curve (Ng et al. (2016); Ni et al. (2019)). The range of root volume ratios found in the pots is shown in the plot

(for further details, see Table 4). It was observed that the air-entry value and the retention capacity of the vegetated soil have decreased.

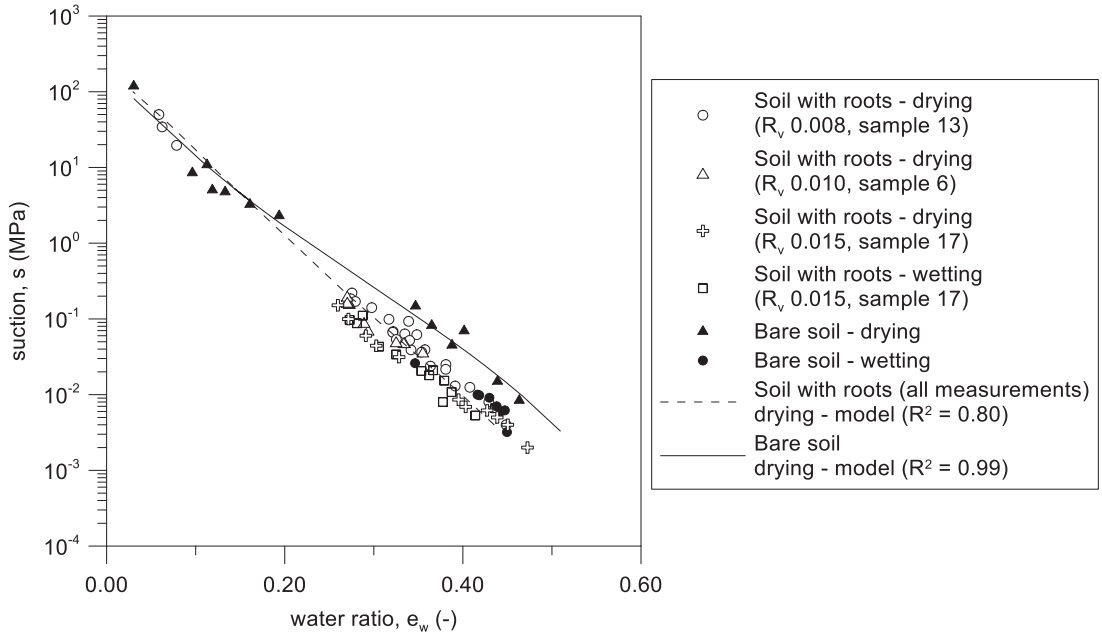

Figure 10 Main drying curves for bare and root permeated soil. Measurements were done with T5x tensiometer and WP4 psychrometer.

Moreover, this phenomenon is accentuated in specimens containing a larger quantity of roots. Finally, all the retention measurements converge at suctions close to 3 MPa. This kind of behaviour was also observed by Ng et al. (2014), for a lightly compacted soil seeded with the same grass of this study.

2.5.2 Volume changes upon drying

The characterization of the entire soil state and stress evolution ($e_w;e;s$) was completed with paraffin tests (ASTM D7263 (2018)). To carry out these tests, cubes with a size of approximately 30 mm were trimmed out of fallow (5 cubes) and root-permeated pots (9 cubes) with an oil-lubricated spatula (to minimize friction with soil), and at different suctions (measured in the soil pot, by tensiometer or hygrometer, as described in Section 2.5.1) and water contents (measured in the soil pot, by oven-checking, as described in Section 2.5.1). In the case of root-permeated pots, the 9 cubes were trimmed out on plants' vicinity. As the standard requires, the cubes were firstly weighed (with a laboratory balance with a precision of 0.1 mg) without paraffin: in the case of vegetated

soil (Figure 11a), the plant's aerial part (shoots) was cut with scissors before weighing. Soil cubes' disturbance was evaluated by visual inspection. Samples were then immersed, face after face, in liquid paraffin at a temperature of 60°C. Once paraffin was solidified (Figure 11b), cubes were weighed again (precision 0.1 mg). Finally, soil covered by paraffin was weighed while being totally submerged in water (precision 0.1 mg). These three measurements allowed calculating the total volume of the soil cubes, with the equation:

$$V_{tot} = \left(\frac{W_2 - W_3}{\rho_w}\right) - \left(\frac{W_2 - W_1}{\rho_p}\right) \quad (4)$$

where W_1 is the mass of the cube without paraffin, W_2 is the mass of the cube covered by paraffin, W_3 is the submerged mass of the covered cube, ρ_w and ρ_p are the water and paraffin density respectively. Moreover, in the case of fallow soil cubes, W_1 consists in the sum of the masses of the liquid (W_w) and the solid (W_s) phases that are linked by the water content.From these two formulations, it is possible to calculate the masses of the two phases (W_w and W_s) and their respective volumes (V_w and V_{solid}), which allowed estimating the void ratios.

In the case of vegetated soil cubes, the value of volume (V_{tot}) calculated according to equation (4) included the volume of roots (as schematised in Figure 3a). As the aim of this test is to calculate the volume of voids (V_{voids}) and the volume of solids (V_{solid}), it was necessary to calculate the volume of roots (V_{roots}) and subtract it to the total volume. So, after submerged weighing, vegetated soil cubes were destroyed to recover the roots present inside them. The weight and the water content of the soil deprived of its roots were respectively measured and estimated. Then, it was possible to estimate the volume of solid particles, knowing their mass. Finally, roots volume was measured with a pycnometer, according to the procedure detailed in Section 2.4.2. Then, the volume of the pores was calculated as the difference:

$$V_{voids} = V_{tot} - V_{solid} - V_{roots} \quad (5)$$

With this procedure it was possible to evaluate the void ratio of the vegetated soil.

Figure 11 Paraffin tests on vegetated soil: a) before and b) after soil covering

Results, in terms of void ratio, have been interpreted with the laws expressing volumetric deformations during suction changes proposed by Alonso et al. (1990):

$$d\varepsilon_{vs}{}^{el} = \frac{\kappa_s}{(1+e)}\frac{ds}{(s+p_{at})}, s < s_0 \quad (6)$$

$$d\varepsilon_{vs} = \frac{\lambda_s}{(1+e)}\frac{ds_0}{(s_0+p_{at})}, s > s_0 \quad (7)$$

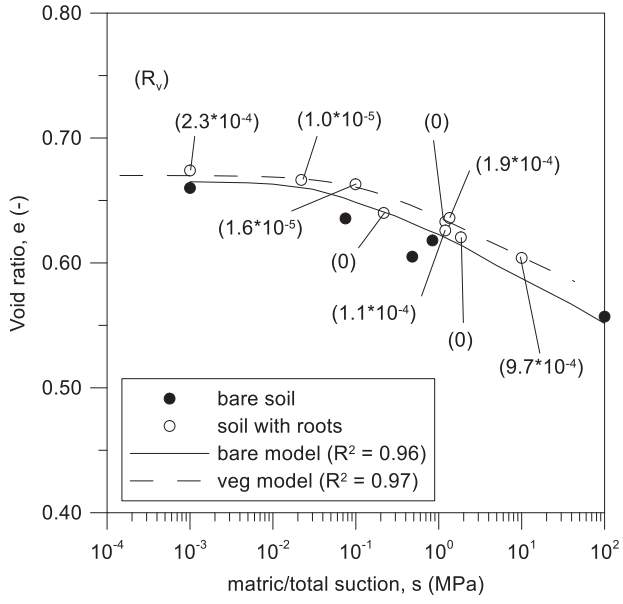

Figure 12 Observed and predicted volumetric deformations, expressed in terms of void ratio along suction increase Root length density values are plotted jointly to their relative points.

The parameters κ_s and λ_s are the stiffness values with respect to suction changes along elastic and virgin states, e the void ratio at which soil was before suction variation (ds) and p_{at} the atmospheric pressure. The term s_0 indicating the maximum suction

experienced by the material and, according to Alonso et al. (1990) it is the point above which irreversible strains are occurring. The maximum suction experienced by all the cubes was $s_0 = 40$ kPa, which is the suction at which material was just after compaction. The parameter κ_s was calibrated and found to be 0.0015 and 0.0010 for bare and rooted soils, respectively. The parameter λ_s was 0.011 and 0.009 for bare and rooted soils, respectively. Results corresponding to volumetric deformations occurred during the drying phase experienced by the samples and fitted curves to equations (6) and (7) are shown in Figure 12. The lower κ_s and λ_s values calibrated for root-permeated soil are indicating that this soil was stiffer than bare soil: this means that its volume is decreasing less than the bare soil, and that it remains at higher porosities than the bare soil, upon suction variations.

These results are in line with those shown by Milleret et al. (2009): the authors observed an increase of the specific volume within a vegetated soil, with respect to a bare soil, along a drying process.

2.5.3 Saturated water permeability

Large-cell oedometer tests (ASTM D2435-M (2011)) and falling-head permeability tests (ASTM D5084 (2003)) were used to evaluate the saturated water permeability of the soil before and after root growth. One bare and one root-permeated soil samples were tested in large oedometer cells (150 mm in diameter, 70 mm in height, Figure 13a). Plants were left to grow for 3 months within the equipment. At test starting, samples were connected to a graded water tank to be saturated and kept under controlled hydraulic gradient conditions throughout all the loading/unloading steps. These steps allowed gradually applying vertical stresses:10/20/40/90/130 kPa on loading and 90/50/10 kPa on unloading. These stresses were chosen to be representative of the stresses which characterise the shallowest parts of the ground, in which roots grow. A permeameter with a diameter of 92 mm and a height of 221 mm (Figure 13a) was used to carry out a falling head permeability test. The soil was statically compacted in the cell at an initial state and stress expressed in Table 6 and seeded with *Cynodon dactilon*. The seeding density was the same as for the other pots used in this study. To allow plants growth, the soil was wetted at zero vertical stress up to gravimetric water content of $w = 21$ %. After roots growth (5 months after seeding), the specimen was completely

saturated under a controlled hydraulic gradient close to the one imposed at test beginning.

Table 6 Initial state and stress variables of soil in the permeameter.

Soil initial state and stress	Value
Gravimetric water content, w (%)	15
Water ratio, $e_w = \rho_s w/\rho_w$ (-)	0.40
Void ratio, e (-) °	0.87
Matric suction, s (kPa) $^{+}$	8
Max compaction vertical stress, $\sigma_{v,0}$ (kPa) *	20

° calculated as $e = (\rho_s/\rho_d) - 1$

$^{+}$ measured by tensiometer

All the values of soil water permeability were plotted together (bare and root-permeated) as a function of their void ratio (Figure 13): results obtained by Oorthuis et al. (2018) for the same bare soil are also included. In the case of root-permeated soil, void ratio is defined as the one at the initial state of compaction (permeameter) or the one calculated according to the volumetric deformations occurred (oedometer test). The maximum vertical stresses applied on the material and the root volume ratio (R_v) measured within the samplesare indicated as labels.

Root growth increased the soil water permeability. Anyway, root-permeated soil permeability tends to the bare soil's values as void ratio reduces. Even if the root volume ratio (R_v) within the oedometer specimen is higher than the one within the permeameter, the effects of roots on soil water permeability are less pronounced. These results are in good agreement with other authors (Vergani and Graf (2016); Ng et al. (2014)) that found that the hydraulic behaviour of a root-permeated soil does not depend only on roots properties and their evolution in time but also on soil confinement and density.

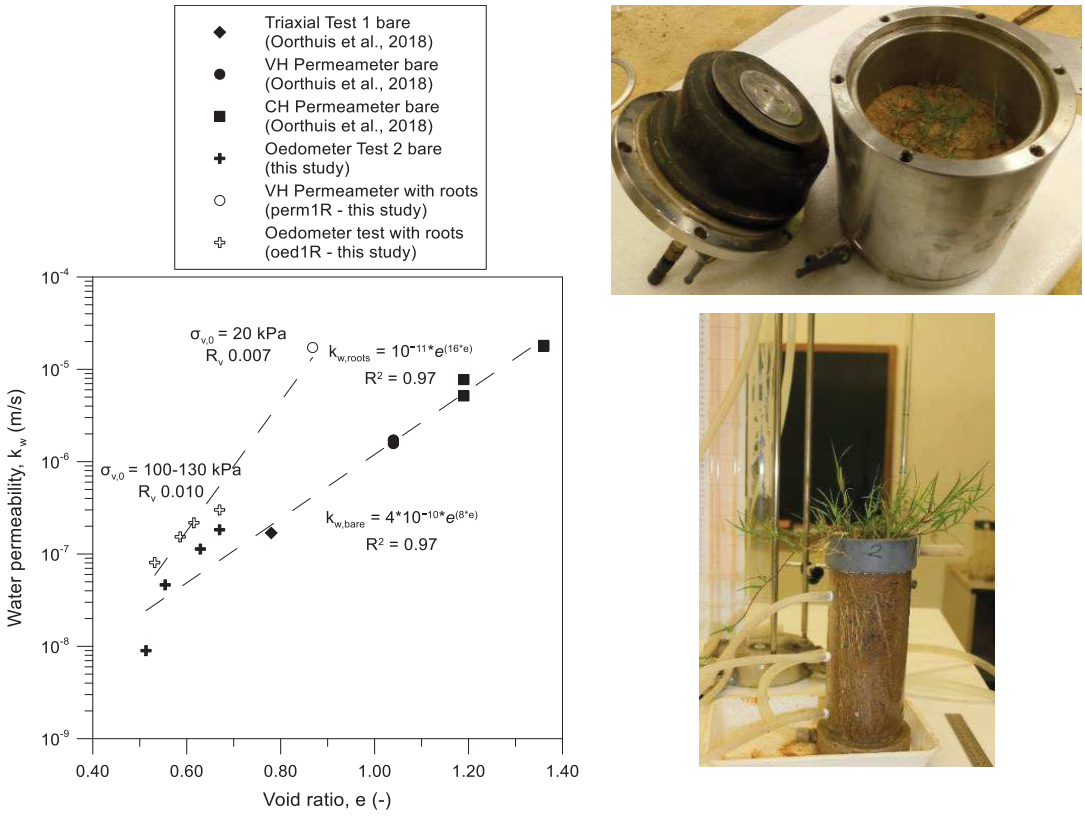

Figure 13 a) Water permeability for bare and vegetated specimens evaluated for different void ratios and with different laboratory tests. Dashed lines indicate the best-fit tendency (R_v = root volume ratio, R^2 = coefficient of determination for the tendency lines). B) Specimen with roots installed in an oedometer cell and in a permeameter.

The latter might have an influence on roots ability to displace grains and generate fissures during their growth. Moreover, the increasing vertical stress imposed on the vegetated soil could have made the root-generated fissures to reduce.

2.6 Plant effects at the microscale

It is assumed that roots affect soil structure due to different processes: pores chemical and physical clogging and soil fissuring due to roots growth and development. The domains involved by these phenomena correspond well to the porosity ranges that can be investigated by the two techniques used: Mercury Intrusion Porosimetry and X-ray microtomography.

2.6.1 Distribution of large-pore sizes

The images coming from the seven X-ray microtomography scans (one example is shown in Figure 14), previously analysed to determine the root volumes, have been furtherly processed to assess the effects of plants on the soil structure.

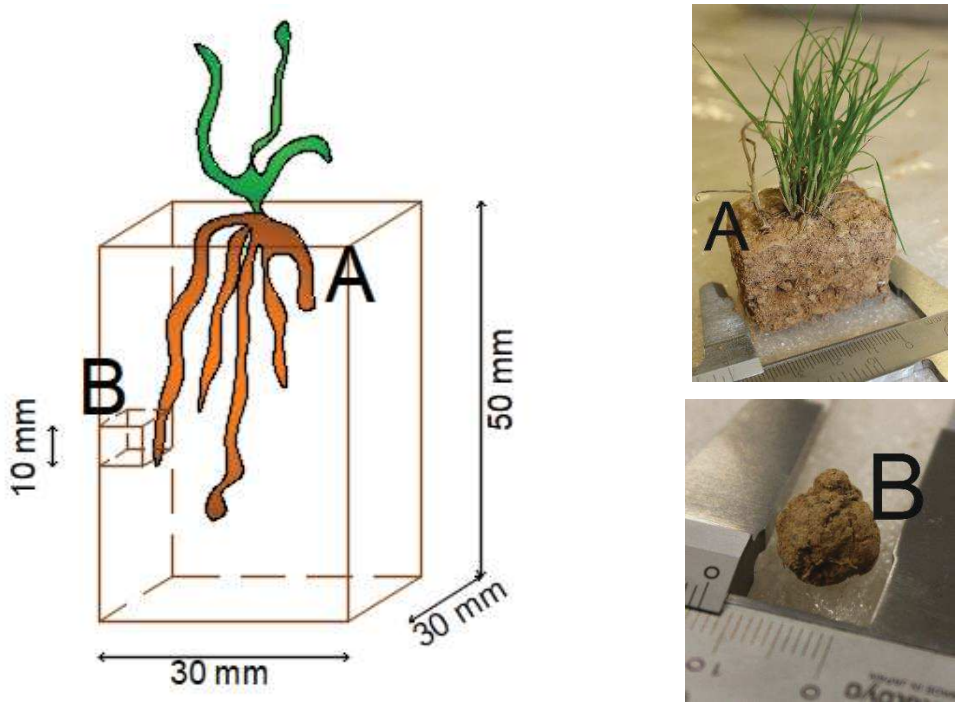

a *b*

Figure 14 a) Schematic of a sample scanned by micro-tomography and tested by MIP, and b) sample scanned by micro-tomography (A) and retrieved sample for MIP (B).

Pores and solid particles were identified through an automatic threshold operation, using *ImageJ*, calculated on the histogram of the grey values of the entire image stack and using the *Default* method. The threshold point was always close to 120 (Figure 3b). The image stack containing the roots phase (previously showed in Figure 4d) was then superimposed to the one showing solid and void phases (Figure 15a), in such a way that the roots are again virtually included into the sample (Figure 15b).

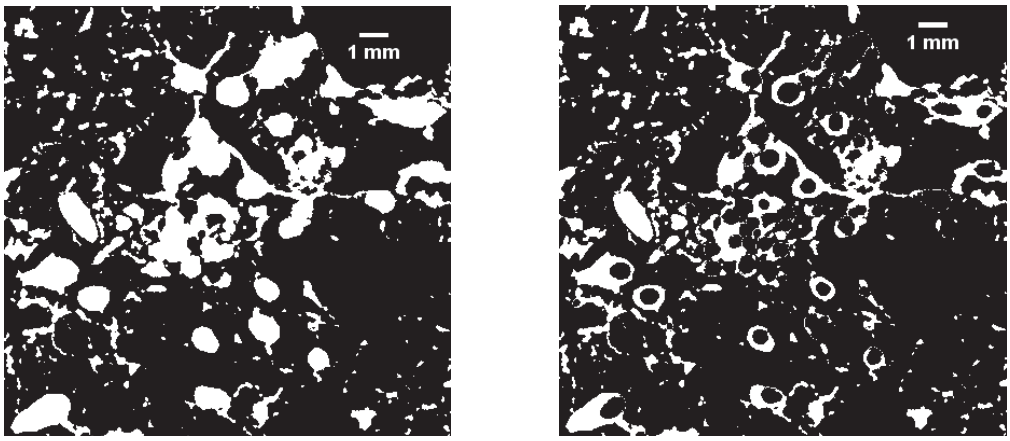
1 mm
1 mm

a *b*

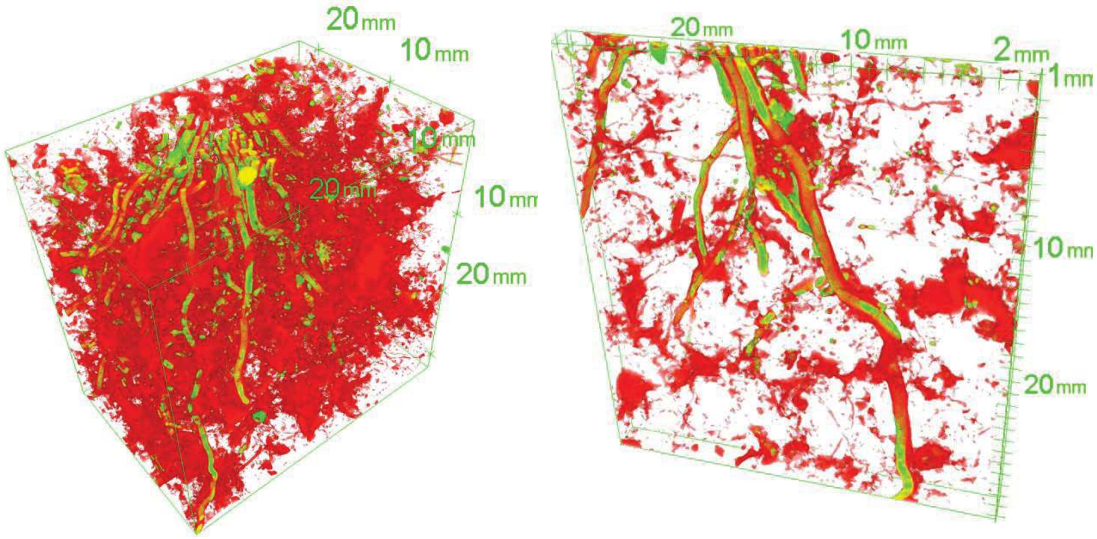
20 mm
10 mm
10 mm
20 mm
10 mm
20 mm
20 mm
10 mm
2 mm
1 mm
10 mm
20 mm

c *d*

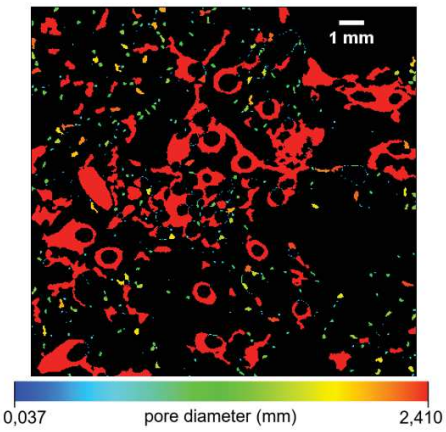
1 mm
0,037
pore diameter (mm)
2,410

e

Figure 15 a) Automatic threshold to separate voids (white pixels) from solid particles. b) Inclusion of the root phase within the image (voids in white). c-d) 3D rendering of roots (yellow) and pores (red) within the ROI and a slice of it. e) Individuation of the different pore diameter classes.

This step allowed building a 3D rendering of roots and voids (Figure 15c-d) that gave a first qualitative insight into the phenomenon: roots are often surrounded by fissures. To better quantify this effect along the hydraulic path studied (Figure 2), a pore-size distribution was assessed for each scanned sample. The analysis was carried out with the *ImageJ* plugin *Pore size distribution* (Münch and Lorenz (2008)). The tool can perform a 3D simulation of mercury intrusion within the voxels representing voids and to evaluate the volume occupied for each class of pore diameter (in Figure 15e the identification of the different diameters by the plugin is showed). Resulting images displayed a clear distinction between pores generated by root penetration (usually between 1 and 2.41 mm in diameter) and pre-existing ones. The tool described allowed investigating pores with a minimum diameter of 37 μm, which is the voxel size for the microtomography images.

2.6.2 Extension to the micro-pores range

Five vegetated and four bare soil cubes with a size smaller than 10 mm have been carefully trimmed from the samples (Figure 14) previously scanned by X-ray micro-tomography (at unvaried water content and suction (Table 2)) and used to perform Mercury Intrusion Porosimetry. Before testing, all the cubes were freeze-dried to remove pore water avoiding soil volumetric deformations (Romero (1999)). Tests were carried out in a porosimeter (AutoPore IV 9500, Micromeritics Instrument Corporation, Norcross, GA, USA). This technique allowed investigating pore sizes from 7 nm to 400 μm.

2.6.3 Roots effects on soil pore-size distribution

The pore size distribution (PSD) represents the cumulative void ratio occupied up to a given pore diameter, starting from the maximum diameter observed. In the case of X-ray micro-tomography, the cumulative void ratio for a given entrance pore size x* was calculated by:

$$e_{cum}^{(x^*)} = \frac{\sum_{x=x_{max}}^{x^*} V_v^{(x)}}{V_s} \quad (8)$$

where $V_v^{(x)}$ is the volume of voids (white pixels in Figure 15b) occupied by a generic entrance pore size x and V_s is the volume of solid particles, calculated as the total volume of the black pixels in Figure 15a. In the case of the results given by MIP, the cumulative void ratio is evaluated directly from mercury intruded volume, as explained in Romero et al. (1999).

Results have been joined to make the upper end of the microtomography curve coincide with the lower end of the MIP curve (Figure 16). In the plot, there is a comparison between PSD curves obtained for bare and root-permeated soils at a water ratio equal to $e_w \approx 0.33$ ($e \approx 0.64$, $S_r \approx 0.52$). The two curves almost approached the same final cumulative void ratio but did not reach the value at which they were originally compacted. Moreover, root-permeated soil's cumulative void ratio at 7 nm was always slightly higher than the bare soil's one, for each water ratio tested. This means that a general increase in void ratio was observed in vegetated soil with respect to bare soil. This agrees to what observed by paraffin tests.

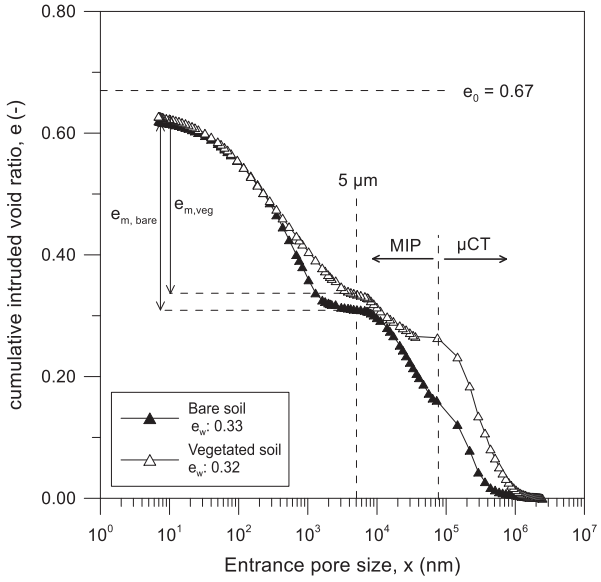

Figure 16 Cumulative PSD for a bare and a vegetated sample, both initially compacted at void ratio 0.67.

Results will be furtherly presented as PSD derivatives with respect to the logarithm of pore diameter: this operation allows better individuating the different pore modes of the material (Figure 17). In Figure 17a-b, there is an overview of all the results, detailing

the water ratio at which they were tested. The pore sizes below 5 μm are corresponding to the clay aggregation range, which cannot be physically penetrated by roots or root hairs (Lamont (1983); Grierson and Schiefelbein (2002); Wulfsohn and Nyengaard (1999)). Comparing Figure 17a and b, one can note that, upon water ratio e_w decrease, the diameter at the peak (mode) of the clay aggregates in the bare soil undergoes a much larger shifting towards smaller pore diameters (from 2.5 to 0.3 μm) than the vegetated one (from 1 to 0.5 μm). This means that aggregates undergo lower shrinkage in the rooted soil. Aggregates mechanical stability generated by roots, is in turn linked to a higher stiffness against volumetric shrinkage previously observed at the macro-scale (Figure 12).

Above the threshold value of 5 μm, different and counterposed effects of soil-roots interactions are expected:

- soil fissuring during roots growth;
- channel formation after roots decay;
- increasing gap between roots and soil matrix during the drying phase;
- pores clogging by root hairs;
- pores clogging by mucilage released.

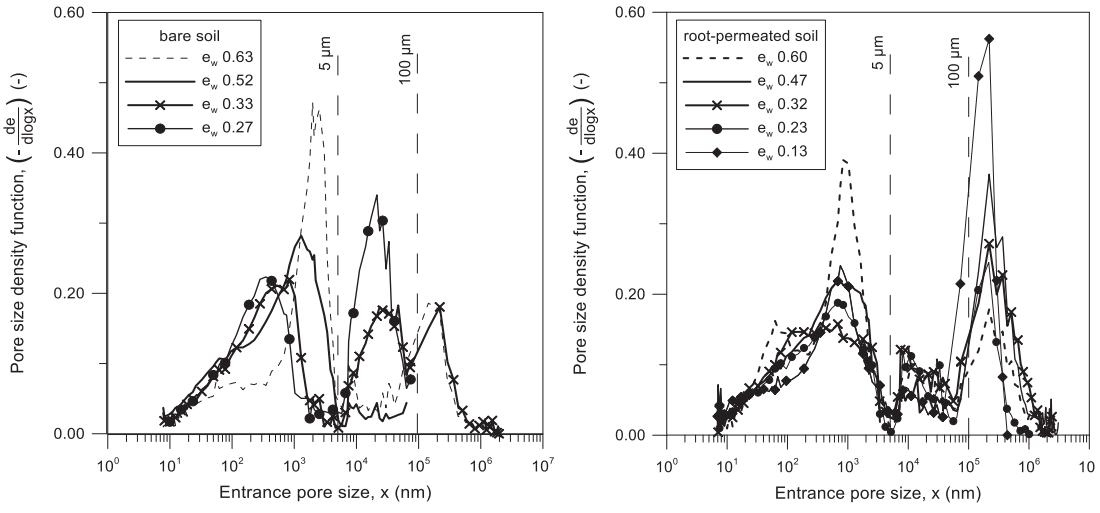

a *b*

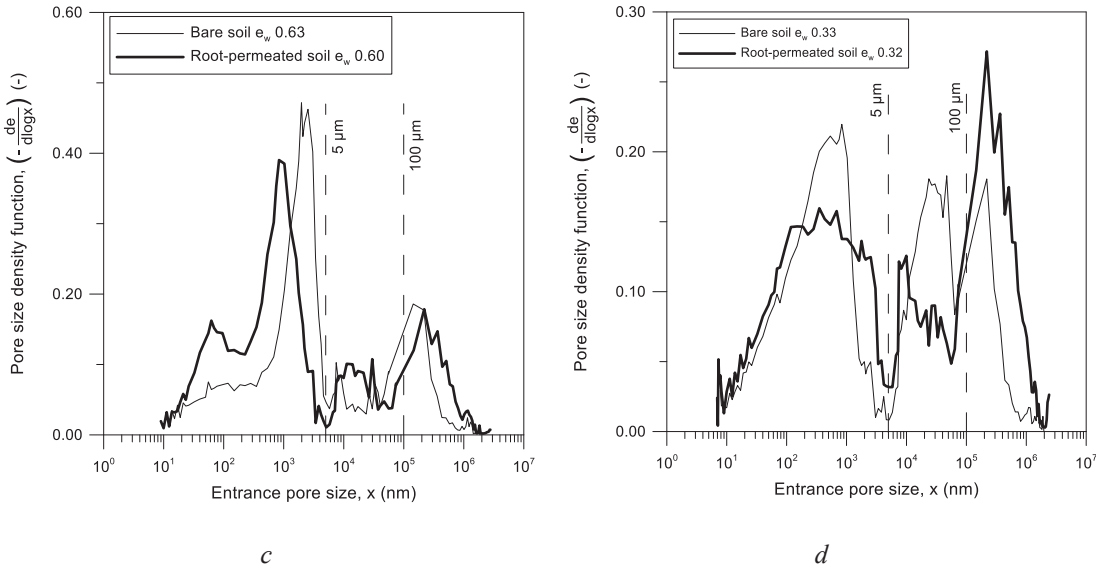

c *d*

Figure 17 Pore size density functions for: a) all the bare samples, b) all the root-permeated samples, c) bare and root-permeated samples close to saturation (e_w = 0.60) and d) after a drying phase (e_w = 0.33).

Comparing Figure 17a and b, the abovementioned effects are noticeable. In the pore size range 5 to 100 µm, pores volume density is in average 1.60 times lower in root-permeated soil compared to bare soil, which can be explained by soil pores being penetrated by fine roots and root hairs. These two root types were characterized by WinRhizo with a unique class of diameter φ ($0< \varphi <0.10$mm). The average root length calculated in the samples, for this diameter class, was 940 mm (σ = 590 mm). Above 100 µm an opposite trend is observed: pores volume density generally increased in the rooted soil. These pore sizes are corresponding to the fissures visible around the roots in Figure 15b and computed in Figure 15e. In addition, the volume of this range of porosity is clearly increasing as the soil dries out, jointly with a shifting of the volume density peak towards lower pore diameters. Such a phenomenon depends on the concurrent shrinkage of soil and roots (Jones (2007); Carminati et al. (2013); Liu et al. (2015)).

Bare and root-permeated pore size density functions calculated for samples at similar water ratios were compared (Figure 17c-d). At a water ratio equal to $e_w \approx 0.60$ ($e \approx 0.67$, $S_r \approx 0.90$, Figure 17c), the volume of pores above 100 µm is almost equal between the two soils, even if the peak value corresponds to a larger pore size within the vegetated sample. This observation is in line with findings shown by Carminati et al. (2013), who

evidenced the capacity of roots to clog the whole fissures generated by their growth, when soil is saturated. In the pore diameter range 5-100 μm, pore size density is increased by roots, while for pore diameters below 5 μm some porosity is reduced and other ones are enhanced. Jointly to a partial pore clogging due to mucilage production, some pores in aggregates might have increased in volume due to other chemical activities in soil. Indeed, high water contents increase soil nutrient mineralization due to metabolic and enzymatic activities (Borken and Matzner (2009); Manzoni et al. (2012)): this is strictly linked to plants nutrition (Singh and Schulze (2015)). At a lower water content (Figure 17d, $e_w \approx 0.33$, $e \approx 0.64$, $S_r \approx 0.52$) most of the vegetated soil's intra-aggregate (inside aggregates) and inter-aggregate (outside aggregates) pores between 5 and 100 μm appear reduced in volume compared with bare soil. This observation is caused by a combined effect of chemical and physical clogging, for instance linked to mucilage production that increases upon drying (Watt et al. (1994)). Porosities above 100 μm are instead evidencing higher pore size densities and pore diameter peaks, due to fissures generated and widened by roots.

2.7 Roots traits and soil microstructure on drying

Soil microstructure evolution on drying is quantitively defined by the intra-aggregate void ratio e_m; this variable is defined on the pore size distribution curve (Figure 16) as the difference between the final cumulative intruded void ratio and the one reached at the pore size of 5 μm. This value is close to the one used by Romero (2013) to identify aggregates porosities in clayey soils. The microstructural variable is linked to the total void ratio by:

$$e = e_m + e_M \tag{9}$$

where e_M is the void ratio of inter-aggregate space.

Intra-aggregate void ratio is plotted in Figure 18 as a function of the water ratio at which samples were tested. In fact, for the bare soil, the graph is representing the swelling and shrinkage reversible behaviour of clay aggregates along the hydraulic path. This behaviour is indicated by the parameter β with the following equation in line with the one proposed by Romero et al. (2011):

$$e_m = e_m^* + \beta e_w \tag{10}$$

where e_m^* is the intra-aggregate void ratio at water ratio $e_w = 0$ and β is a microstructural parameter: both parameters depend on the specific surface of clay particles (Romero (2013)). Calibrated parameters for bare soil were $e_m^* = 0.25$ and $\beta = 0.24$: they are in good agreement with results showed by Romero (2013) for similar kind of soils.

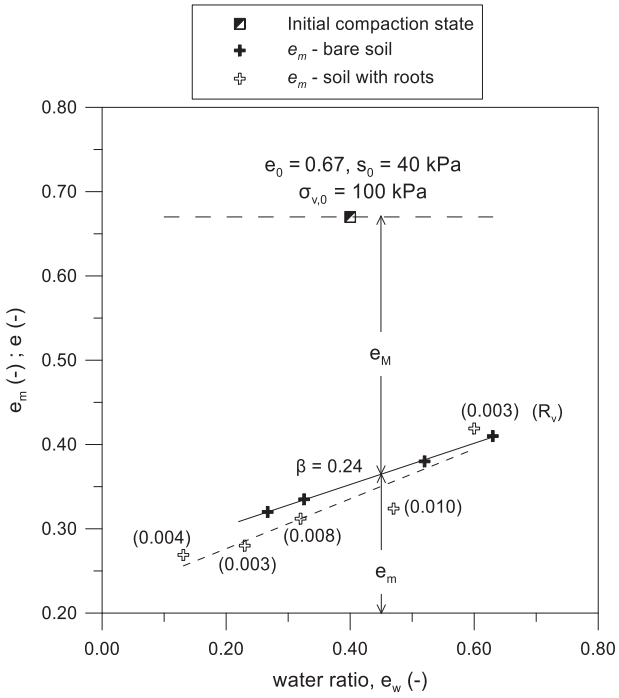

Figure 18 Inter-aggregate void ratio evolution with the water ratio, for bare and root-permeated specimens. Roots volume ratio is indicated for the correspondent vegetated samples.

The interpretation of the points for the root-permeated soil is more complex. Fissures volume is increasing, due to previously commented effects, during drying in the rooted soil: this is expressed by an increase of the macroscopic void ratio, e_M, with a consequent decrease of the intra-aggregate void ratio, e_m.

By looking at the root volume ratio values in correspondence of each sample, one can notice a good correlation with the macroscopic void ratio generated. WinRHIZO scans revealed that all the roots had very similar diameter distributions and lengths: in this case, the root volume ratio is directly proportional to the number of roots. Hence, the higher is the number of roots, the more significant is the volume of fissures generated upon drying. Moreover, the values of the root volume ratio evaluated within samples for microscopical investigations are comparable with those calculated within samples

for larger-scale tests. Hence, results obtained on soil structure can be directly used to predict and to justify the behaviour observed at the phenomenological scale.
In addition, the slope of the linear fitting curve of the root-permeated soil is steeper than the bare soil's one. This means that, apart from a natural shrinkage of the clay aggregates (intrinsic for a given material and for clay particles specific surface (Romero (2013)), the vegetated soil has a higher rate of reduction of micro-voids thanks to root mucilage production (a statistical analysis of this assumption will be provided in Section 3.3 of this thesis).

2.8 Micro and macroscale interactions

Pore-size distributions were used to evaluate soil water retention curves. Concerning the part of the PSD obtained by MIP, suction has been calculated from the mercury pressure values achieved for each intrusion step, according to Romero et al. (1999), assuming the mercury intrusion process (ruled by Wasburn equation) to be similar to air intrusion (Young-Laplace's equation). Concerning the part of the PSD obtained by X-ray microtomography, suction was deduced by the Young-Laplace's equation, considering that suction is generated only by capillary effects within this range of large porosities. The degree of saturation of the gas phase was calculated as the ratio between the cumulative void ratio at a given pore diameter and the total cumulative void ratio (Romero et al. (1999)). The water phase was calculated from the gas phase degree of saturation ($S_{r,g}+ S_{r,w} = 1$, where $S_{r,g}$ is the gas phase degree of saturation and $S_{r,w}$ is the water phase degree of saturation), and then the water ratio was calculated (Romero et al. (1999)). Results were plotted jointly with soil retention measurements (Figure 19): two curves coming from the bare and vegetated samples at a water ratio $e_w \approx 0.33$ ($e \approx 0.64$, $S_r \approx 0.52$, Figure 17d) and the other one from the vegetated sample at a water ratio $e_w \approx 0.60$ ($e \approx 0.67$, $S_r \approx 0.90$, Figure 17c).

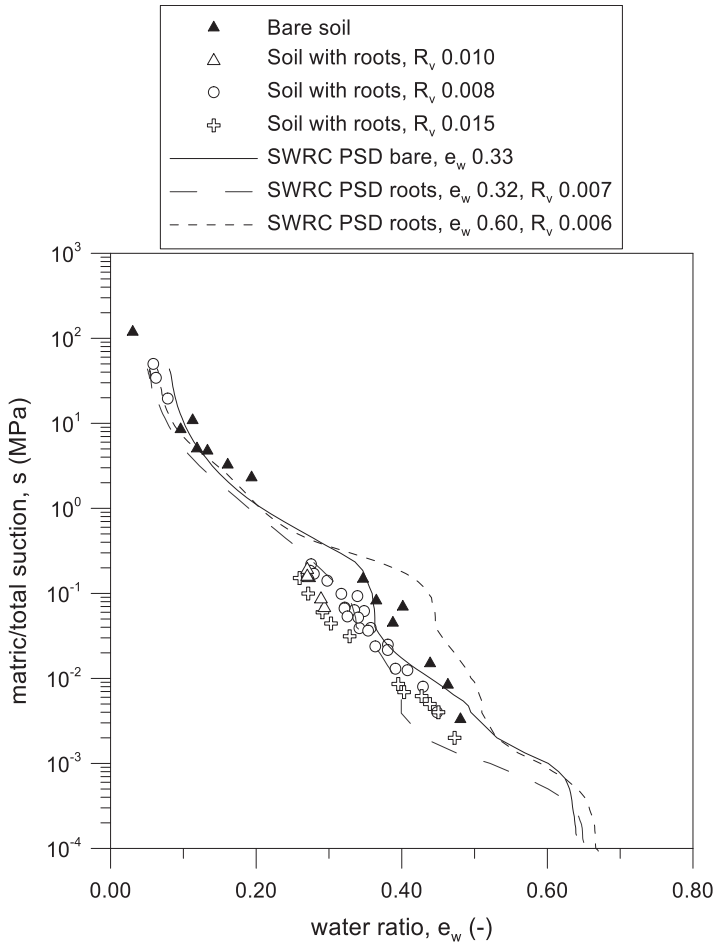

Figure 19 WRCs of bare and root permeated soil measured by tensiometer and psychrometer and calculated from pore-size distributions.

For the latter sample, the predicted air-entry value is close to the one calculated for the bare sample. The slope after the air-entry value becomes much smaller than the bare soil's one. As a consequence, in a range of suction, the predicted retention behaviour of a root-permeated soil would be above the bare soil (higher suction for a given water ratio). This is the retention curve that the vegetated soil would have if the soil structure were always the same along drying, starting from a saturated condition. Indeed, several authors observed similar trends in the retention curves of root-permeated soil (Ng et al. (2016); Garg et al. (2015)), for values of suction below 0.1 MPa.

Nevertheless, in this thesis, it was observed (Section 2.5.1) that, as the soil dried, its water retention properties became affected by the opening of fissures. This situation is clearly observed in the retention curve obtained from the PSD evaluated for the soil with roots at a water ratio equal to $e_w \approx 0.33$ ($e \approx 0.64$, $S_r \approx 0.52$, Figure 17d). Fissures

are dramatically affecting the air-entry value and the first part of the curve, which is characterised by a higher slope of the SWRC. Subsequently, the decrease in pores volume within the clay aggregates pores is progressively controlling the macroscopic behaviour by reducing the slope of the curve. This response could be linked again to chemo-physical modifications produced by roots exudates on the water contained in the soil. Indeed, it was observed that the surface tension of the liquid present within the rhizosphere is dramatically decreasing and its viscosity was increasing with respect to pure water at 20 °C (Read et al. (2003); Hinsinger et al. (2009); Carminati et al. (2017)). Finally, the curves converge in correspondence to 1 MPa of suction, which is representing what is being measured with tensiometers and psychrometers.

2.9 Concluding remarks

The hydro-mechanical behaviour of a root-permeated and compacted soil was investigated considering phenomenological and microstructural scales. The soil was seeded by *Cynodon dactilon,* at a fixed density of 34 g/m^2 and tested after 3 months of growth. Attention was paid to the initial soil state and stress and to the hydro-mechanical paths followed during the tests. Air-entry value, slope, saturated soil water permeability and shrinkage behaviour changed considerably between vegetated and fallow soil. The causes of these changes were assessed by investigating the effects of roots on soil microstructure. Two complementary techniques evidenced macro-pores volume increasing and micro-pores clogging, at different points of the same soil-root system. The two phenomena had consequences on soil hydro-mechanical behaviour. The former reduced soil air-entry value and increased its saturated permeability. The latter affected the retention curve at high suction ranges and the shrinkage behaviour. Root volume ratio was estimated by three techniques and used to correlate effects occurring at the different scales of the problem.

The information obtained in this study could provide the basis to build a constitutive framework able to predict soil hydro-mechanical behaviour starting from a given bare condition and considering plants features and physiology.

3. Hydro-mechanical framework to predict root effects on a compacted silty soil

3.1 Abstract

In this study, a hydro-mechanical multi-scale framework was built to predict the behaviour of a compacted silty soil penetrated by roots. The framework includes a model proposed to predict the evolution of soil microstructure along hydraulic paths and depending on roots geometrical features. The latter has been calibrated according to pore size distribution curves obtained from bare and vegetated samples, at different hydraulic states. Macroscopic volume change behaviour under hydro-mechanical paths was introduced into the framework and calibrated through shrinkage and oedometer tests. Finally, a soil water retention law for aggregated soils with double-porosity pore network was calibrated on bare soil data and used in conjunction with the rest of the framework to predict the vegetated soil hydro-mechanical response. Hence, the framework has been validated thanks to the prediction of three water retention curves and saturated permeability values obtained from vegetated soil samples. A statistical analysis quantified the good quality of the modelled results.

3.2 Introduction

The research aimed at producing predictive models on the influence of root geometrical and physiological traits on soil hydraulic behaviour is very recent (Wang et al. (2013) Leung, Garg and Ng (2015); Ng et al. (2016); Cao et al. (2018); Ni et al. (2019)). So far, engineering models predicting roots effects on soil hydro-mechanical behaviour have been often based on empirical correlations between macroscopic observations (air-entry value andretention capacity – saturated permeability changes), roots geometrical

features and soil initial compaction state (Ng et al. (2016); Ni et al. (2019)). These relationships were built deducing the possible causes (roots effects on soil microstructure, void ratio changes, soil fissuring, pores clogging, roots decay) from the phenomenological effects observed (water permeability/retention behaviour). Indeed, there are few studies on roots direct effects on soil fabric: among them, Scholl et al. (2014) deduced the effects of roots on the pore size distributions of a fine-grained soil by an inverse estimation, while Koebernick et al. (2017) performed high-resolution X-ray micro-tomography on loose silty sand, focusing on a single soil-root interface. The latter observed an occlusion of the soil pores with sizes between 5 and 300 μm due to root hairs but could not assess what was happening outside this range of pore sizes.

Models coming from agronomy, instead, are more focused on linking vegetated soil's hydraulic behaviour to chemical alterations induced by roots on soil structure (organic matter increase, water surface tension decrease) but neglecting the mechanical implications of roots growth (fissures/interfaces generation, soil grains displacement) (Ohu et al. (1987); Karup et al. (2017); Read et al. (2003)).

To unify the different fields of knowledge and the multi-physics processes involved in the problem, plants effects on the hydro-mechanical behaviour of a silty soil have been observed at different scales of behaviour and hydraulic states in Chapter 2. Important alterations in terms of water retention properties, permeability and shrinkage upon drying have been evidenced. The causes of these changes were clear after evaluating the soil multi-modal pore-size distribution, before and after roots growth. The use of complementary techniques (X-ray CT and MIP) allowed having an overview of the main phenomena observed within different porosity ranges: fissures generation due to roots growth and opening upon drying, micro-pores clogging by fine roots and released fluids (roots mucilage). For each sample, roots geometrical features (root volume ratio, root length density, tips number, diameter classes) have been identified.

Given these observations, a hydro-mechanical framework is proposed to predict the water retention curve and the soil water permeability of a vegetated silty soil, by considering microstructural changes induced by roots on soil. In the framework, a model in line to the one proposed by Romero et al. (2011) and formulated in equation (10) is adapted to predict the evolution of the micro- and macro-porosity along water content changes and to include dependence on the characteristics of the roots. The

adapted model was then included within a constitutive law for double-porosity soils (Dieudonné et al. (2013)). Observed soil volumetric strains due to mechanical stresses and suction variations are also considered through the laws proposed by Alonso et al. (1990). The model is calibrated with bare soil retention measurements and validated by predicting 56 retention measurements carried out on three vegetated samples and the soil water permeability measurements done on vegetated and bare soil.

3.3 Methods

The soil characteristics and the hydro-mechanical tests on which this Chapter is based were mainly presented in Chapter 2. Those tests are dealing with pore volume changes during suction changes, and under unconfined conditions (i.e. no vertical/lateral stresses applied on samples).

3.3.1 Oedometer tests

Tests presented in Chapter 2 will be complemented, in this Chapter, with oedometer tests carried out on one bare and one vegetated sample. Oedometer tests (ASTM D2435-M (2011)) are used to observe how pore volumes are varying when soil is submitted to vertical stresses, while remaining at constant water content. The samples were prepared and statically compacted in the oedometer cells resulting in a diameter of 150 mm and a height of 70 mm (Figure 20). Samples were compacted at a void ratio $e \approx 0.73$, water ratio $e_w \approx 0.40$, suction $s_0 \approx 40$ kPa and at a mean net stress $p''_0 \approx 25$ kPa (values representing initial state of the specimens in the campaign for soil hydraulic characterization). Roots were let to grow inside the soil after compaction and under saturated conditions. Compaction method and maximum vertical stress, hydraulic path, seeding density and root growing period within the samples were the same as discussed in Section 2.3. Vertical loading steps were of 10/20/40/90/130 kPa and unloading ones were of 90/50/10 kPa. Oedometer cells were closed for 6 hours to allow suction and water content equalisation within the specimen. Water content in samples was checked before and after tests with oven-drying method on two points of the samples' upper and lower surface (ASTM D2216 (2019)). Then, vertical loading steps were applied by a pneumatic actuator air cylinder. Vertical displacements of the specimen upper surface were registered by an LVDT with full scale of 10 mm and resolution of 0.002 mm. The

lower surface was in contact with the base of the cell: in this way, its downwards displacements were prevented. Moreover, lateral displacements in this kind of test were not allowed (ASTM D2435-M (2011)). At the end of the test, vegetated soil samples were washed with water using a sieve with mesh opening of 0.074 mm. Roots were retrieved and scanned to be recognised by WinRhizo (procedure detailed in Section 2.4.1).

Figure 20 Large size oedometer cell, with vegetated sample inside.

3.4 Micro-scale model formulation and calibration

The microstructural model is based on the soil pore-size distribution (PSD, example in Figure 21) described in Section 2.6.3 for bare and vegetated compacted soils. The intra-aggregates (or microstructural) void ratio e_m was calculated on the PSD curves as the cumulated void ratio below the pore size of 5 μm. A similar value for characterizing the clay aggregates was used by Romero (2013). The evolution of this microstructural variable with water ratio changes ($e_w = \rho_s w/\rho_w$) is presented in Figure 22. The evolution of the total void ratio, measured with paraffin tests in Section 2.5.2, was also shown in the same figure. The total (e) and the intra-aggregates (e_m) void ratio are linked by the equation:

$$e = e_m + e_M \tag{11}$$

where e_M is the inter-aggregates (or macrostructural) void ratio. Close to each vegetated e_m point, the value of root length density, R_{ld} (ratio between the total root length and the bulk soil volume), is indicated as a label.

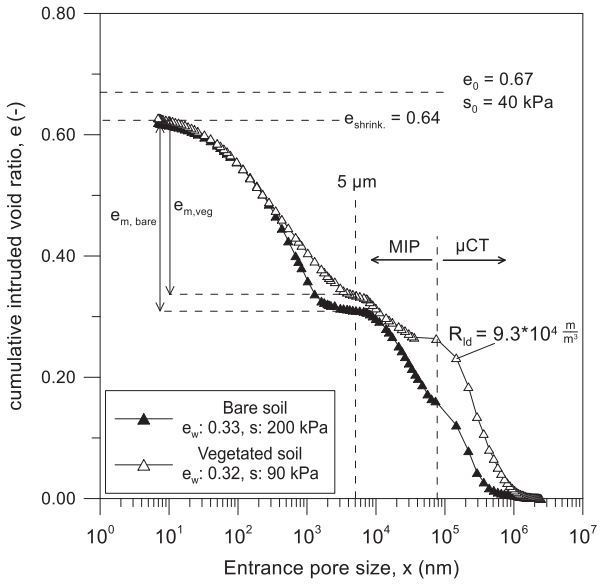

Figure 21 Comparison of PSDs of bare and root-penetrated soils at given water ratio. Root length density within the vegetated soil is indicated in the graph. Data from Chapter 2.

This parameter was evaluated by scanning the washed roots with the software WinRHIZO (see Section 2.4.2 for further details). Its value within the different samples is summarised in Table 7, jointly with other root features (samples: *veg1* to *veg5*). For the vegetated soil points (Figure 22), an increase of the macrostructural void ratio and a decrease in the intra-aggregate values was observed during drying. To express this reduction, the law proposed by Romero et al. (2011), previously indicated in equation 10 was adapted as follows:

$$e_m = e_m^* + (\beta + \gamma)e_w - \alpha R_{ld} \qquad (12)$$

in which γ and αR_{ld} are parameters added to the original model. The product αR_{ld} is indicating the quantity of macropores generated by a given root quantity. The parameter γ controls the coupled effects of roots presence and water ratio variations (i.e. soil fissures opening due to soil and roots shrinkage and clogging due to roots swelling on wetting (phenomenon observed by Carminati et al. (2013)), as well as the evolution of micropores during drying and due to chemical activities. The parameter γ is added to β, which is the slope of the microstructural evolution with water ratio. According to Romero (2013), β depends on the total specific surface of the different clays. The parameters α and γ were calibrated by minimizing the mean squared error between measurements and predictions of e_m with equation 12 ($R^2 = 0.96$): their values are $7 \cdot 10^{-7}$ m^3/m and 0.030, respectively. A good correlation ($R^2 = 0.95$) was also found

expressing the model as a function of the root volume ratio, R_v, which is the ratio between roots total volume and bulk soil volume:

$$e_m = e_m^* + (\beta + \gamma^*)e_w - \alpha^* R_v \quad (13)$$

New calibrated values for α^* and γ* were 2.2 and 0.028 respectively. The reason for the two formulations is the fact that R_{ld} could make it easier to extend the model to other types of plants. In contrast, R_v is more easily measurable in field applications involving plants with similar characteristics to those studied.

Table 7 Root parameters found with WinRhizo scans (mean, variance and peak root diameters were evaluated as parameters of a gamma distribution of probability).

sample name	**testing soil water ratio (-)**	**R_{ld} root length density (m/m^3)**	**R_v root volume ratio (m^3/m^3)**	**mean root diameter (mm)**	**peak root diameter (mm)**	**soil bulk volume (mm^3)**	**tips density (n.tips/ mm^3)**
veg1	0.23	$5.0 \cdot 10^4$	0.003	0.41 (σ^2 = 0.04)	0.31	$8.36\ 10^4$	0.04
veg2	0.13	$4.6\ 10^4$	0.004	0.38 (σ^2 = 0.03)	0.30	$3.50\ 10^4$	0.04
veg3	0.32	$9.3\ 10^4$	0.008	0.44 (σ^2 = 0.05)	0.32	$8.0\ 10^4$	0.07
veg4	0.60	$4.0\ 10^4$	0.003	0.42 (σ^2 = 0.01)	0.40	$1.49\ 10^5$	0.02
veg5	0.47	$8.1\ 10^4$	0.010	0.47 (σ^2 = 0.07)	0.32	$1.25\ 10^5$	0.08
oed1R	0.60	$4.7\ 10^4$	0.010	0.44 (σ^2 = 0.04)	0.35	$1.24\ 10^6$	0.02
oed2R	0.32	$1.1\ 10^5$	0.014	0.31 (σ^2 = 0.02)	0.25	$1.24\ 10^6$	0.04
perm1R	0.60	$3.5\ 10^4$	0.007	0.39 (σ^2 = 0.05)	0.25	$1.47\ 10^6$	0.04
sample6	0.28-0.60	$7.6\ 10^4$	0.010	0.41 (σ^2 = 0.06)	0.25	$1.24\ 10^6$	0.04
sample13	0.08-0.60	$5.0\ 10^4$	0.008	0.34 (σ^2 = 0.03)	0.24	$1.24\ 10^6$	0.01
sample 17	0.28-0.60	1.710^5	0.015	0.30 (σ^2 = 0.002)	0.29	$1.24\ 10^6$	0.03

The use of the root length density (R_{ld}) comes from the assumption that soil fissuring is occurring at the soil-root interface and that fissures volume is depending mainly on the length of the interface rather than on other roots properties (such as diameter). For reasons of brevity, the rest of the study will be presented in terms of R_{ld}, however, the same results have been obtained in terms of R_v.

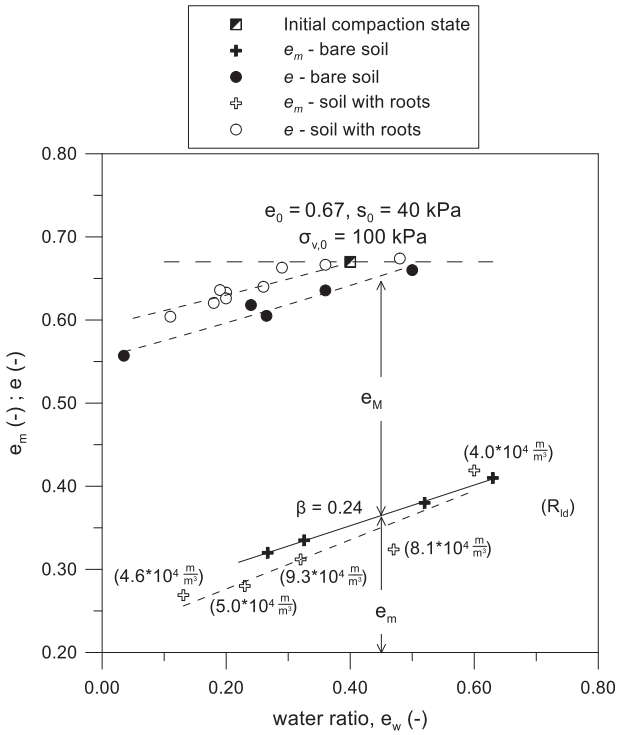

Figure 22 Microscopic and total void ratio evolutions with water ratio during a drying path. Root length density values are plotted jointly to their relative points. Data from Chapter 2.

3.5 Macroscopic hydro-mechanical framework

3.5.1 Oedometer test results

Once the microstructural void ratio law is formalised, it is necessary to introduce the equations describing the macroscopic volumetric deformations, to fully characterize the state and stress (e, e_m, s, e_w, p) evolution along hydro-mechanical paths. In this regard, paraffin (Section 2.5.2) and oedometer (Section 3.3.1) tests were carried out on the bare and root-permeated soil.

One large oedometer test with and one without roots are presented in Figure 23. The tests were carried out at a constant water ratio $e_w \approx 0.32$ ($S_r \approx 0.44$). Initial suction was 190 kPa and 150 kPa in the bare and root-permeated sample, respectively. Root length

density (evaluated by WinRhizo, Section 2.4.1) of the tested sample is shown in Figure 23 (other roots features are presented in Table 7 - sample *oed2R*). The yield stress in the vegetated sample appeared lower than that of bare soil, probably due to the collapse of the fissures generated by roots. Nevertheless, the vegetated soil exhibited a higher stiffness than the bare one, particularly in the virgin part of the curve.

Elastic and total volume strains upon loading were interpreted according to Alonso et al. (1990):

$$d\varepsilon_{vp}{}^{el} = \frac{\kappa}{(1+e)}\frac{dp''}{p''}, p'' < p''_0 \quad (14)$$

$$d\varepsilon_{vp} = \frac{\lambda(s)}{(1+e)}\frac{dp''_0}{p''_0}, p'' > p''_0 \quad (15)$$

Where κ and $\lambda(s)$ are the soil stiffness against changes in net mean stress in elastic and virgin states, respectively. Calibrated values are summarised in Table 8.

Table 8 Soil stiffness parameters calibrated for the laws formalized by Alonso et al. (1990). κ_s *and* λ_s *calibrated from paraffin tests detailed in Section 2.5.2*

	Bare soil	**Soil with roots**
κ	0.0063	0.005
λ	0.065	0.026
κ_s	0.0015	0.001
λ_s	0.011	0.009

As observed in Figure 23, the equations are well representing the test results. The oedometer tests results were predicted considering suction variations, according equations (6) and (7), within the samples due to volumetric deformations at constant water ratio: indeed, the void ratio is decreasing, saturation degree is increasing, and consequently suction is decreasing during loading.

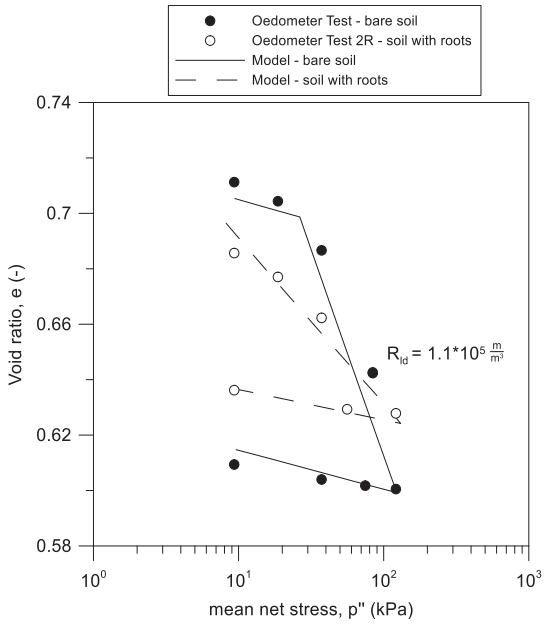

Figure 23 Oedometer tests carried out at constant water content with and without roots. Measurements and hydro-mechanical modelling.

3.5.2 Macroscopic framework development

So far, in the thesis, some components of the framework have been explained: a law describing the intra-aggregate void ratio evolution with water ratio and root length density (equation (12 detailed in Section 3.4) and a macroscopic framework in which the total void ratio evolution is described as a function of suction and loading (equations (6),(7) and (14),(15)). The last component of the framework is a law to predict the water retention behaviour in a double porosity soil (Dieudonné et al. (2013)). This law is based on the assumption that the water retention response of soil within the intra-aggregate's space can be superimposed to the retention response of the inter-aggregate's structural level (Dieudonné et al. (2013)). This assumption is represented by the equation that links water ratio values that fill micro- and macro-pores to suction, given by Dieudonné et al. (2013):

$$e_w(s) = e_{wm} + e_{wM}$$
$$= e_m \left[1 + \left(\frac{s}{s_0^{(m)}}\right)^{n^{(m)}}\right]^{-m^{(m)}} + (e - e_m)\left[1 + \left(\frac{s}{s_0^{(M)}}\right)^{n^{(M)}}\right]^{-m^{(M)}} \quad (16)$$

It is worth remarking that the two structural levels are expressed separately with a van Genuchten (1980) retention curve. The quantities e_{wm} and e_{wM} are indicating the water

ratio in the micro- and in the macro-pores, respectively. e_m is the micro-pore void ratio, whose evolution as a function of the water ratio has been formalized in equation (10) and equation (12) (for vegetated soil). $(e - e_m)$ is the difference between the total void ratio and the micro-pore void ratio, which corresponds to e_M according to equation 11 Suction is expressed by s while n and m are model parameters, differentiated for the micro- and the macro-structures by the lowercase and uppercase exponent ((m) or (M), respectively). Finally, s_0 is associated with the air-entry suction, and is expressed by the equations given by Dieudonné et al. (2013):

$$s_0^{(m)} = \alpha_1^{(m)} \exp\left(-\alpha_2^{(m)} e_m\right) \quad (17)$$

$$s_0^{(M)} = \alpha_1^{(M)} \exp\left(-\alpha_2^{(M)} \frac{e - e_m}{e}\right) \quad (18)$$

where α_1 and α_2 are model parameters.

The macrostructural and microstructural parameters of the retention curve just detailed have been calibrated on bare soil retention measurements, as showed by the algorithm in Figure 24.

Void ratio at saturation was assumed as e = 0.67 (p'' ≈ 90 kPa). For each suction value (s), inputs of the i-steps iterative process are the mean net stress (p''), the water ratio (e_w) measured for the bare soil in the Chapter 2, and a tentative void ratio (e_i). The variables $e_{w,m}$ and $e_{w,M}$ are the water ratios within the micro- and the macro-voids, respectively. Suction changes along drying were used to compute volumetric strains according to equations (6) and (7). Iterations continued until void/water ratios predicted were in good agreement with the tentative/measured ones. The convergence parameters (errors on predicted void ratio and water ratio) ε_e and ε_{ew} were equal to 0.001. The calibrated parameters of the retention curve (Dieudonné et al. (2013)) are summarised in Table 9.

Macroscopic volumetric strains expressed by equations (6) and (7) are not dependent directly on the PSD of the material. The evolution of microstructural and macrostructural void ratio is evaluated at each hydraulic state and loading step assuming that intra-aggregates void ratio depends only on the water content and is not affected by total void ratio changes (Romero (2013)).

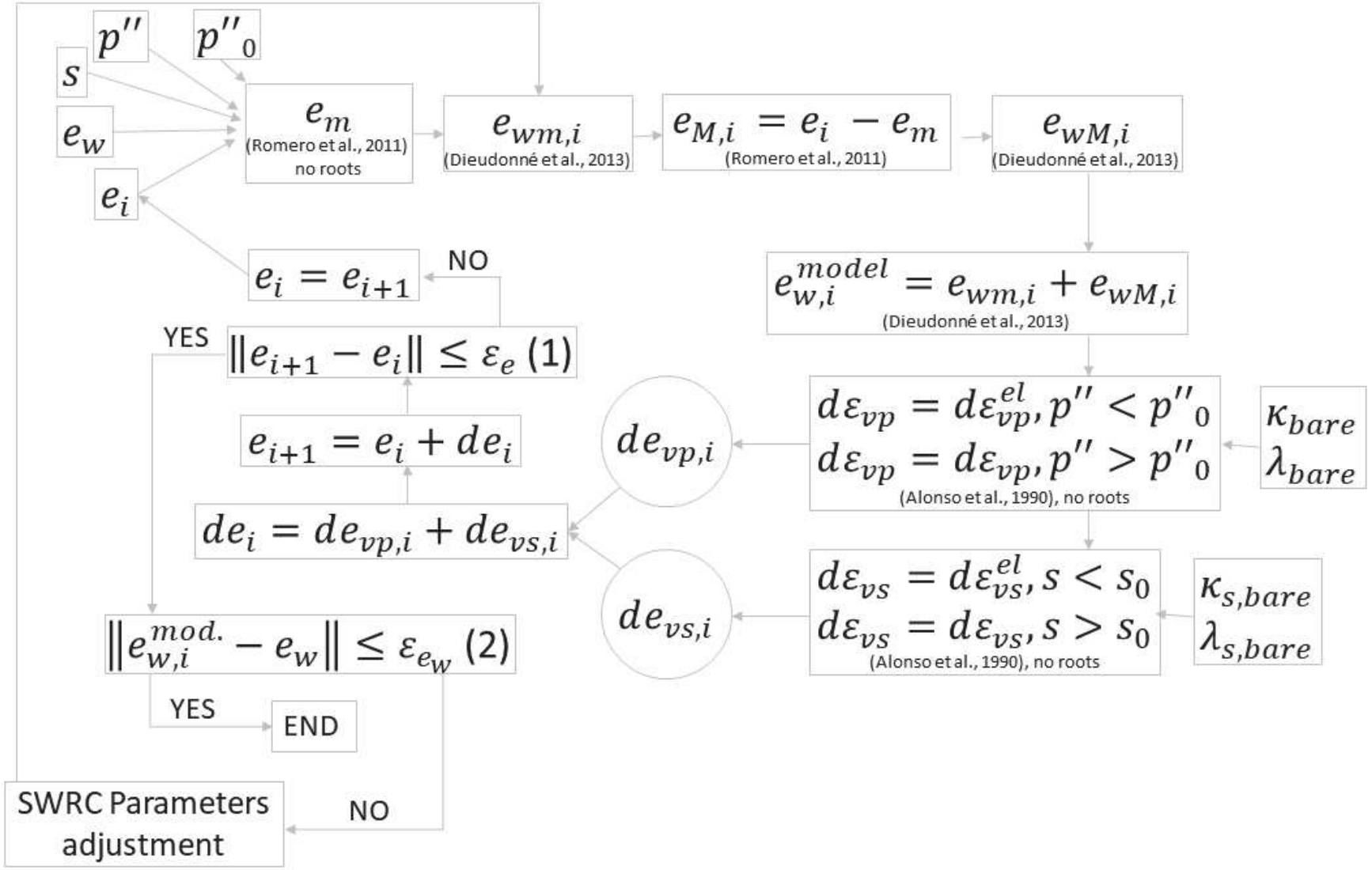

Figure 24 Algorithm used for the calibration of the SWRC parameters through the hydro-mechanical framework and using the bare soil measurements

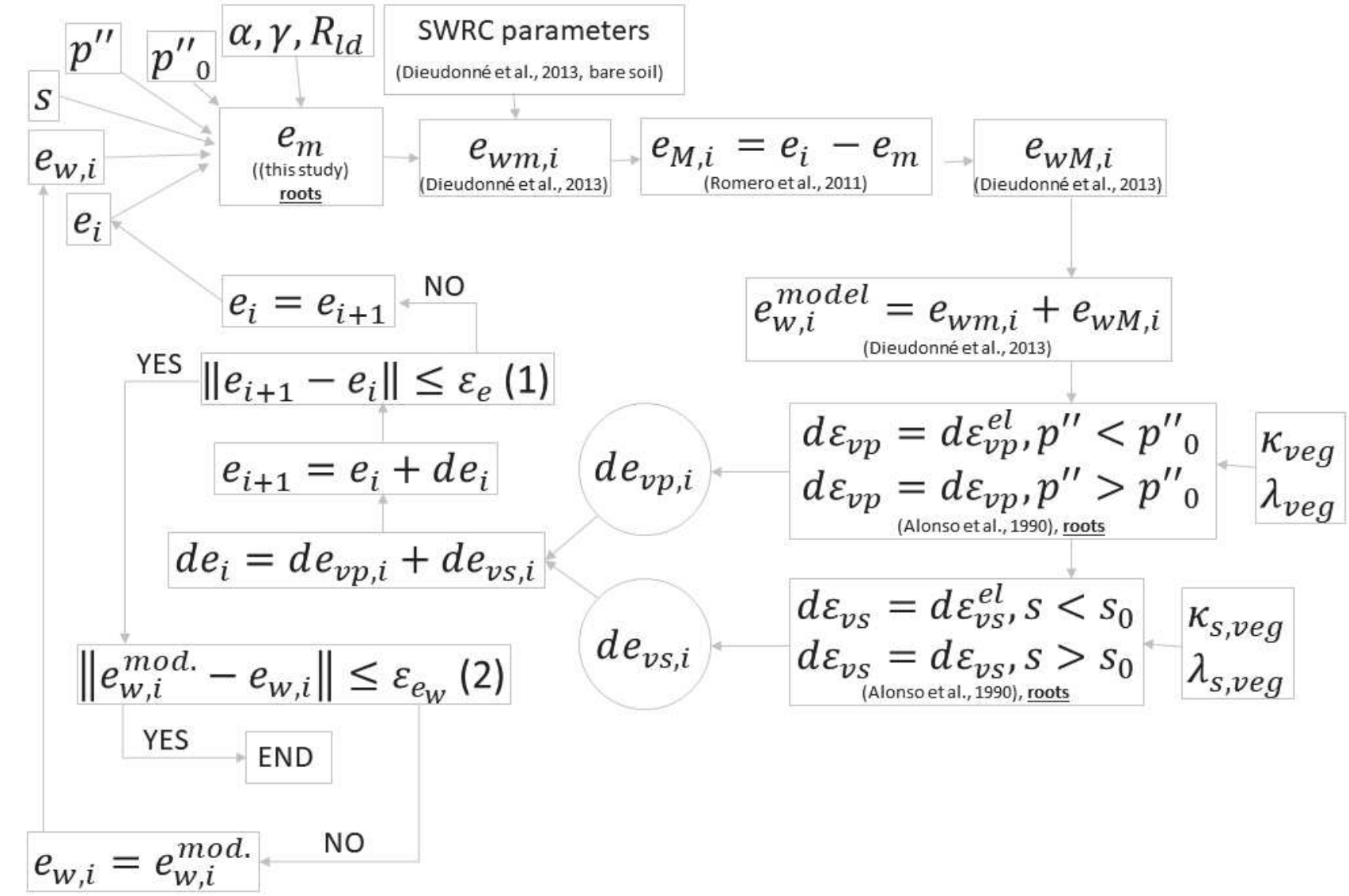

Figure 25 Algorithm for predicting the SWRC curve for the vegetated soil through the hydro-mechanical framework.

Table 9 Parameters calibrated for the double-porosity SWRC law formalized by Dieudonné et al. (2013). *Calibration from bare soil retention measurements.*

$\alpha_1^{(m)}$ (MPa)	$\alpha_2^{(m)}$ (-)	$n^{(m)}$ (-)	$m^{(m)}$ (-)	$\alpha_1^{(M)}$ (-)	$\alpha_2^{(M)}$ (MPa)	$n^{(m)}$ (-)	$m^{(M)}$ (-)
10^{-1}	10^{-10}	5.92 10	4.23 10^{-3}	7.38 10^{-4}	7.88 10^{-3}	3.23 10	1.36 10^{-1}

3.6 Model validation and performance

Once the retention curve parameters have been calibrated, they were used to predict the behaviour of a soil presenting a given root length density (*samples 6-13-17* in Table 7). Equation 12 was used in the framework (algorithm in Figure 25) to predict the micro-structural void ratio (e_m) evolution. The parameters calibrated by shrinkage and oedometer tests for the vegetated soil were used in equations (6) ,(7), (14) and (15) to predict volumetric strains due to loads and drying. Iterations lasted until water and void ratios predicted were in good agreement with the tentative initial values, for given suction *s* (Figure 25). The curves predicted by the hydro-mechanical framework, for the bare and for a vegetated sample, are shown in Figure 26, jointly with the points measured in Chapter 2.

The drying behaviour was reproduced by assuming elastic volumetric deformations below suctions of 40 kPa and elasto-plastic strains above (as described in Alonso et al. (1990)). The wetting phase was reproduced by equation (6) in the framework, assuming a purely elastic strain behaviour, (s_0 moved to 100 MPa consequently to drying, as indicated by the suction increase yield surface in Alonso et al. (1990)). On wetting, the vegetated soil recovers higher water ratios than the bare soil. This is because vegetated soil had remained at higher void ratios than those of bare soil, during the drying/wetting path, as observed experimentally in Figure 12.

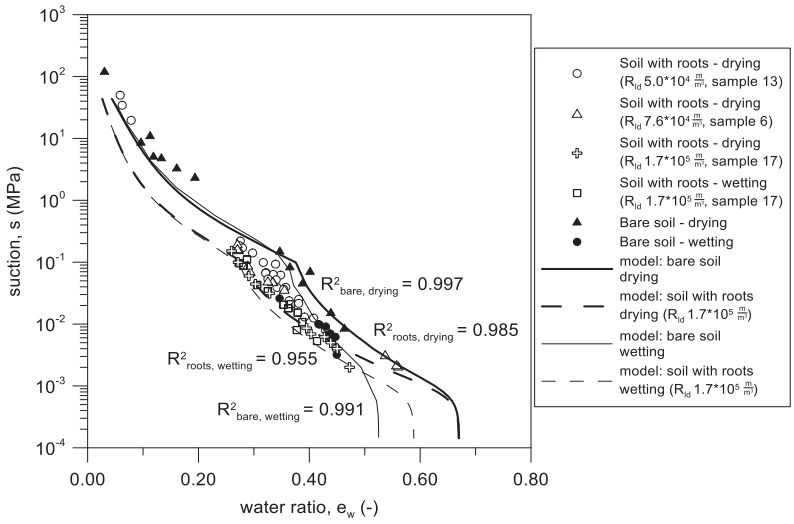

Figure 26 Modelled soil water retention curves on drying and wetting. Measurements from Chapter 2.

A good agreement between the retention model and measurements is evident in Figure 26. For the remaining samples, their retention curves were also modelled by introducing the corresponding value of R_{ld} in the algorithm. The coefficients of determination (R^2) were calculated considering the different measurements obtained for the three vegetated samples and the bare soil tested (Table 10). Each measurement is a couple of water ratio e_w and suction, s; and the number of measurements, for each couple, is indicated in Table 10. The coefficient of determination slightly decreases as the R_{ld} increases. This may be due to several variables that need further investigation. The framework might have overestimated the fissures volume when dealing with high values of root length density, since it is not considering possible "group effects" of roots, depending on their different architecture. Indeed, the same length density can produce different volumes of fissures, if roots are more sorted or spaced. Also, the model is not considering the root diameters distribution, which may have a role in the generation of fissures. Nevertheless, the model is capable of predicting well the behaviour of a vegetated soil in a large range of root length density values. Further investigations are needed to find a dependency of α and γ on the other abovementioned root features.

The framework also predicts changes in the retention properties due to confinement stress changes, according to the algorithm in Figure 25. As an example, bare and vegetated soil retention curves are compared when loading from $\sigma_{v,0} \approx 100$ kPa (which is the stress at which samples for retention measurements were compacted) to $\sigma_{v,0} \approx 730$

kPa. The lower compressibility showed by the vegetated soil allows it keeping a higher porosity and then, to develop higher water ratios at saturation (Figure 27).

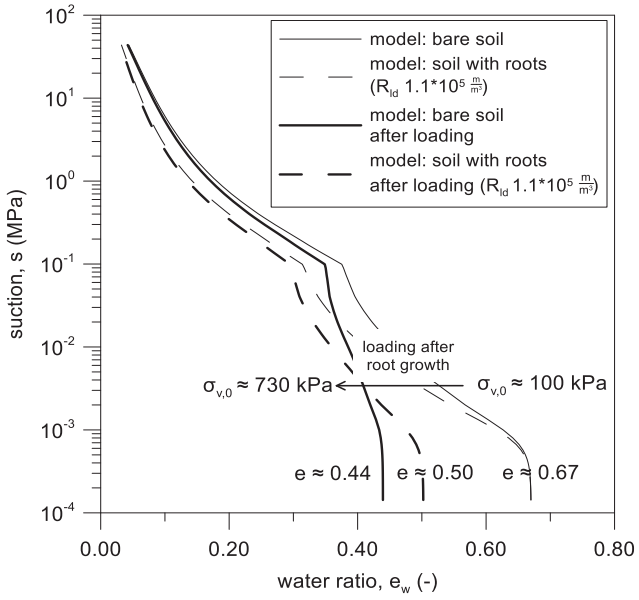

Figure 27 Prediction of bare and vegetated swrc before and after loading.

The micro-scale model (equation 12) was also used to predict measurements of permeability carried out in Chapter 2 and by Oorthuis et al. (2018) (Figure 28a).

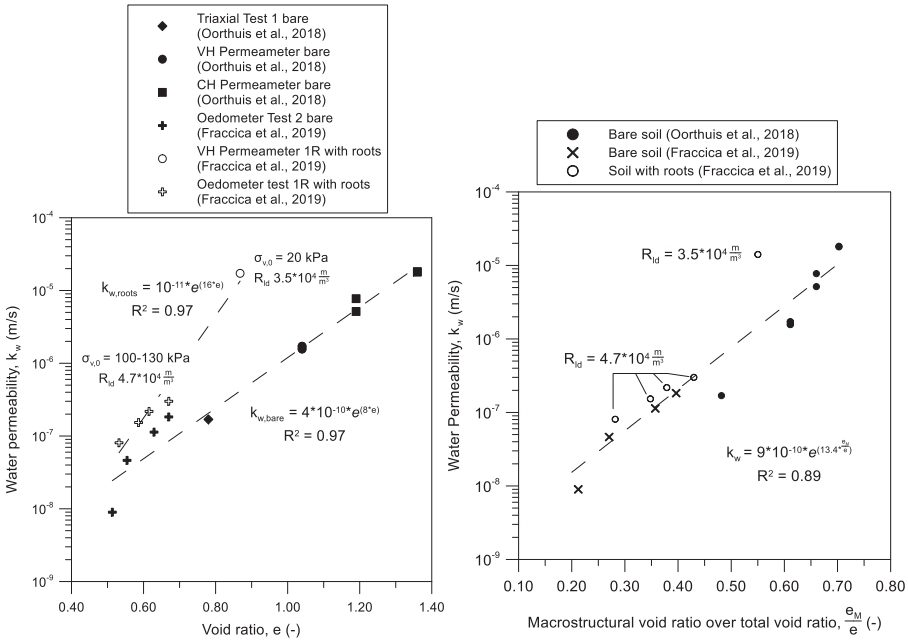

Figure 28 Soil water permeability of bare and root-permeated soil as a function of a) the void ratio and b) the degree of macro-pores. For the vegetated soil, the degree of macro-pores was calculated considering the measured root length density and the void ratio at compaction.

The macropore volume was evaluated for the samples in which permeability was measured, knowing their root length density (samples *oed1R* and *perm1R* in Table 7). Soil water permeability was plotted as a function of the ratio between the macrostructural and the total void ratio. The quantity of macropores as a fraction of the total volume of voids has a direct influence on soil permeability. As it can be seen in Figure 28b, the results obtained by an oedometer test with roots done under saturated conditions (*oed1R*) are well aligned with the bare measurements. The point representing the permeability measured by the permeameter (*perm1R*) is the most far from the tendency, presenting a higher value with respect to those predicted. This case is evidencing another limitation of the model: the equation developed, in fact, is not considering the number of different roots within the samples. This last feature is linked to the *tips density*, which is given by the ratio between the number of root tips and the soil bulk volume (see Table 7). Given the same root length density, the different number of roots developed may affect the total volume of fissures generated within the soil. Indeed, considering Table 7 and Figure 28a, one can note that, even if permeameter test 1R and oedometer test 1R have a similar root length density and volume ratio, the *tips density* in the permeameter test 1R is two times higher than the other test. Finally, the model does not even include the effect of the initial void ratio (higher in the permeameter) on plants development and growth.

Table 10 Root length density, coefficients of determinations and number of measurements of each modelled SWRC.

swrc	**R_{ld} (m/m^3)**	**R^2 (model/measurements)**	**n. of measurements**
bare drying	-	0.996	14
bare wetting	-	0.991	7
sample 13 (roots) drying	$5.0\ 10^4$	0.996	18
sample 6 (roots) drying	$7.6\ 10^4$	0.989	11
sample 17 (roots) drying	$1.7\ 10^5$	0.985	15
sample 17 (roots) wetting	$1.7\ 10^5$	0.955	12

The lower confinement imposed by the soil to plant roots may have amplified the phenomenon of fissuring with respect to what it is happening in more compacted soils.

3.7 Conclusions

Information about soil microstructure and root properties have been used to develop a model able to predict the macro- and micro-pores volume generated by a specific root quantity. The parameters calibrated are controlling soil-root chemo-hydro-mechanical interactions, and they are dependent on the type and the architecture of roots and the soil type. Observations at the specimen scale (shrinkage and loading) made it possible to develop a hydro-mechanical framework to predict soil volumetric strains. A double-porosity model for soil water retention curve was coupled to the microstructural vegetated model proposed in the study and to the macroscopic framework. The parameters for the retention curve were calibrated on the bare soil measurements and used to predict the behaviour of the soil with roots. The introduction of laws defining soil yielding upon suction and loading changes allowed predicting both drying and wetting retention curves. Soil behaviour was also simulated after a particular loading stage, evidencing different tendencies with respect to what observed at lower confinement. Macropores increase predicted by the new model allowed explaining the increase in permeability observed in the vegetated samples. The model predicts well the behaviour of a silty soil penetrated by roots and it can be easily extended to other types of soils and plants.

.

4. Mechanical behaviour of a vegetated soil at different hydraulic states

4.1 Abstract

The objective of this study is to assess the effects of *Cynodon dactilon* roots on the shear and tensile strength of a compacted silty soil, under different hydraulic states and after different plants growing periods. Triaxial compressions were carried out within large cell equipment to evaluate the shear strength increase and the volumetric deformations induced by roots. A new equipment was developed to evaluate soil tensile resistance by pulling at constant water content.

Soil shear and tensile resistance increased with suction, jointly with an accentuation of its brittle behaviour. Vegetated soil presented a greater resistance and two different stress-displacement responses, depending on whether it was dry or moist. Moreover, roots growing periods had an impact on the results.

Roots affected both soil friction angle and cohesion. Results were interpreted according to two constitutive laws for partially saturated soils and considering soil suction, degree of saturation and roots geometrical and mechanical features. Finally, a correlation was found between the increase in shear strength, roots properties and soil hydraulic state.

4.2 Introduction

Global warming has led to longer periods of drought and heavier rainfalls. These events are particularly damaging in fine-grained soils: dyring and wetting cycles generate fissures and alter their hydro-mechanical and structural properties (Albrecht and Benson (2001); Cordero et al. (2017)). This affects the behaviour of slopes and embankments made with those kind of soils, causing a faster response to rainfall, affecting their

behaviour at the service state and producing phenomena of shallow or deep instability (Vardon (2014); Sánchez et al. (2014)). In the framework of sustainable engineering it is important to understand which is the role of vegetation in preventing such detrimental effects on the response of geotechnical structures (Oorthuis et al. (2018)). Plant roots contribute to enhance soil shear resistance thanks to their tensile strength (Wu et al. (1979); Mickovski et al. (2009); Preti and Giadrossich (2009)). So far, the most commonly used laboratory test to quantify this reinforcement is the direct shear one (Gonzalez-Ollauri and Mickovski (2017); Ghestem et al. (2014); Yildiz et al. (2018); Veylon et al. (2015); Mickovski et al. (2009)). Gonzalez-Ollauri and Mickovski (2017) carried out direct shear tests on partially saturated vegetated soils, finding out that root effectiveness in reinforcing the soil was strongly coupled to soil suction. Standard triaxial equipment was also used to test vegetated soil (Zhang et al. (2010); Ji (2019)).
Few knowledge has been provided so far on the volumetric deformations upon shearing occurring in vegetated soils (Yildiz et al. (2018)). Moreover, there are still few insights on how soil micro-structural changes generated by roots growth could affect the overall mechanical behaviour.
To the author's best knowledge, vegetated soils haven't been tested under tension: the soil behaviour following such stress path has an impact on the tensile cracks formation under drying/wetting cycles. Few examples of bare soil tensile strength assessment were provided in literature (Lakshmikantha et al. (2012); Murray and Tarantino (2019)). The former observed a peak and a subsequent decrease of tensile strength in the material, below a certain value of degree of saturation: this was due to a decrease of the number of capillary bridges inside the soil despite an increase in suction. Divya et al. (2014) and Trabelsi et al. (2018) performed tensile tests on soil reinforced by natural fibres manually distributed within the matrix.
Attention has to be paid to roots' features when interpreting geotechnical tests including them. The first analytical model to correlate the increase in soil cohesion to typical plant parameters is the model given by Wu et al. (1979): it was calibrated from in situ large direct shear tests, root diameter measurements in escarpment areas of landslides, tensile tests on singular roots and back-analysis. In this model it is assumed that all roots fail at the same time: this prediction is unlikely to happen, since it is known that not all soil roots are equal and that their resistance varies according to their diameter and the rupture

mechanism due to their spatial arrangement in the soil. Nevertheless, the use of the plant traits included in this model (roots tensile strength and area), was proved to give good predictions of the results, in more recent investigations (Mickovski et al. (2009)).

Roots reinforcement also depends on soil hydraulic conditions: Pollen (2007) observed that in a wet soil the roots have a greater tendency to be extracted by sliding (pull-out) while they fail by breakage, in a drier soil. Schwarz et al. (2010) confirmed the importance of suction and water content in modelling roots reinforcement in soil. Mickovski et al. (2007), performed pull-out tests on model roots included in soils at different water contents (a totally dry and a partially saturated sand), performing Particle Image Velocimetry on roots, by means of a transparent wall. The macroscopic behaviour observed, in terms of force-displacement, was that the roots included in the totally dry sand were extracted in a "ductile" way, after large displacements whereas roots embedded in a partially saturated sand showed a more brittle behaviour, with a sharp drop in the pull-out force, as showed in Figure 29a. The authors observed, by means of evaluating the velocity fields within roots, two different mechanisms of root failure: roots in dry sand were slipping-out the soil, mobilizing also lateral deep roots (Figure 29 b), whereas roots in partially saturated sand broke after reaching their tensile strength and without mobilizing the deep lateral roots (Figure 29 c). The authors attribute the latter behaviour to the fact that the effective stresses in the soil have increased, thanks to the suction developed in the soil. Moreover, as soon as the soil dries, it shrinks around the roots, holding them tighter.

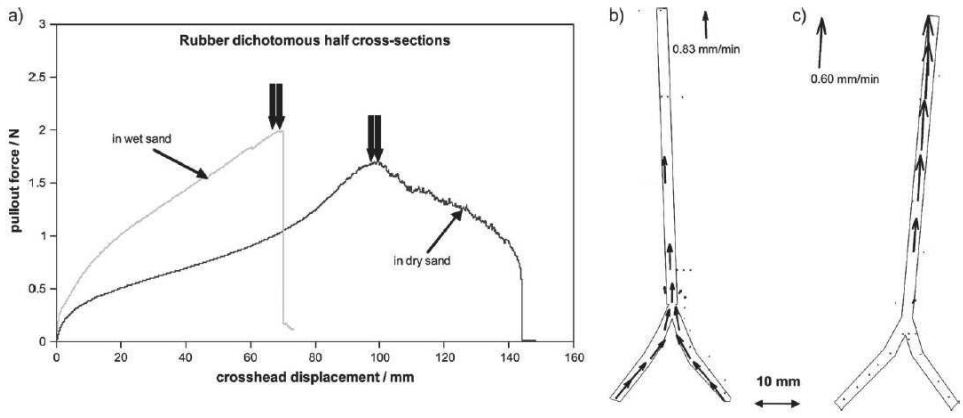

Figure 29 a) Pull-out behaviour of model roots in a partially saturated and in a dry sand, in terms of force-displacements. Velocity fields for roots in a dry sand (b) and in a partially saturated sand (c)(from Mickovski et al. (2007))

The objectives to be achieved in this Chapter are: to undersand which is the effect of vegetation on the shear and tensile strength of a silty sand lightly compacted, to characterise the roots' geometrical and mechanical features that most affect soil's behaviour and to implement those features within a constitutive law for partially saturated soils. The aim is to produce a model to predict the soil shear strength increase due to vegetation.

4.3 Soil properties and compaction

The laboratory characterization of the material retrieved in situ is presented in Figure 30 and Table 11. The soil was sieved at 4.76 mm (ASTM E11 (2017)). By means of the grain-size distribution it has also been possible to estimate the average diameter of pores in the soil as:

$$d_{pores,aver.} = 0.3 * d_{50,solids} \tag{19}$$

where $d_{50,solids}$ is the solid particle size corresponding to 50% of soil passing fraction. According to this formula, the average pore size is 0.10 mm. This implies that it is likely that roots larger than this diameter will create fissures in the material during their growth.

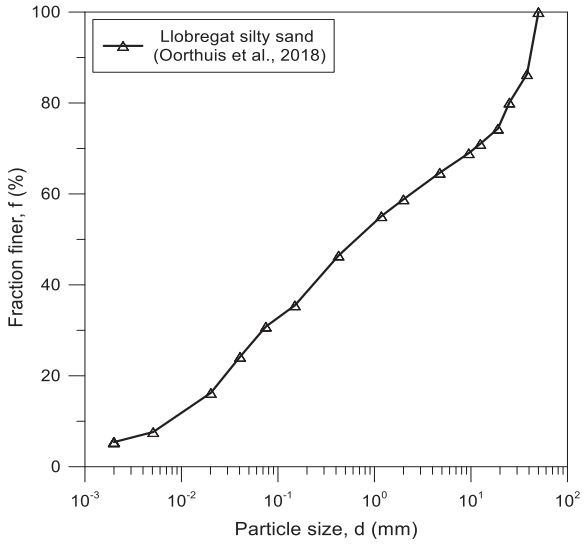

Figure 30 Particle size distribution of non-sieved soil (Oorthuis et al., 2018) and sieved soil for the laboratory study (in Fraccica et al. (2019)).

Table 11 Soil properties - a(Oorthuis et al., 2018) b(Fraccica et al., 2019).

Soil property	*Value*
Soil fraction < 2 mm (%)	58.8[b]
Soil fraction < 75 μm (%)	30.8[b]
Soil fraction < 2 μm (%)	5.4[b]
Liquid limit (%)	29.5-34.4[a]
Plasticity index (%)	9.6-13.5[a]
Density of solids, ρ_s (Mg/m^3)	2.65-2.70[a]
Hydraulic conductivity (m/s)	$7.7*10^{-8} – 1.8*10^{-7}$ [a]

Samples were statically compacted ($\sigma_{v,max} \approx 100$ kPa) at the dry side of the optimum, as indicated by the point A in Figure 31, obtaining a void ratio, $e \approx 0.67$ at a water content $w \approx 15\%$. After compaction, the soil was wetted under unconfined conditions up to a suction equal to 1 kPa (corresponding to a water content $w \approx 21\%$), monitored by tensiometer, to allow plants growth. In fact, the process of germination and growth of the plants was carried out entirely in correspondence with the state characterized by the letter B in the Figure 31. Samples were then left to dry to be tested under triaxial compression or tensile tests at different water contents (points between B and C, Figure 31). Drying was carried out in a controlled temperature/relative humidity room (T = 20 ± 1 °C, RH = 50%). Bare samples were subjected to the same compaction and hydraulic trajectory.

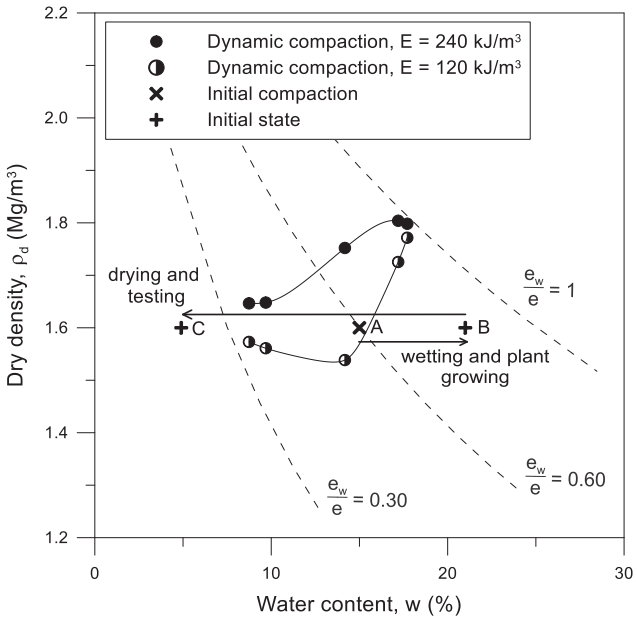

Figure 31 Dry density – water content plot. Compaction and hydraulic path followed in this study.

Samples for direct tensile tests were prepared in ABS 3D-printed moulds (Φ 100 mm and h 40 mm) are indicated in Figure 32. Samples for triaxial compression tests were compacted in PVC moulds (represented in Figure 33) (Φ 200 mm and h 400 mm).

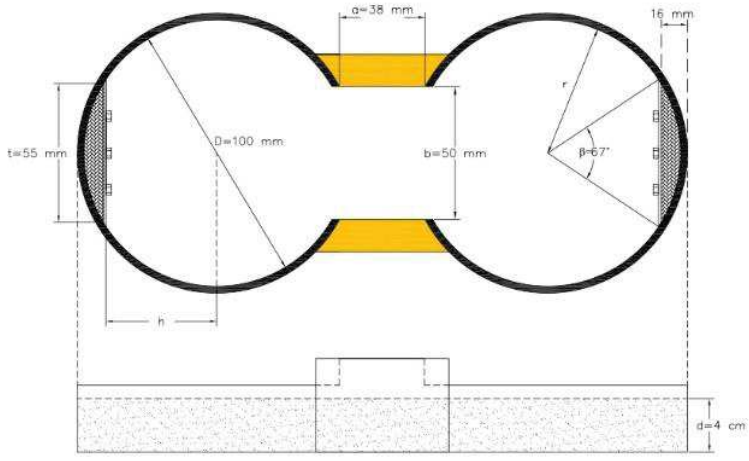

Figure 32 Moulds for direct tensile and shrinkage tests

4.4 Roots growth and characterization

The growth of plants took place inside the moulds (Figure 33), after soil compaction. The seeds of the plants are inserted into the soil through holes spaced 30 mm apart generated with a mini soil corer and with a seeding density of 34 g/m^2.

Figure 33 Plants seeding in 40 mm spaced holes and after 3-months growth in moulds for triaxial and direct tensile tests

Plants in triaxial tests samples were left to grow for 8 months while, in direct tensile moulds, growth period varied from 1 to 3 months. This choice aimed at finding out the effect of different quantities of roots on the tensile strength of the soil.

After triaxial and tensile tests (ASTM D7181 (2011)), soil samples were washed within a woven geotextile (apparent opening size: 0.212 mm, ASTM D4751 (2020)) to retrieve the roots (Figure 34a) and characterize their geometrical and mechanical properties. This characterization will allow to better interpret the results of the geotechnical tests presented below. For triaxial tests, roots volume was characterized by pycnometry (Figure 34b) whereas roots diameter, tips number and length for each diameter class were characterized by image acquisition and treatment through WinRhizo software (Figure 34c).

a

b

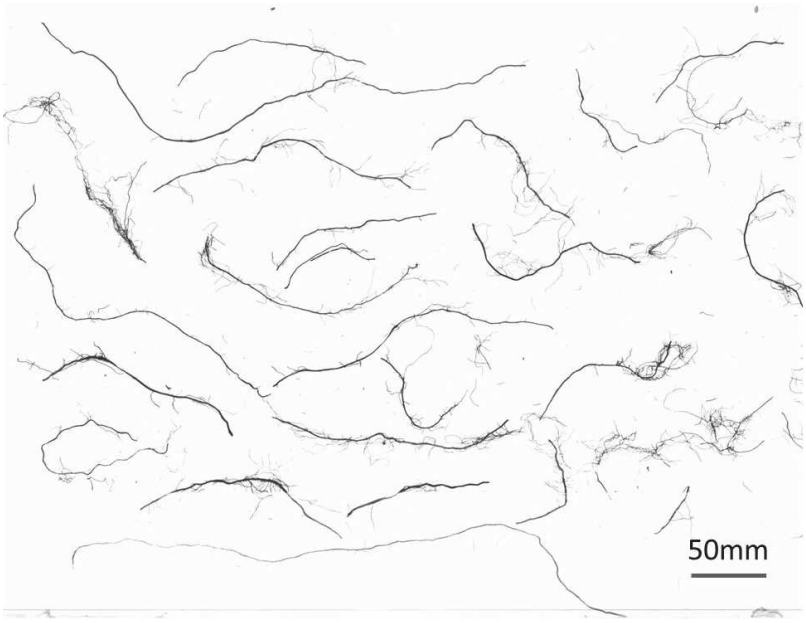

c

Figure 34 a) roots retrieved from soil sample, b) pycnometer test to calculate roots volume, c) WinRhizo scan to evaluate roots geometrical properties (diameter, length).

After direct tensile tests, the roots crossing the fissure produced by the tests were counted. The respective diameters and lengths were measured by a calliper with an accuracy of 0.02 mm. Finally, the volume of each root was obtained by pycnometry.

From further image analysis with ImageJ (Schindelin et al. (2012)) on data obtained by WinRhizo, it was possible to build the average root length distribution as function of root diameters: this information was gathered by individuating the segments for each

root diameter class from a binarized root image (Figure 35a). This last was used as training image of a machine learning algorithm (ImageJ plugin: Trainable Weka Segmentation –Arganda-Carreras et al. (2017)) for which some lines are indicated and correlated to size-known roots diameters (classes in Figure 35b). In this way, the plugin gives as output a segmentation pattern (Figure 35c), based on a probability map of the different classes' spatial distribution (root diameters). Once segmented, the objects for each class have been separately counted with another ImageJ tool (Find Maxima). Finally, the root average length was calculated dividing the sum of all roots' lengths by the number of roots, for each diameter class.

a b c

Figure 35 Image treatment to calculate the average root length for each diameter class. A) original binarized image, b) machine training with recognised diameters Sections (lines), c) roots characterized by diameter's classes.

Distributions were built for plants at different growing periods (Figure 36).

Some of the retrieved unbroken roots have been furtherly tested in tension: for this purpose, roots from the same individual and with different diameters were chosen. The tensile strength of fresh roots was plotted as a function of its diameter. The tests have been carried out with special traction equipment (Figure 37a) with a load cell with a maximum capacity of 5 N (accuracy 0.003 N, rate 0.5 mm/min) and results are shown in Figure 37b.

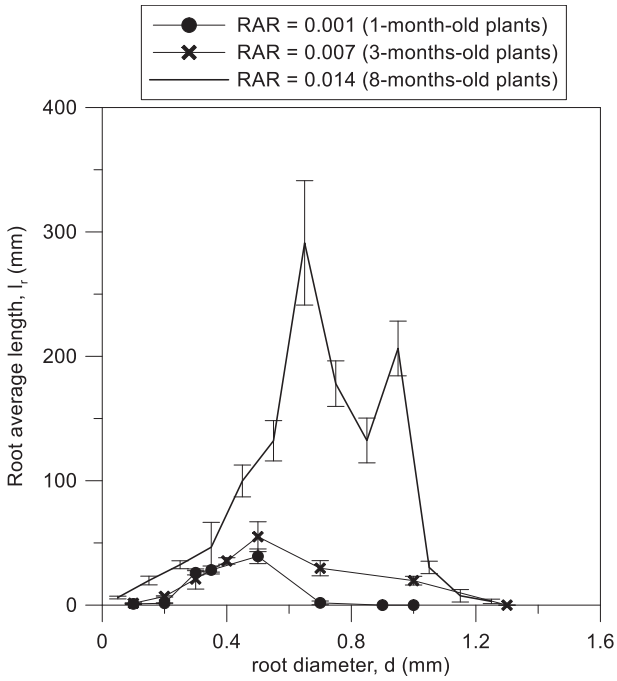

Figure 36 Distribution of average root length for each class of root diameter and for different plants growing periods.

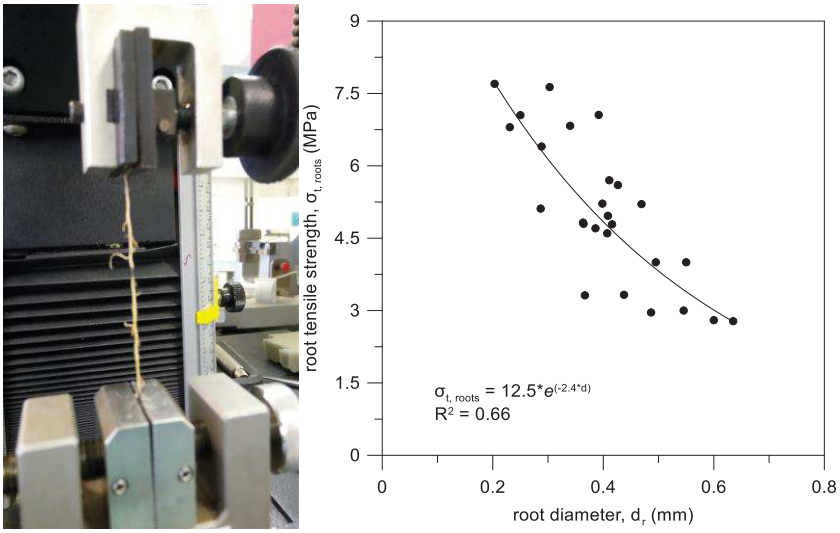

Figure 37 a) root installed in the traction equipment b) tensile strength of Cynodon dactilon roots as function of their diameter

4.5 Methodology

4.5.1 Triaxial Compression Tests

Triaxial compression tests were carried out on soil with and without roots, using equipment that allows the testing of large samples (Φ 200 mm and h 400 mm). Soil

samples were firstly let to dry up to the desired water content (as explained in Section 4.3), then sealed in plastic film for 24 hours to allow suction and water content equalisation. Before testing, water content was measured by separately oven-drying four small soil specimens retrieved in four point of the cylinders (two on the upper surface and two on the lower one). An average value out of the four measurements was considered (the water content difference was less than 0.3%, for each specimen). In the same way, suction was evaluated in four points of the specimen. If suction in soil was lower than 200 kPa, a ceramic tip tensiometer with a 100 mm shaft was used (T5x, UMS, München, Germany). The tensiometer was completely inserted within the sample, to have matric suction measurements 100 mm below the upper surface and above the lower surface of the sample. The measurement time was of 5 minutes. Above suction of 200 kPa, a chilled mirror dew point hygrometer (WP4, Decagon Devices, Pullman, WA, USA) was used.

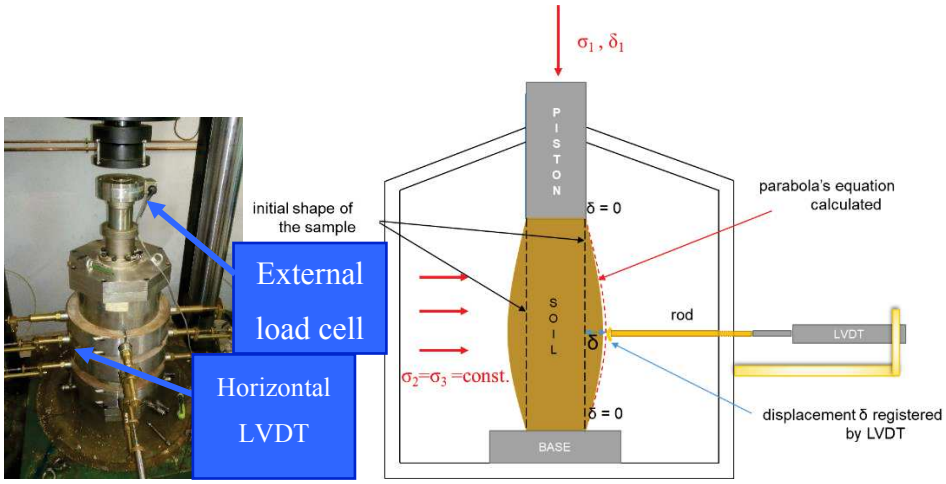

Figure 38 a) triaxial cell and horizontal LVDT supports used in the investigation. B) schematic section of the equipment and the radial displacement measuring system

In this case, soil for total suction measurements was retrieved in four points of the two samples' surfaces.

Before triaxial compression, samples were subjected to isotropic consolidation. Confinement was imposed by air pressure, checked by a pressure transducer. Consolidation step was considered concluded when volumetric strain rate observed in the sample was lower than 0.1%/day. Triaxial drained compression was carried out with displacement control (displacement rate = 0.016 mm/min) and at constant soil water content. Axial and radial displacements in the soil were measured by one vertical and

eight horizontal LVDTs. Horizontal transducers were placed to be in contact with iron rods, which in turn are in contact with the sample's membrane at three different heights (90-180-270 mm with respect to the specimen base) and along two orthogonal orientations (x- and y-axis, with z-axis the vertical one), as shown in Figure 38a-b. For each horizontal displacement registered, a parable equation was calculated along three points: the upper and lower boundaries of the specimen (assuming a zero-horizontal displacement for both) and the height of each LVDT (scheme in Figure 38b). Subsequently, the definite integral of the parable was calculated along the whole height of the sample (considering axial strains) and divided by the same height: in this way, horizontal displacements measured at one point of the sample were averaged along its height. Each one of the averaged displacements was averaged again with all the others along the same vertical and orientation. Finally, the averaged displacements were divided by the initial diameter of the specimen to obtain the radial strains and to calculate the volumetric deformation as the algebraic sum of the strains along the three principal directions ($\varepsilon_{vol} = \varepsilon_x + \varepsilon_y + \varepsilon_z$). The equipment was designed in the UPC geotechnical laboratory and presented in all his components by Alvarado de Menéndez (2017). After tests, soil water content and suction were measured in the same way as explained before in this Section.

4.5.1 Direct tensile test

A new prototype was designed in the UPC, in order to determine soil tensile strength. This mould consists of two independent cylinders made in ABS (ρ = 1.05 Mg/m3, tensile strength (printed) = 27.59 MPa, elastic modulus (printed) = 1.20 GPa (Weng et al. (2016)), water absorption after 24h of saturation = 0.2-0.4% (Interstate Plastics Inc. (2019)) joined by L-shaped pieces (orange pieces in Figure 39), which are removed, after compaction, to start the experiment. Cylinders are fixed on sliding rails with minimized friction (dynamic friction coefficient = 0.002). One of them is connected to a motor and the other one, to a load cell (RSC-1 type, Remberg, Spain, FS = 500 N, precision 0.2 N, Figure 39). An LVDT was installed to measure the horizontal displacement of the mobile mould. The internal base of the equipment presents grooves that enhance the adherence with soil.

A ceramic-tip tensiometer with a 5 mm long shaft (matric suction measurements up to 0.2 MPa) was used to measure suction, recording the value of suction throughout the testing period. The instrument was installed at a depth of 20 mm and 70 mm away from the central section of the equipment, to minimise the alteration on soil's mechanical response. The average variation of suction observed between the beginning and the end of each test was $\Delta s = (5 \pm 2)$ kPa. Matric suction measured in correspondence to the peak of resistance of each test was finally considered to interpret the results. It was impossible to dry the soil above the value of suction of 400 kPa.

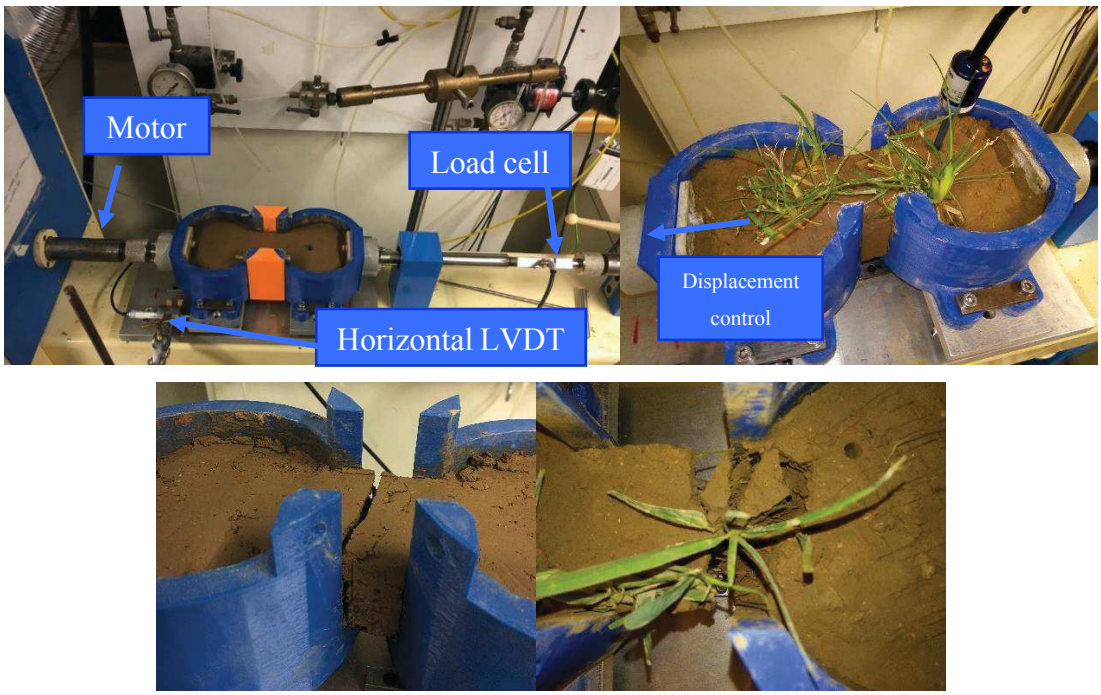

Figure 39 Tensile test equipment in its initial configuration, before testing. A) On the left-hand-side: the motor for controlled displacement and the horizontal LVDT. On the right-hand-side: the load cell. B) Bridge supports removed, and direction of the traction displacement imposed by the motor. C) End of test and fissure generated in bare soil D) End of test and fissure generated by tensile displacement in vegetated soil. Roots visible within the fissure.

The geometrical constraints of the equipment have indeed caused the material to reach the maximum tensile stress (and then, to reach fissuring) it can withstand during shrinkage, close to the above-mentioned value of suction. The water content was measured by an oven drying test at 110 °C at the beginning and at the end of each test. The average difference between the initial and the final measurements was $\Delta w = (0.10 \pm 0.03)\%$. For this reason, an average of the measurements was taken.

Tensile tests were carried out with a controlled displacement rate equal to 0.080 mm/min. Displacement control was adopted to study the post-peak tensile behaviour, especially in the case of vegetated soil. In fact, it was intended to observe the mechanical response of the roots in the soil subjected to pulling and after soil failure (fissuring).

4.5.2 Void ratio measurements in vegetated soil

After triaxial and tensile tests, soil blocks were trimmed out the sample, to check their final void ratio. An average void ratio was considered for triaxial test's specimens: its initial value was back-calculated knowing the final one and the volumetric deformations occurred during the shearing phase. Vegetated cubes were extracted including roots. (the procedure to evaluate void ratio for bare and vegetated soil is explained in Section 2.5.2).

4.5.3 Constitutive laws used

Results coming from triaxial compression and direct tensile tests will be interpreted according to two different failure criterions for partially saturated soils. The first one, proposed by Cárdenas (2018) is formulated as:

$$\tau_f = c'_0 + (\sigma - u_a)tan\varphi' + \frac{s}{a + bs} \tag{20}$$

Where apparent cohesion as function of suction is defined as:

$$c'(s) = c'_0 + \frac{s}{a + bs} \tag{21}$$

Where $(\sigma - u_a)$ is the net stress, s is suction, c'$_0$ is the soil cohesion at null suction, a and b are material parameters.

The second failure criterion used is the one proposed by Alonso et al. (2010):

$$\tau_f = c'_0 + (\sigma - u_a)tan\varphi' + S_r^e s\, tan\varphi' \tag{22}$$

Where apparent cohesion as function of suction becomes:

$$c'(s) = c'_0 + S_r^e s\, tan\varphi' \tag{23}$$

In which the effective saturation degree is $S_r^e = (S_r)^\alpha$, with α a material parameter. Both models include the contribution of suction in increasing soil shear strength. The second one includes the saturation degree as well. The saturation degree implemented in this effective stress formulation shouldn't be intended as a constitutive parameter but as a volume fraction (Jommi (2000)): in fact its value is proportional to the volume and

then to the area of the liquid menisci between soil grains, on which suction is acting and enhancing soil strength. Menisci form only in soil macropores, where water is free to move (Alonso et al. (2010)), whereas immobile water is present within the micro-pores, due to chemical interactions between water and clay particles. Thus, for a soil presenting micro-porosities (clayey/silty soil), the volume/areal fraction of free water is lower than in the case of macro-porous soil (sands), for the same degree of saturation. To include this effect due to soil microstructure, Alonso et al. (2010) introduced the parameter α within the effective stress formulation and calibrated its value for different types of soil: for sandy soils it was close to 1 whereas for clayey soils it was equal to 6.4.

An adaptation to the model proposed by Wu et al. (1979) was adopted to interpret and model vegetated soil behaviour:

$$c'_{0,roots} \approx \gamma\, \sigma_{t,roots,aver.} RAR \qquad (24)$$

Where γ is a parameter depending on the type of plant, $\sigma_{t,roots,aver.}$ is the average roots tensile strength and RAR is the root area ratio (A_{roots}/A_{soil}): this parameter is used in the literature to quantify the amount of roots within the soil matrix. The average roots tensile strength used was assigned according to Figure 37 and in correspondence to the average diameter evaluated from the distributions in Figure 36.

4.6 Results

4.6.1 Hydraulic state and stress evolution during tests

Figure 40a shows the retention measurements (water content (w), suction (s)) and Figure 40b the void ratio changes with suction along drying, obtained within samples for direct tensile tests. In the case of vegetated soils, a decrease in air entry value and retention capacity is observed compared to bare soil. Thanks to paraffin tests, it was possible to follow the evolution of the void ratio with suction in the soil. For vegetated soil, void ratio values shown are the ones obtained by correction for root volume explained in Section 4.5.2. Figure 40b presents void ratio evolution obtained with samples for direct tensile tests. Void ratio is slightly higher in rooted soil than in bare soil.

From this characterization of the stress and state (e, w, s) variables, it was possible to evaluate the degree of saturation S_r for each tested sample and to follow the evolution of this variable along suction changes.

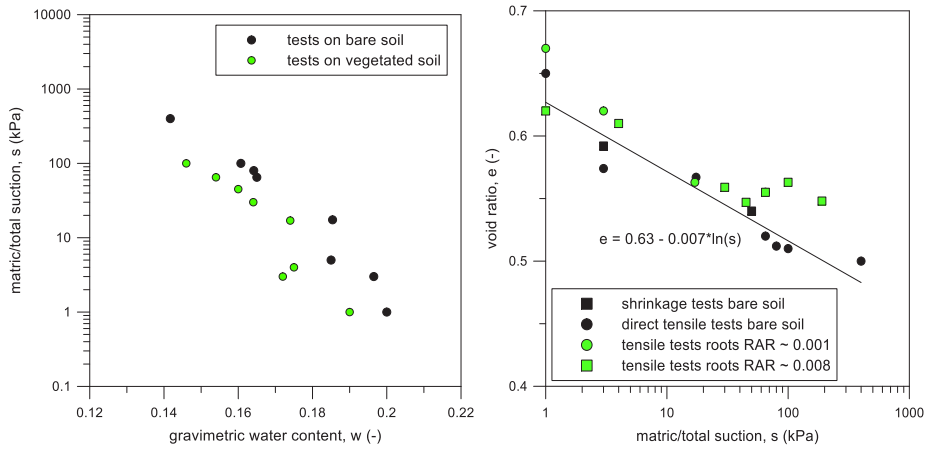

Figure 40 a) Average water content and suction at peak resistance for direct tensile tests and b) evolution of void ratio with suction along drying

4.6.2 Triaxial Compressions

Triaxial compression tests were carried out on ten bare and eight root-permeated samples, at different confinement stresses and at different water contents. The obtained results, in terms of deviator stress and axial strains are shown in Figure 41a-b. From the curves, it is possible to observe how soil stiffness (initial moduli) and strength is increasing with suction and/or with cell pressure (σ_3), as observed by Cui and Delage (1996). The stress and state variables corresponding to each test are presented in Table 12. Close to each stress-strain curve for vegetated samples is indicated the average R_v (root volume ratio) contained by the soil sample. Since it was impossible to evaluate the RAR in the shear bands produced by the compression, this ratio was considered as the 2D equivalent of the root volume ratio R_v (V_{roots}/V_{soil}), which was finally calculated. Therefore, on average, root area ratio and root volume ratio have been given the same value.

Figure 42 presents a comparison in the mechanical behaviour of bare and vegetated soil done at similar suction and confinement stress. As it's possible to observe in Figure 42a, no deviatoric stress plateau is reached in vegetated soil at low suction. This is due to the general root failure mechanism occurring at low suction: roots pull-out with large displacements. In Figure 42b, a deviatoric stress plateau is almost reached: this is due

to the general root failure mechanism expected at high suction: breakage with small displacements.

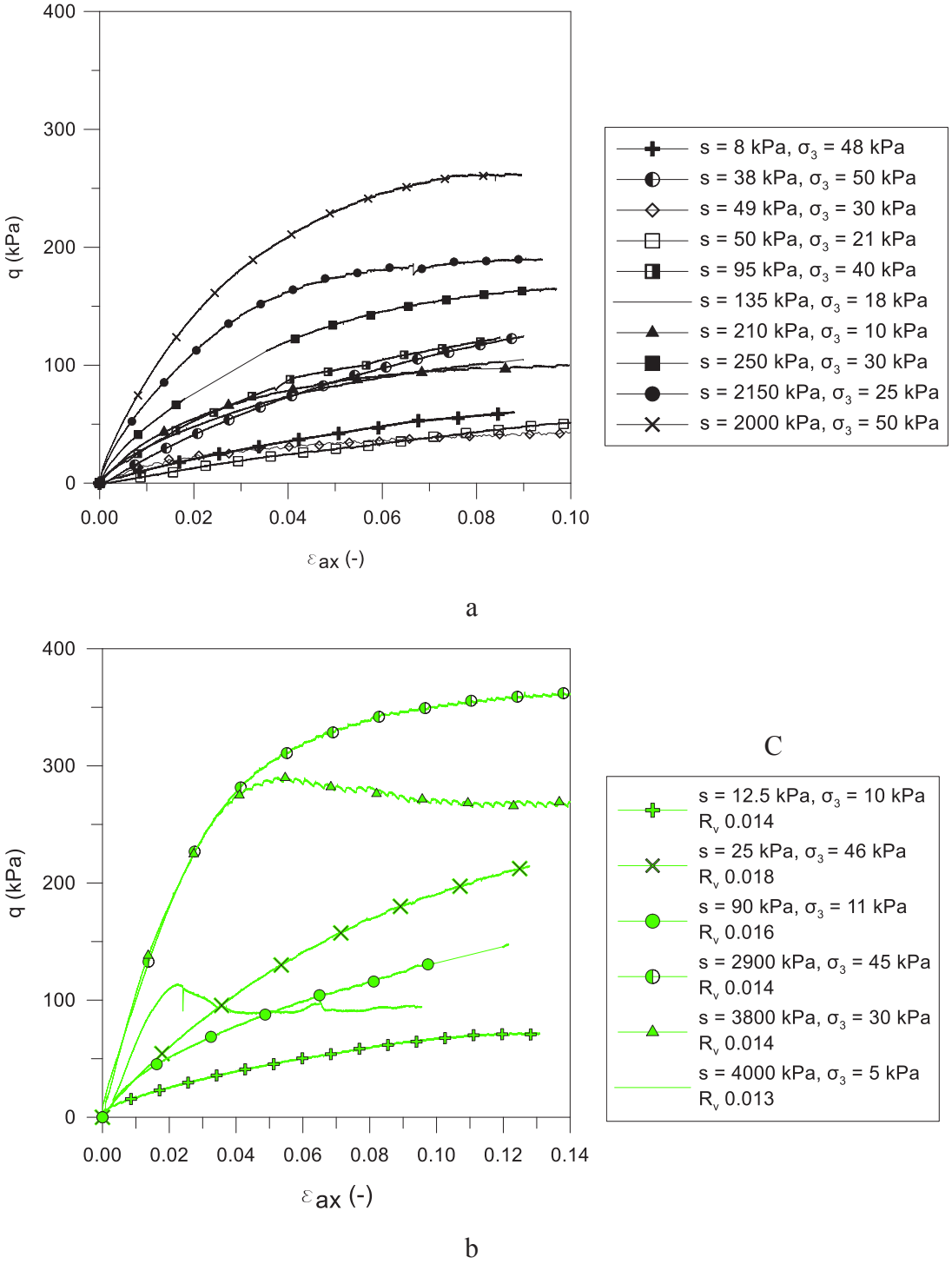

Figure 41 Deviatoric stress vs axial strain curves obtained during triaxial compression tests of: a) bare soil b) vegetated soil

The volumetric behaviour on shearing is showed in Figure 42c-d. Larger compression deformations were generally observed in the vegetated soil due to fissures generated by roots, already showed and quantified in the Section 2.6.3. In some cases, for extremely high suction values and low confinement stresses, soil presented a brittle behaviour with a peak in the deviatoric stress (Figure 42e) and a volume behaviour on shearing characterized by dilatancy after an initial stage of contraction (Figure 42f). From visual inspections after the tests, shear bands were observed within those specimens, with the cylindrical samples completely divided in two or more pieces (Figure 42g). Thus, volume change plotted in terms of axial and volumetric strain (Figure 42f) is representative of the behaviour within the totality of the sample only before the deviatoric stress's peak: close to this point, in fact, shear bands are commonly forming in soil, with a consequent strain localization (Andò (2013)).

Table 12 Triaxial compression tests (TRX). B=Bare soil, V=Vegetated soil. w_{in}, w_{fin} = initial and final measured water content, $e_{average}$ = average void ratio (between values after consolidation and after shearing). $S_{r,average}$ = average saturation degree, s_{in}, s_{fin} = initial and final measured/estimated suction.

test #	w_{in} (-)	w_{fin} (-)	e after consolidation (-)	e after shearing (-)	e average (-)	S_r average (-)	s_{in} (kPa)	s_{fin} (kPa)
TRX B2	0.075	0.062	0.624	0.567	0.595	0.301	1800	2200
TRX B3	0.152	0.150	0.631	0.533	0.582	0.693	11	5
TRX B4	0.126	0.122	0.667	0.589	0.628	0.527	90	100
TRX B6	0.136	0.130	0.672	0.590	0.631	0.546	39	59
TRX B8	0.145	0.138	0.649	0.571	0.610	0.619	30	45
TRX B9	0.127	0.122	0.644	0.578	0.611	0.544	130	140
TRX B10	0.146	0.140	0.682	0.606	0.644	0.593	30	70
TRX B12	0.113	0.114	0.699	0.614	0.657	0.462	200	220
TRX B13	0.114	0.104	0.674	0.600	0.637	0.457	200	300
TRX B15	0.091	0.083	0.654	0.588	0.621	0.375	1280	2230

TRX V1	0.127	0.124	0.680	0.570	0.625	0.536	77.5	100
TRX V2	0.062	0.057	0.658	0.658	0.658	0.242	3400	4210
TRX V3	0.060	0.054	0.664	0.657	0.661	0.213	3420	4495
TRX V4	0.178	0.175	0.699	0.512	0.605	0.779	10	15
TRX V5	0.075	0.068	0.684	0.549	0.616	0.311	2800	3000
TRX V6	0.154	0.149	0.653	0.505	0.579	0.697	20	30
TRX V7	0.202	0.200	0.664	0.481	0.573	0.938	1	1
TRX V8	0.191	0.183	0.662	0.462	0.562	0.887	5	6

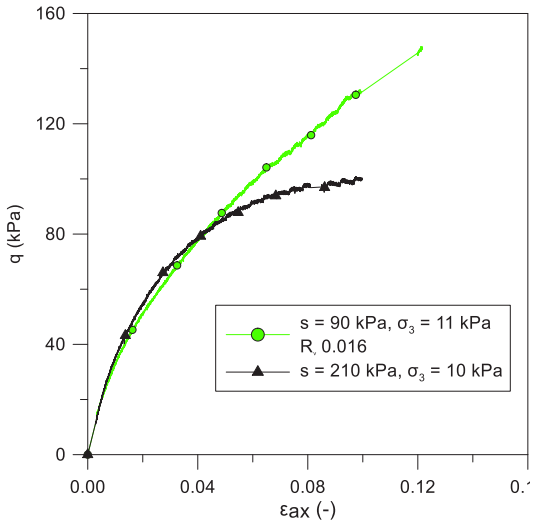
q (kPa)
εax (-)
s = 90 kPa, σ3 = 11 kPa
Rv 0.016
s = 210 kPa, σ3 = 10 kPa

a

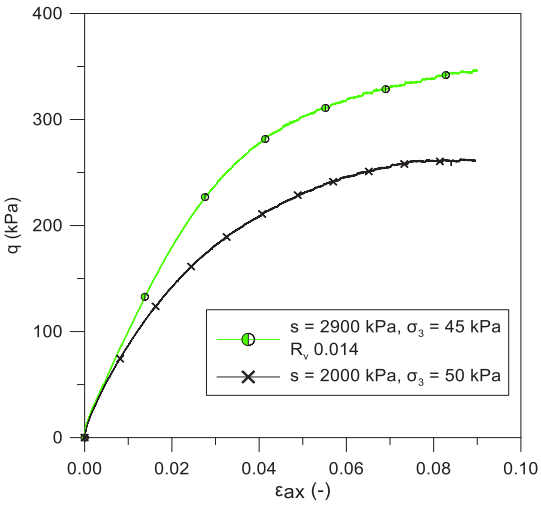
q (kPa)
εax (-)
s = 2900 kPa, σ3 = 45 kPa
Rv 0.014
s = 2000 kPa, σ3 = 50 kPa

b

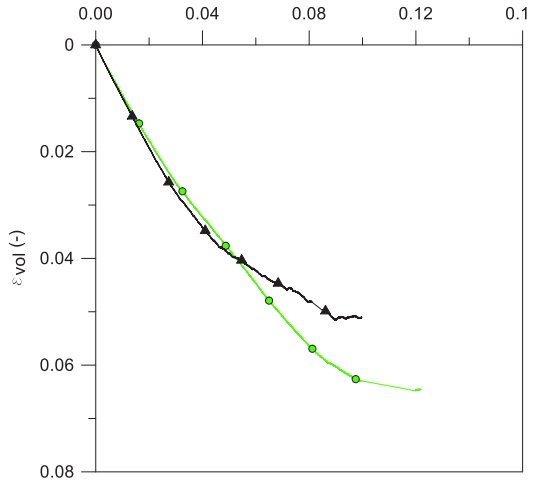
εvol (-)

c

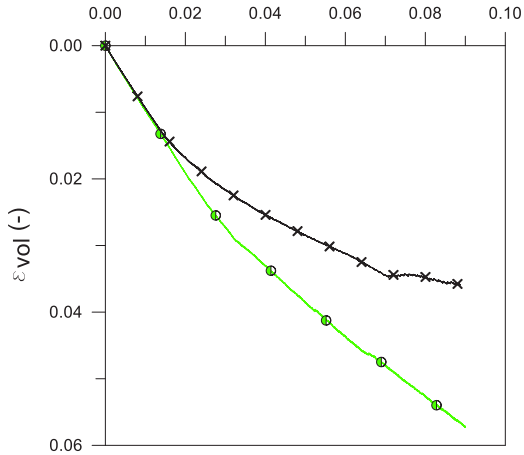
εvol (-)

d

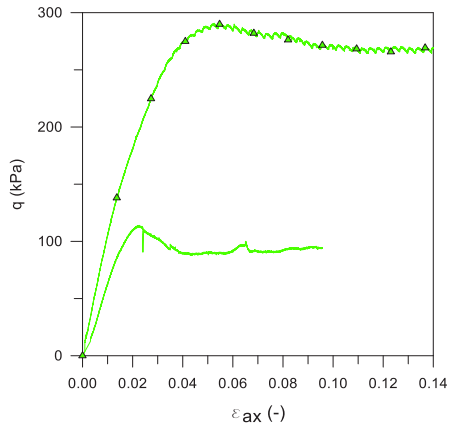
q (kPa)
εax (-)

e

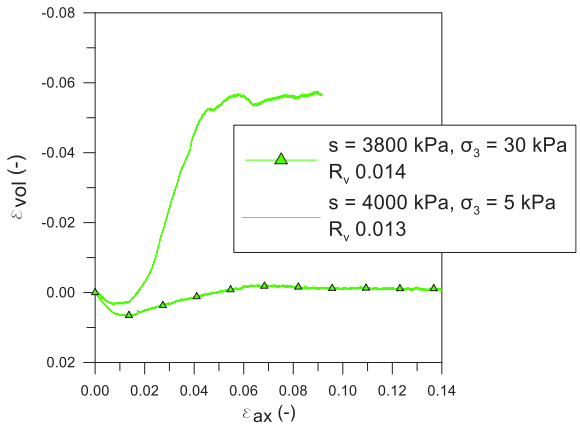
εvol (-)
εax (-)
s = 3800 kPa, σ3 = 30 kPa
Rv 0.014
s = 4000 kPa, σ3 = 5 kPa
Rv 0.013

f

g

Figure 42 Stress strain behaviour under triaxial compression of bare and vegetated soils at a) low suction, low confinement b) high suction, high confinement stress. The respective volumetric deformations are in c and d. E) samples in which brittle behaviour was observed, with a peak in the deviatoric stress and f) respective volumetric behaviour. G) shear band observed during visual inspection of a vegetated sample after triaxial compression

In Figure 43 a and b the failure envelopes obtained by analysing the results are shown. The friction angle, the cohesion at null suction $c'_{(0)}$ and the parameters required by the two laws expressed in equations (20) and (22) were calibrated, at the minimum squared error. Results obtained have been plotted as deviator stress vs normalized mean stress axis. As it is possible to observe in the figure, minor effects on soil friction angle were observed in the vegetated soil.

The evolution of apparent cohesion calculated with the two laws is shown in Figure 44. In the legend of the figure and in Table 13, the calibrated parameters for the two laws are indicated. Calibrated cohesion at null suction was $c'_{(0)}$ = 0 kPa in bare soil whereas higher values of cohesion ($c'_{(0)}$ = 9-10 kPa) have been calibrated for the vegetated soil (Table 13).

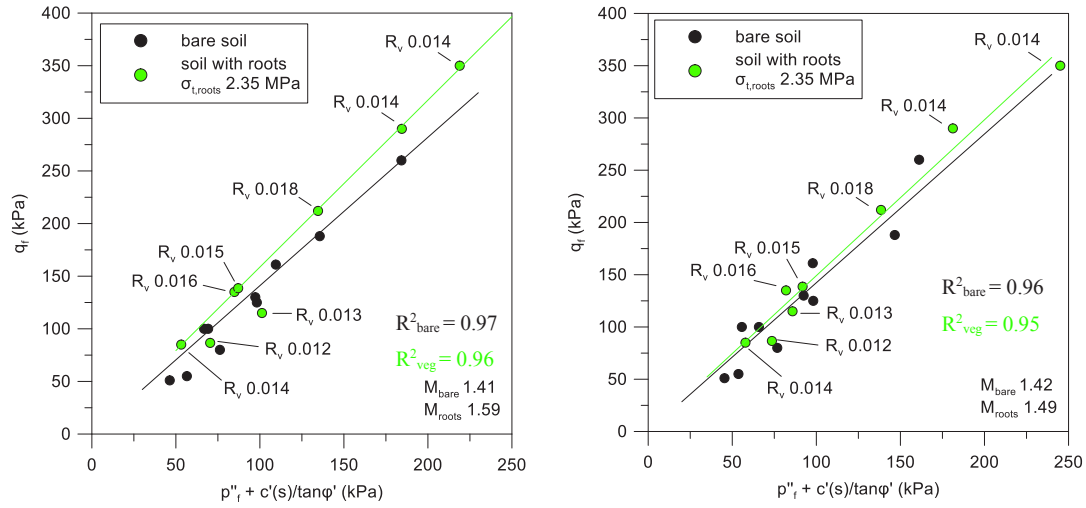

a b

Figure 43 Calculated failure envelopes for soil with and without roots with two different cohesion evolution laws: a) Cárdenas hyperbolic model (2018) and b) (Alonso et al., 2010).

Table 13 Mechanical parameters calibrated with triaxial tests and according to two different failure criteria for partially saturated soils

	Model from Cárdenas (2018):	Model from Alonso et al. (2010):
Bare soil	c'(0) = 0 kPa ; φ' = 34.8° a = 7.3 b = 0.027	c'(0) = 0 kPa ; φ' = 35.1° α = 3.67
Vegetated soil	c'(0) = 9 kPa ; φ' = 38.8° a = 3.9 b = 0.026	c'(0) = 10.3 kPa ; φ' = 36.6°, α = 3.20

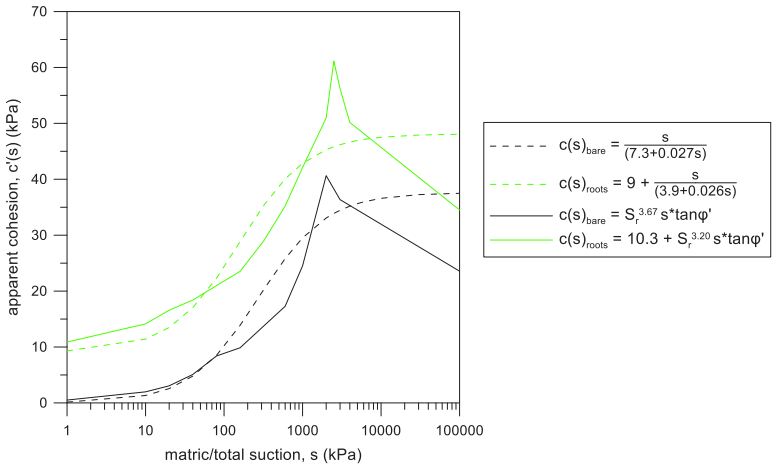

Figure 44 Evolution of apparent cohesion calculated through triaxial compression tests in soil with and without roots and with two laws of evolution of cohesion as a function of suction and degree of saturation.

4.7 Direct Tensile Tests

Figure 45 shows the results of the tensile tests performed on bare and vegetated soil. The legend shows the values of the estimated suction at the time of the stress peak. More information about the stress and state variables in each test can be found in Table 14.

The material reaches tensile stress values that are gradually higher as the suction increases. The stress-displacement behaviour is more ductile at low suction values and more fragile at high suction values. In fact, at low suction values, it was observed that the crack initially opened on the surface and propagated due to induced displacement. At higher suction values, on the other hand, the crack opening extended almost instantaneously over the entire height of the bridge.

For the vegetated soil samples, the legend indicates the RAR (Area of roots divided by the soil bridge section (50x40 mm^2)) values measured within the crack induced by the test (Figure 46) and the suction measured during the peak resistance. It is important to note that, after the peak, the tensile strength does not suddenly drop to zero, but that the roots continue to withstand the induced stresses, even if the soil is partially or totally cracked.

Analysing the results of tensile tests on a sample of bare soil and on two samples with plants grown at 1 and 3 months, at the same suction, it is obtained, as a result, that the tensile stress peak is clearly influenced by the quantity of roots that are in the area of

failure. Figure 47 shows that, at the same suction, the sample with a lower RAR has a strength of approximately 4 kPa: just slightly above the tensile strength of the unrooted soil. The sample with the highest RAR reaches almost 10 kPa of resistance.

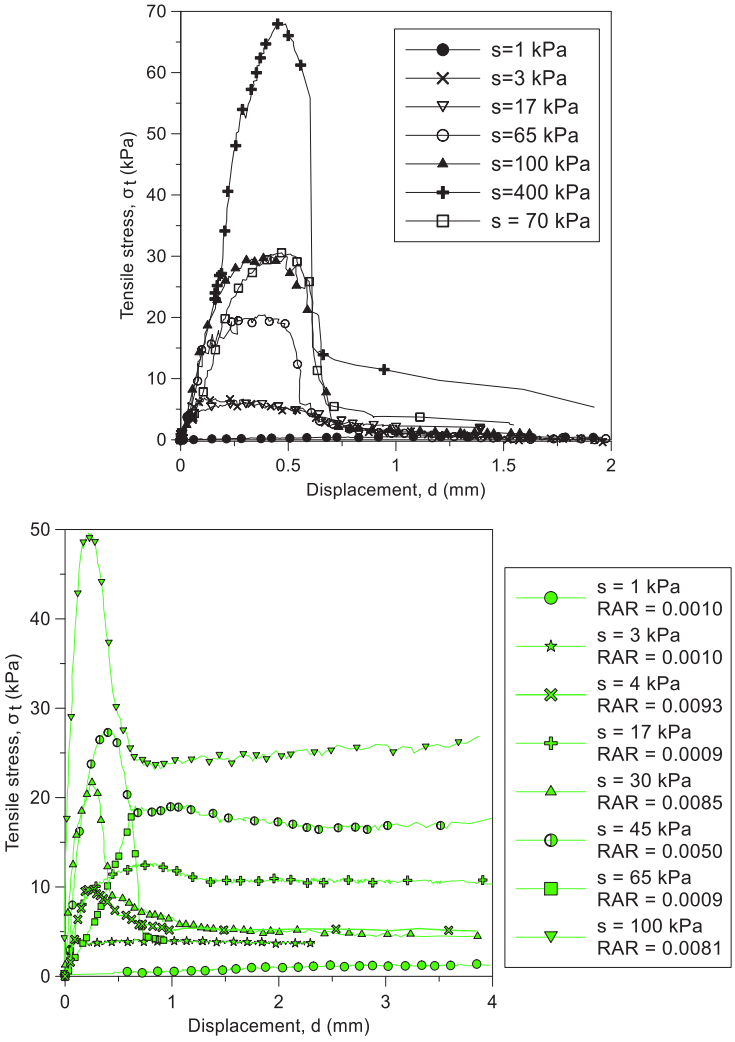

Figure 45 Curves from direct tensile tests on bare and vegetated soil at different water contents

Table 14 Direct Tensile Tests. B = bare soil, V = vegetated soil. w_{in} and w_{fin} = gravimetric water content before and after the test. s_{in} and s_{peak} = suction at the beginning and at the maximum stress observed during tensile test. $S_{r,\ average}$ = average saturation degree during the test.

test #	w_{in} (-)	w_{fin} (-)	e_{fin} (-)	s_{in} (kPa)	s_{peak} (kPa)	$S_{r,\ average}$ (-)
DT B2	0.202	0.198	0.651	1.0	1.0	0.815
DT B3	0.168	0.165	0.522	63.5	65.0	0.841
DT B5	0.163	0.161	0.513	100.3	100.5	0.837
DT B7	0.195	0.192	0.574	2.0	3.0	0.910
DT B9	0.189	0.185	0.580	3.5	5.0	0.852
DT B11	0.185	0.180	0.567	17.0	17.4	0.865
DT B12	0.168	0.164	0.512	78.5	80.0	0.849
DT B14	0.146	0.142	0.503	n.m.	400.0 (estim. by SWRC)	0.753
DT V19	0.192	0.190	0.670	0.7	1.0	0.752
DT V20	0.177	0.174	0.563	16.5	17.7	0.819
DT V21	0.175	0.172	0.620	2.2	3.0	0.735
DT V22	0.156	0.154	0.555	63.5	65.3	0.735
DT V24	0.168	0.160	0.547	42.8	45.0	0.761
DT V25	0.140	0.146	0.563	98.0	101.2	0.701
DT V26	0.162	0.164	0.559	31.0	30.0	0.778
DT V27	0.178	0.175	0.610	3.5	4.0	0.760
DT V28	0.195	0.191	0.621	1.5	1.0	0.812
DT V29	0.115	0.112	0.548	188.7	190.5	0.544

Figure 46 Unbroken roots after test, within the fissure generated by the tensile test

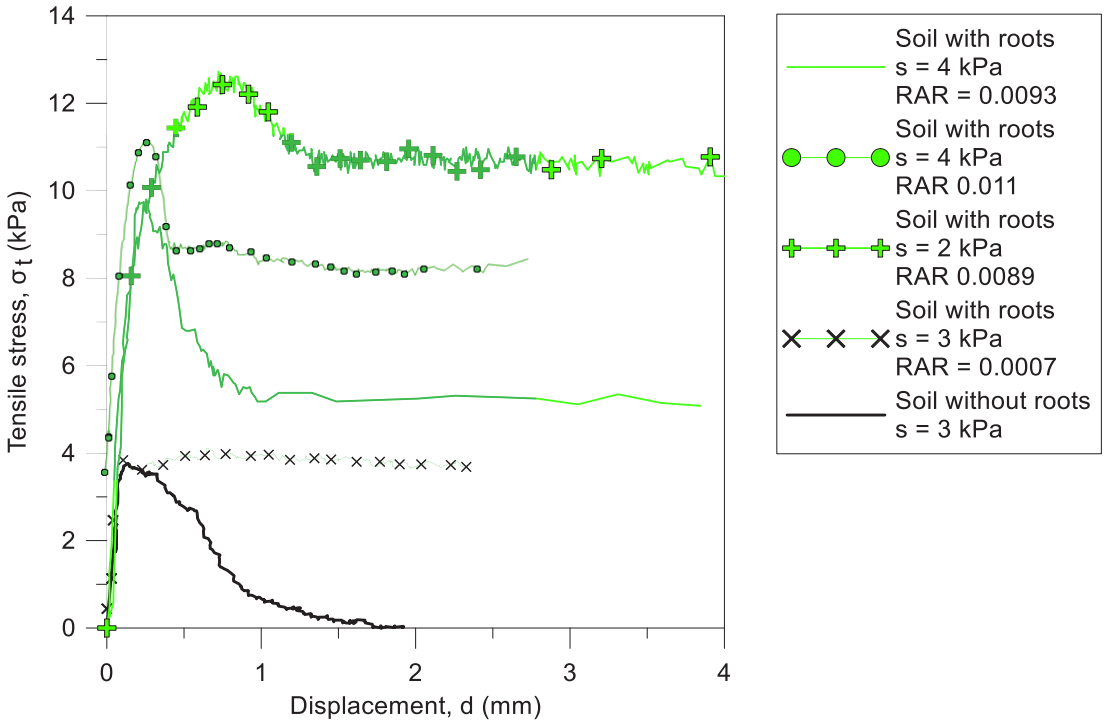

Figure 47 Bare soil and vegetated soil with different roots quantities, for the same suction value.

Bare and root permeated tensile tests were compared at the same suction in Figure 48. Compared to bare soil, at a low suction value (Figure 48a), vegetated soil presents a higher strength, reached after a larger displacement. This might have been caused by the fact that, at high soil water content, roots pull-out phenomenon is prevailing and occurring after large displacements. At high suction (Figure 48b), the soil response is more fragile: in this case, roots breakage at small displacements is the most likely phenomenon.

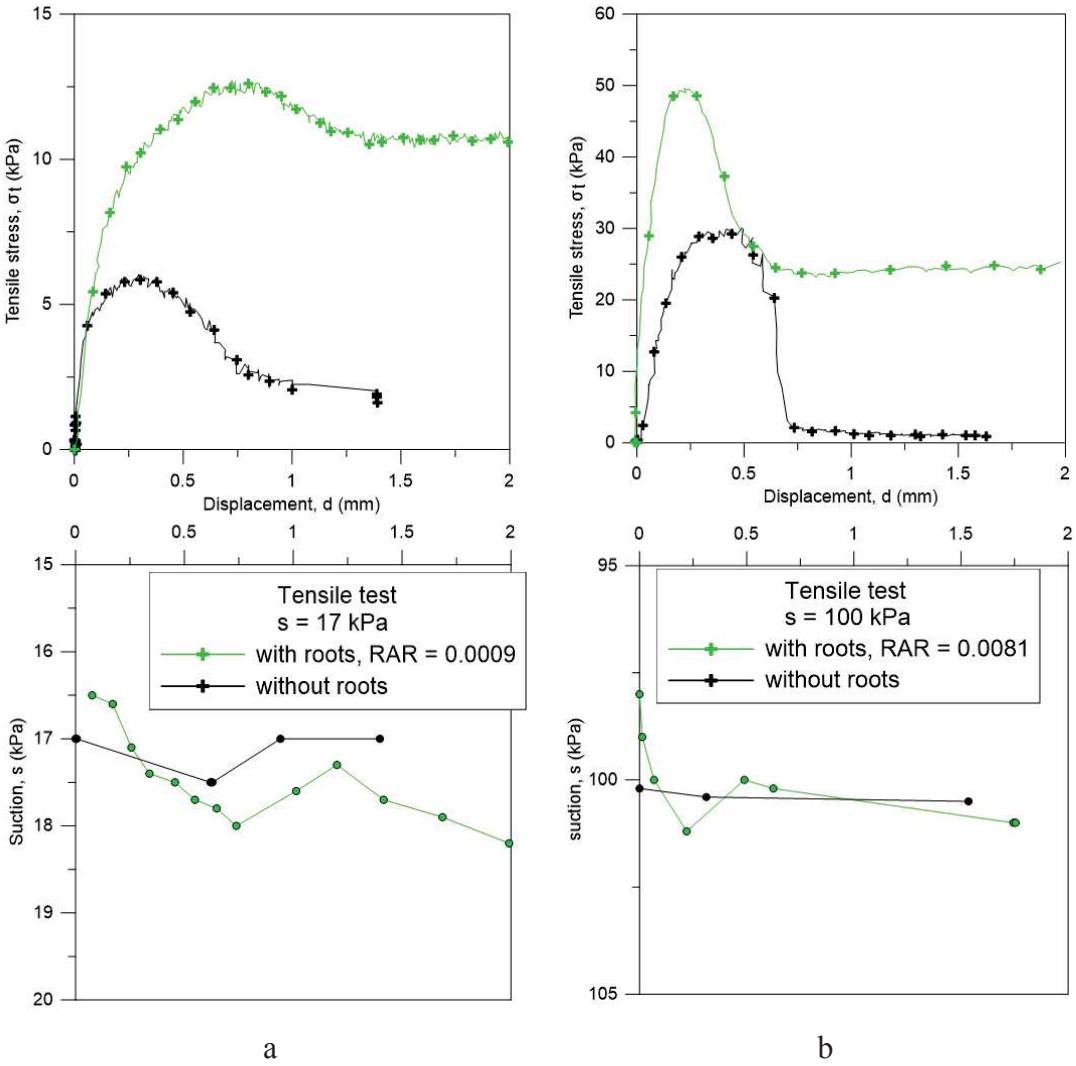

Figure 48 Comparison of direct tensile tests carried out at different suction, for bare and root-permeated soil. A) test carried out at suction equal to 17 kPa, B) test run at 100 kPa

4.8 Joint interpretation of the results

Tensile strength values observed with direct tensile tests have been plotted as a function of suction. (Figure 49). Vegetated results were differentiated by growth periods (1 and 3 months). Samples with 1 month-grown plants showed an average RAR of 0.001±0.0001 whereas 3 months-grown plants were characterized by an average RAR of 0.007±0.002. Roots traits characterized within this study are summarised in Table 15.

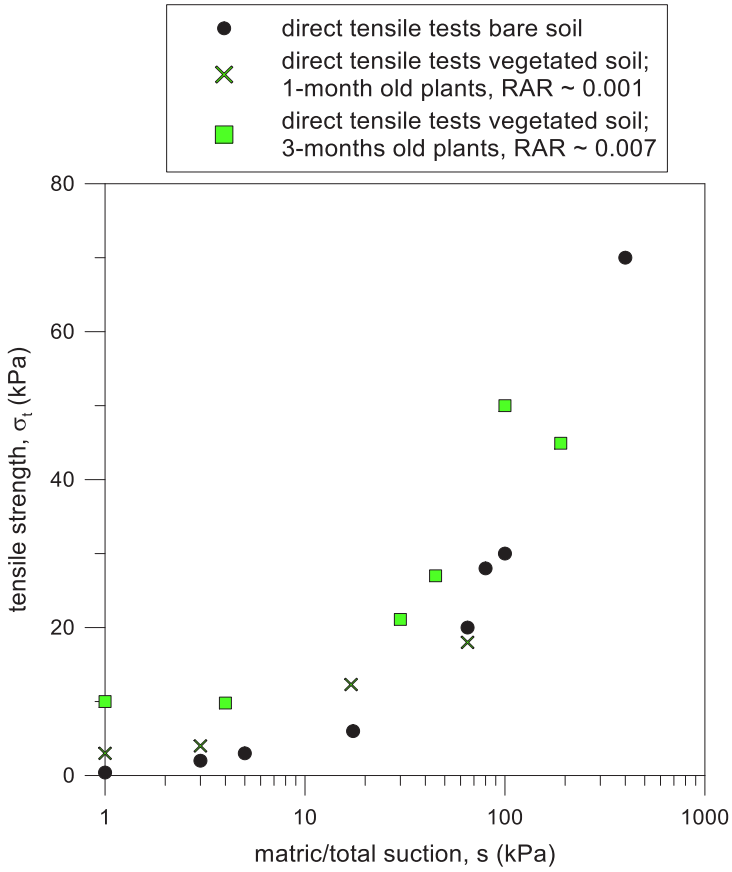

Figure 49 Tensile strength with suction

Tensile strength clearly tends to increase with suction, reaching values close to 70 kPa, for suction values of approximately 400 kPa.

In order to compare these results with those obtained in the triaxial compression tests, the apparent cohesion was calculated, from tensile strength values, using the formula:

$$c'(s) = \sigma_t(s) tan\varphi' \quad (25)$$

which was derived from the Mohr-Coulomb failure criterion (Coulomb (1776); Mohr (1900)). The friction angle used was calibrated by the triaxial compression tests, according to the two laws previously described (equations (20) and (22). Results have been interpreted through the two laws describing the evolution of apparent cohesion with suction indicated in the equations (21) and (23). In order to calibrate the parameters of the respective laws of evolution of cohesion, all the direct tensile tests carried out on vegetated soil were analysed together: to do so it was assumed, for each test, that cohesion at null suction is given by the model proposed in equation (24). The two laws were adapted in this way:

$$c'(s) = \gamma * \sigma_{t,roots,aver.} * RAR + S_r^{\alpha} s \tan\varphi' \quad (26)$$

$$c'(s) = \gamma * \sigma_{t,roots,aver.} * RAR + \frac{s}{a + bs} \quad (27)$$

Knowing the average values of water content and void ratio in each test, it was possible to calculate the degree of saturation of each sample. For each vegetated soil sample, the root area ratio (RAR) and the average roots tensile strength were also known ($\sigma_{t,roots,aver.}$ = 4.8MPa for samples with RAR = 0.001 and $\sigma_{t,roots,aver.}$ = 3.5MPa for samples with RAR = 0.007). Thus, only the values α, γ and the values of a and b were calibrated for vegetated soil through an estimation at the minimum squared error. For the bare soil, the value of c_0 was additionally calibrated, resulting, anyway, close to zero. All the calibrated parameters are indicated in Table 16.

For the law proposed by Alonso et al. (2010), the values of α calibrated were between 3.3 and 4.01: these values are in line with those observed in the literature (Alonso et al. (2010)) for soils with physical characteristics similar to those of the studied soil (silty sand). The lower value of α found for the vegetated soil has a physical meaning: an increase in soil macro-porosity generated by roots growth. This is in line to what observed in the Chapter 2 of this Thesis. The calibrated values of γ were around 0.30 and much below the value of 1.2 predicted by Wu et al. (1979): this is indicating that γ might depend on several factors such as the type of plant, the geometry of roots, the type of soil, its water content.

Table 15 Root properties estimated and/or measured within the different samples tested. TRX = triaxial compression tests, DT = Direct Tensile tests.

Roots growing period	Test	Root Volume Ratio – R_v	Root area ratio – RAR	Average root diameter±standard deviation (mm)	Root length density – R_{ld} (m/m^3)
8 months	TRX V1	0.016	-	0.700±0.020	$2.10*10^5$
	TRX V2	0.014	-	0.685±0.032	$1.89*10^5$
	TRX V3	0.013	-	0.688±0.028	$1.79*10^5$
	TRX V4	0.014	-	0.705±0.024	$1.91*10^5$
	TRX V5	0.014	-	0.710±0.031	$1.47*10^5$
	TRX V6	0.018	-	0.679±0.018	$1.11*10^5$
	TRX V7	0.012	-	0.652±0.027	$6.30*10^4$
	TRX V8	0.015	-	0.704±0.046	$1.89*10^5$
1 month	DT V19	0.0015	0.001	0.384±0.012	$8.17*10^3$
	DT V20	0.0034	0.0009	0.400±0.009	$1.10*10^4$
	DT V21	0.001	0.001	0.398±0.015	$6.75*10^3$
	DT V22	0.002	0.0009	0.405±0.018	$9.78*10^3$
3 months	DT V24	0.011	0.0054	0.532±0.022	$1.04*10^4$
	DT V25	0.012	0.0081	0.526±0.025	$1.42*10^4$
	DT V26	0.015	0.0085	0.531±0.031	$7.47*10^3$
	DT V27	0.013	0.0093	0.557±0.024	$1.23*10^4$
	DT V28	0.009	0.0075	0.499±0.017	$1.18*10^4$
	DT V29	0.010	0.0078	0.509±0.033	$1.20*10^4$

This in turn means that analysing just the number of roots within the fissure is limiting to completely understand the mechanisms of roots reinforcement: roots are in fact redistributing stresses and strains imposed by tension on a broader area of soil, which can extend even far from the fissure position. This phenomenon is already qualitatively observable when comparing the post-failure shape of the fissures observed in almost-saturated bare and vegetated soil (Figure 39).

The apparent cohesion estimated through direct tensile tests are presented in Figure 50 and Figure 51 along with the trends given by the two laws used.

Table 16 Parameters calibrated through direct tensile tests to predict apparent cohesion evolution with suction

	Model from Cárdenas (2018): equation (21) for bare soil, equation (27) for vegetated soil	Model from Alonso et al. (2010): equation (23) for bare soil, equation (26) for vegetated soil
Bare soil	$c'_{(0)} = 0$ kPa; $a = 3.5$; $b = 0.011$ kPa^{-1}	$c'_{(0)} = 0$ kPa; $\alpha = 4.01$
Vegetated soil	$\gamma = 0.31$; $a = 2.3$; $b = 0.019$ kPa^{-1}	$\gamma = 0.23$; $\alpha = 3.3$;

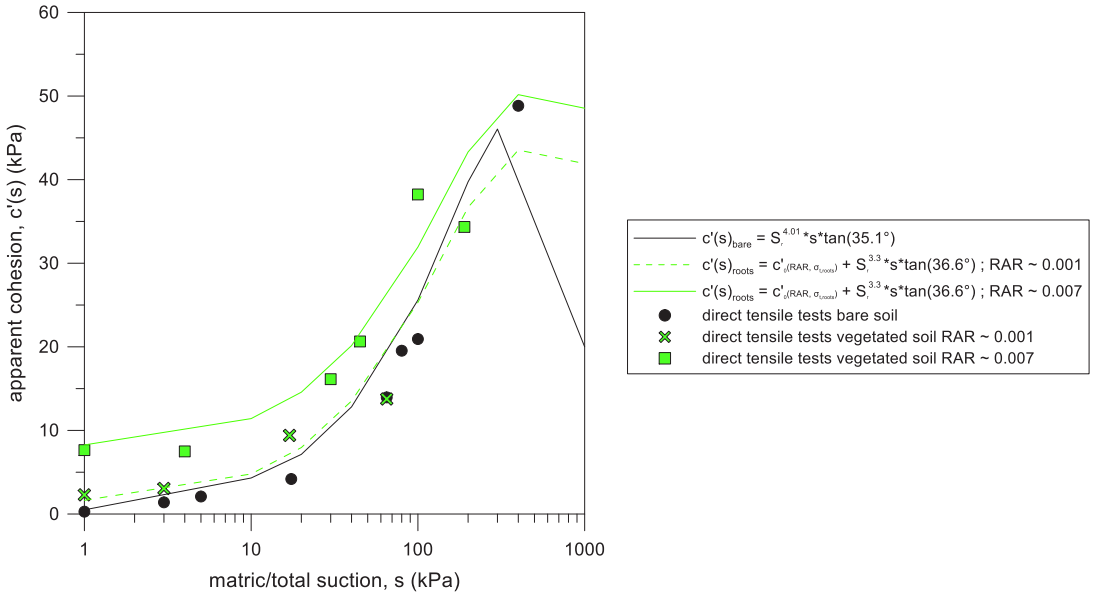

Figure 50 Cohesion evolution with suction, evaluated according to Alonso et al., 2010 (coefficients of determination: $R^2 = 0.97$ (bare soil), $R^2 = 0.93$ (vegetated soil, RAR ≈ 0.001), $R^2 = 0.93$ (vegetated soil, RAR ≈ 0.007))

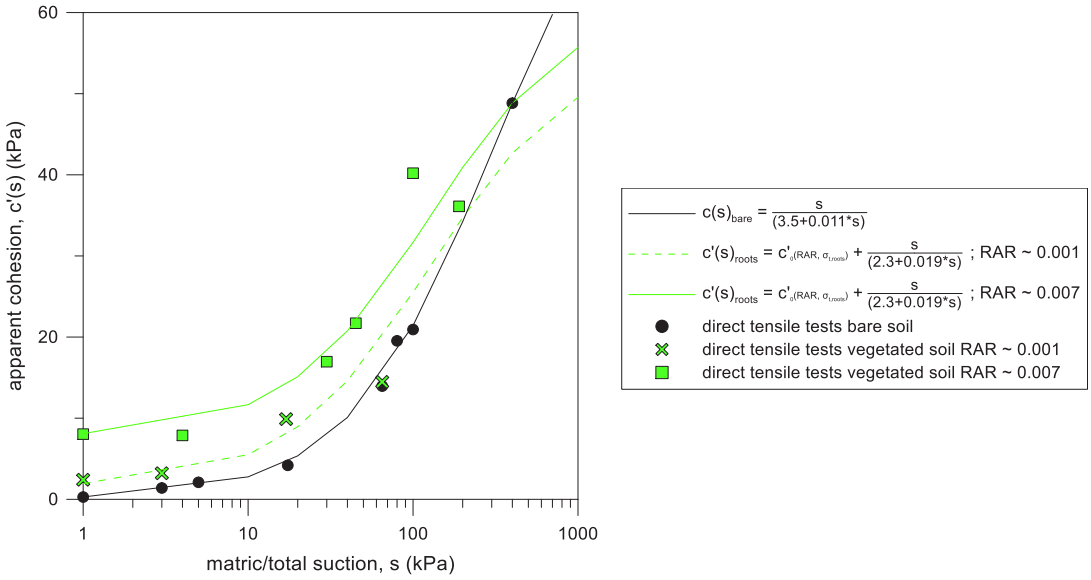

Figure 51 Cohesion evolution with suction, evaluated according to Cárdenas, 2018 (coefficients of determination: R^2 = 0.99 (bare soil), R^2 = 0.99 (vegetated soil, RAR ≈ 0.001), R^2 = 0.94 (vegetated soil, RAR ≈ 0.007))

4.9 Tensile strength interpretation within a shear strength criterion

Results coming from direct tensile tests were furtherly analysed with the constitutive stress framework (mean average skeleton stress *p'*) for partially saturated soils proposed by Alonso et al. (2010) and Vanapalli et al. (1996):

$$p'(s) = p - u_a + S_r^{\alpha} s \tag{28}$$

where p is the total mean stress, u_a the air pressure, s the matric suction, S_r the degree of saturation and α a model parameter that depends on the soil type and microstructure. Tensile (total) stress was considered as the minimum total principal stress σ_3 while total stresses in the other two principal directions are $\sigma_1 = \sigma_2 = 0$ kPa throughout the duration of each test. The assumption of this approach is that tensile strength is ruled by failure in shear, according to the Mohr-Coulomb failure criterion. Deviator stress is defined as $q = \sigma_1 - \sigma_3 = -\sigma_t$. The failure criterion under the axisymmetric extension stress path is given by:

$$q_f = \frac{6c'cos\varphi'}{3 + sin\varphi'} + M_e p' \tag{29}$$

with $M_e = 6 \sin\varphi'/(3+\sin\varphi')$, φ' the friction angle, and c' the cohesion under saturated state. Deviator and mean average skeleton stresses at failure were calculated considering σ_3 equal to the peak tensile (total) stress of the stress – displacement curves. Seven fallow soil and six vegetated soil tests were used to calibrate by least squares fitting two sets of parameters M_e, c' and α. The calibrated parameters of the failure criterion are presented in Table 17. As observed, the vegetated soil displayed cohesion at saturation and a slightly higher friction angle.

Table 17 Calibrated parameters for the Mohr-Coulomb failure criterion.

	Fallow soil	**Vegetated soil**
M_e (-)	0.94	0.98
α (-)	4.92	2.14
φ' (°)	34	36
c' (kPa)	0	6.3

The two failure envelopes and the points at failure (p'_f, q_f) are plotted in Figure 52. For both materials, the model predicts well the results obtained. Moreover, the vegetated soil presents a higher shear strength than the bare soil even at null mean average skeleton stress.

The calibrated shear strength parameters were in good agreement, in terms of φ' and c', to those calibrated with the triaxial tests (Table 13). In spite of the effect of roots on soil hydraulic behaviour (decrease of the retention capacity, as evidenced in Chapter 2), soil mechanical properties were not affected at high suction values.

Close to each point for vegetated soil plotted in Figure 52, the corresponding RAR is indicated as labels. To consider the effect of this morphological plant trait on soil behaviour, the factor $\beta^* \cdot \sigma_{t,roots} \cdot RAR$ was correlated ($R^2 = 0.95$) to the increase in soil shear strength $\Delta q = q_{veg} - q_{fallow}$, where q_{veg} is given by each of the vegetated soils' points in the (p', q) plane and q_{fallow} was evaluated at the same mean average skeleton stress. The tensile strength of the roots considered was $\sigma_{t,roots} = 3.5$ MPa. The calibrated β^* is equal to 0.41. This result demonstrates the usefulness of using these plants' indicators in predicting the contribution of roots to soil shear strength and tensile

strength increase. Moreover, the correlation was found to work well even in extension paths, while so far, it was tested only under triaxial compression stress paths.

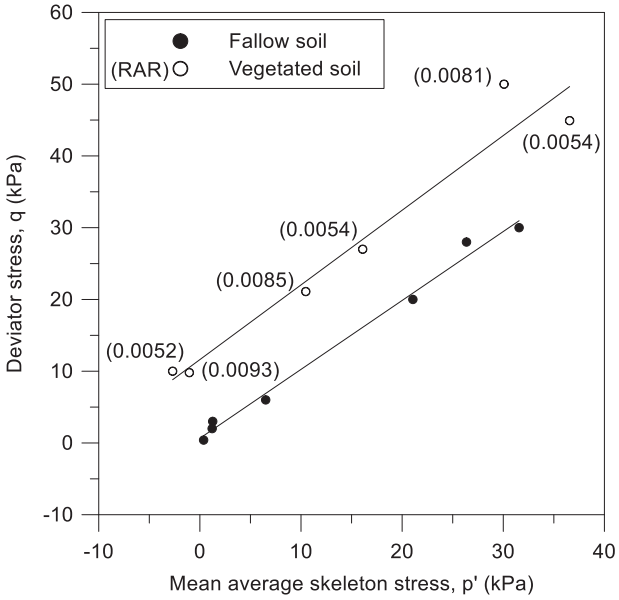

Figure 52 Failure envelopes and stresses at failure for tensile tests on vegetated and fallow samples

4.10 Conclusions

In the current study, an investigation on the effects of roots on the mechanical behaviour of soil was carried out with triaxial compression and direct tensile tests. Tests were carried out after different growing periods (1 and 3 months) and at different hydraulic states. In addition, the characteristics of plants that could affect soil mechanical behaviour were assessed, such as root tensile strength, diameter, root area ratio. These parameters were used in an adapted equation for soil reinforcement with roots. The equation was then implemented in two constitutive laws for partially saturated soils to predict the evolution of soil shear strength and apparent cohesion with suction observed within the laboratory tests.

From the results interpreted in terms of apparent cohesion with suction it was possible to observe that soil with plants had a higher tensile strength and therefore greater cohesion than tests without roots. However, the fissures generated by the growth of the roots, during soil drying, influenced negatively the macroscopic soil mechanical behaviour at high suction values. Moreover, the validity of adapting constitutive laws for partially saturated soils with equations representing roots reinforcement was

demonstrated: in this way, vegetated soil behaviour can be predicted over a good range of suction values. A good agreement between cohesion evolution evaluated by triaxial compression tests and by direct tensile tests was also observed.

5. Numerical analysis of a bare and a vegetated embankment

The results of the hydro-mechanical behaviour of bare and vegetated soil obtained within this thesis were used to assess the effects of different root quantities (RAR ≈ R_v ≈ 0.007 and 0.014) on the stability of the monitored embankment built with the same soil and seeded with the same plant investigated and presented in Oorthuis et al. (2018). Triaxial compression and direct tensile tests have been performed under saturated and partially saturated conditions to quantify the effect of roots on the stress-strain behaviour of soil, in Chapter 4. Results showed that roots provided a noticeable increase of soil strength, even if larger volumetric compressive deformations were traced as shear displacements progressed. Results have been analysed within the context of the shear strength criterion for unsaturated soils proposed by Fredlund and Rahardjo (1993), which is needed in Geoslope (2019) to assess slope stability adopting a limit equilibrium approach. According to this model, the shear strength of a partially saturated soil is given by:

$$\tau_f = c'_0 + (\sigma - u_a)tan\varphi' + s\ tan\varphi^b \quad (30)$$

Where cohesion as function of suction is given by:

$$c'(s) = c'_0 + s\ tan\varphi^b \quad (31)$$

As done in Chapter 4, the c'(s) evolution was re-adapted to consider root reinforcement and to represent the tendency observed by triaxial compression and direct tensile tests, as indicated in equation 32:

$$c'(s) = \gamma\ \sigma_{t,roots,aver.}RAR + s\ tan\varphi^b \quad (32)$$

In which c'_0 represents the cohesion when soil is saturated (suction, s = 0 kPa) and $tan\varphi^b$ is a constant term that represents the increase of cohesion with suction. All the calibrated parameters for this law are presented in Table 18.

Table 18 Parameters for the criterion of Fredlund and Rahardjo (1993) *calibrated with triaxial compression tests and direct tensile tests*

	Bare soil	Vegetated soil
Triaxial Compression Tests	$\varphi' = 34.8°, c'_0 = 0\ kPa$ $\varphi^b = 8°$	$\varphi' = 34.9°, c'_0 = 12\ kPa$ $\varphi^b = 12.3°$
Direct Tensile Tests	no parameters calibration needed	$\gamma = 0.30$

In Figure 53, a comparison between results and models obtained by triaxial compression tests and direct tensile tests is presented. Peak tensile strength values obtained by direct tensile tests have been converted into cohesion by the equation:

$$c'(s) = \sigma_t(s)\ tan\varphi' \tag{33}$$

derived from the Mohr-Coulomb failure criterion. Cohesion values calculated in this way are plotted as points whereas, the models explained in equations 31 and 32, are plotted as lines in Figure 53. In the case of triaxial compression tests, the evolution of cohesion traced by the lines in Figure 53 has been calibrated to make all the deviatoric strength peaks fit the failure envelopes showed in Figure 54.

Roots geometrical and mechanical traits were assessed (see Chapter 4) in order to be used within a soil-root reinforcement well-established model (Fredlund and Rahardjo (1993)), which provided results in good agreement with observations.

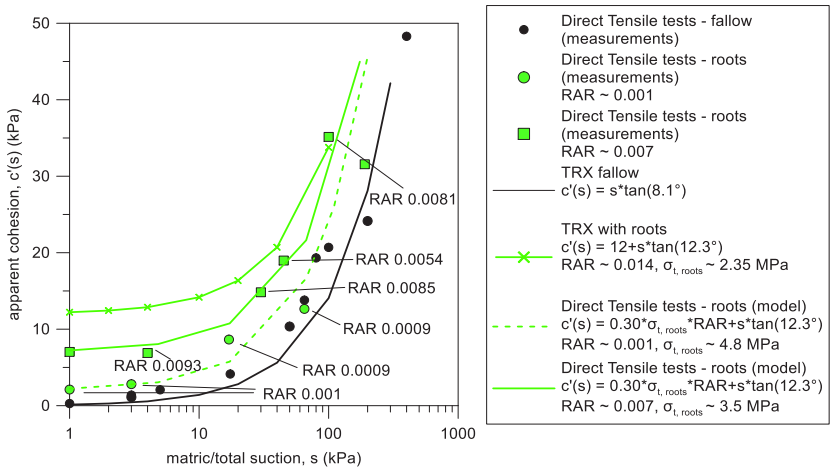

Figure 53 Cohesion evolution with suction according to Fredlund and Rahardjo (1993) *calibrated with triaxial compression and direct tensile tests and for different plant growing periods.*

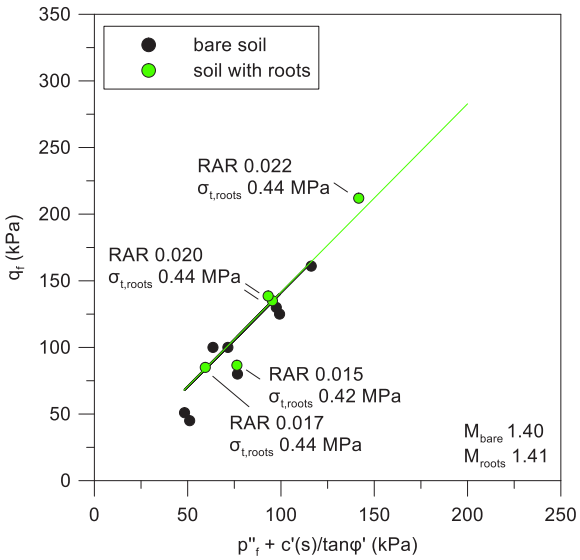

Figure 54 Failure envelope according to Fredlund and Rahardjo (1993*)*

The hydraulic properties of the silty soil were evaluated as well, for the same range of porosity as the mechanical tests (see Chapter 2). Results coming from the analysis of oedometer and permeameter tests evidenced that roots caused an increase of the water saturated permeability, in the order of three times that obtained for bare soil. Retention properties were affected by roots as well: in particular, the air-entry value and the suction correspondent to each water content decreased (see Chapter 2).

The hydro-mechanical model built in Chapter 3 of this thesis was used to obtain the retention curve and the water saturated permeability of the soil before and after roots growth, as indicated in Figure 55.

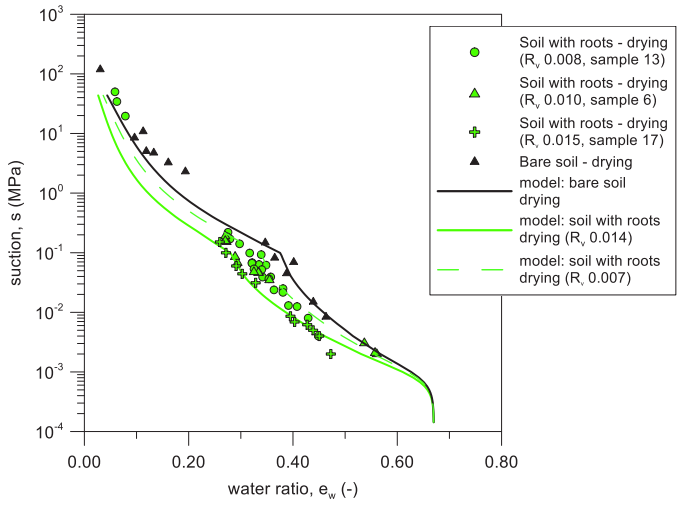

a

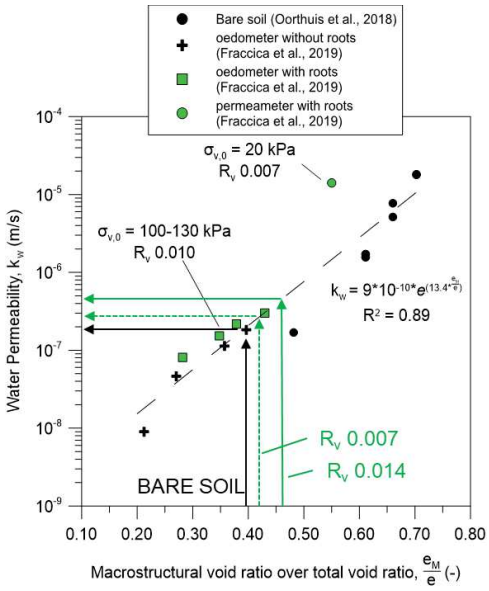

b

Figure 55 Retention curves and water saturated permeability evaluated by the hydro-mechanical framework developed in Chapter 2

The intrinsic unsaturated permeability was evaluated in GeoStudio according to the law proposed by Fredlund and Xing (1994).

These laws were used to simulate the behaviour of an embankment initially under partially saturated conditions and subject to wetting, imposed as a zero pore-pressure condition at the upper boundary of the slope. The geometry of the embankment is showed in Figure 56. A geomembrane with high roughness was used to produce soil breakage in the first 700 mm from the soil surface. The inclination angle of the slope is of 34°.

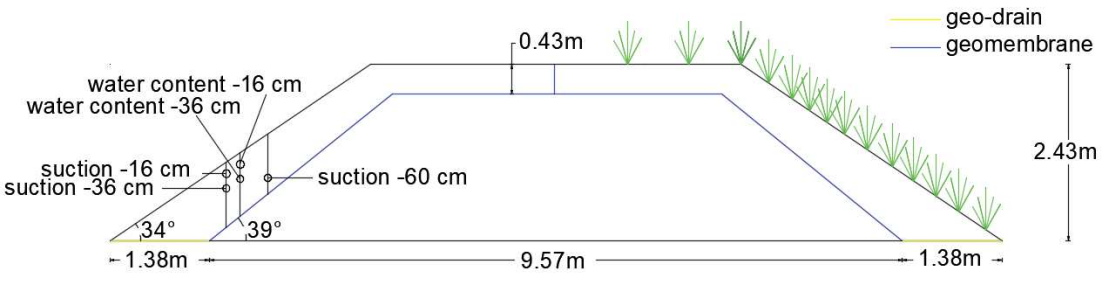

Figure 56 Monitored embankment geometry

The properties of vegetated soil were attributed to the first 400 mm of soil, below the soil surface, as indicated in Figure 57

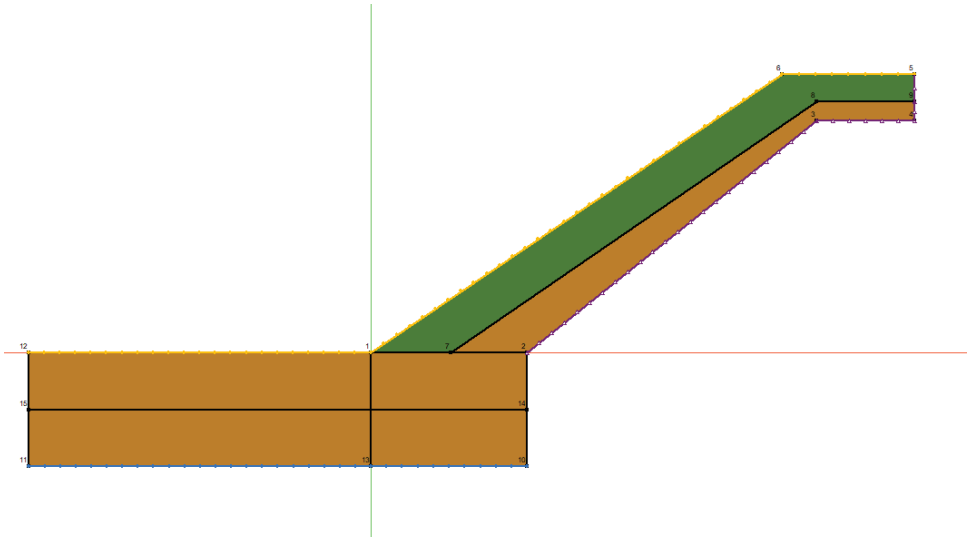

Figure 57 Geometrical model of the vegetated slope of the embankment

The initial boundary conditions given to all the slopes (one bare and two vegetated by different roots quantities) are showed in Figure 58.

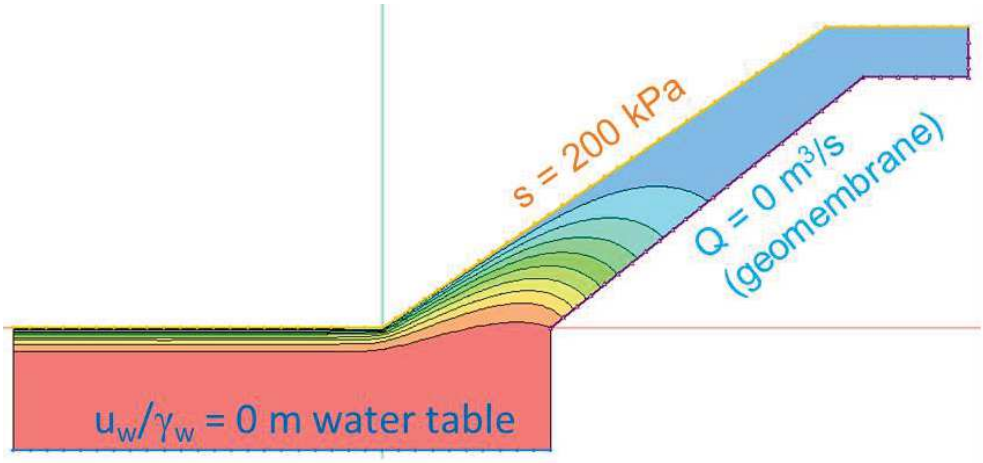

Figure 58 Initial boundary conditions imposed on the embankment slope

A water table one metre below the horizontal surface, suction equal to 200 kPa on the whole upper soil surface and an impervious material (corresponding to the geomembrane) were attributed to the geometrical model. After a first analysis in steady state conditions to allow hydraulic head's equalisation, a rainfall was simulated as a

zero-water-pressure boundary condition on the whole upper surface (Figure 59). A transient analysis in SEEP/W was carried out, jointly with a stability analysis in SLOPE/W, at given time steps.

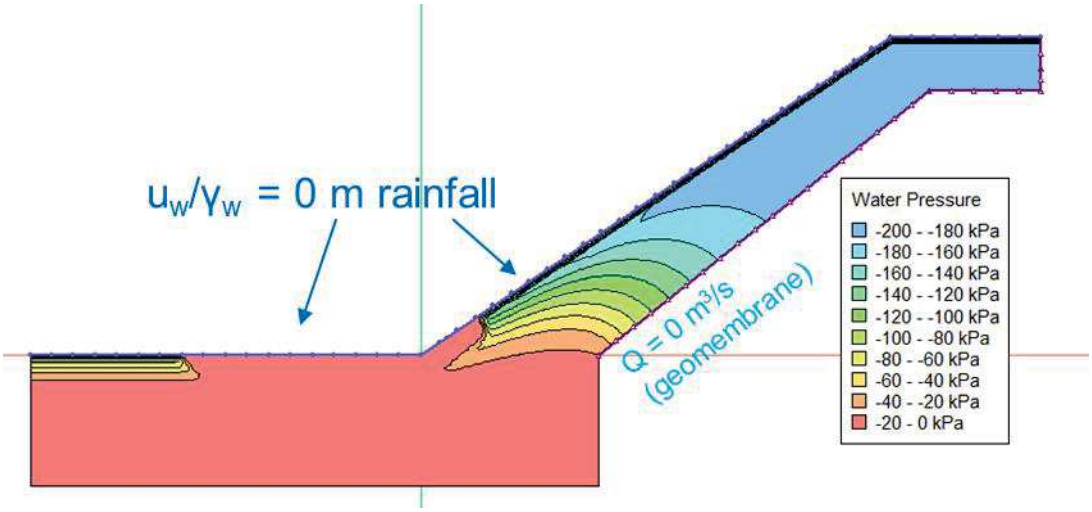

Figure 59 Boundary conditions during transient analysis to simulate rainfall

As expected, at a given simulation time, soil with a highest quantity of roots was found at lower values of suction, with respect to the bare soil, due to the increase in permeability imposed (Figure 60).

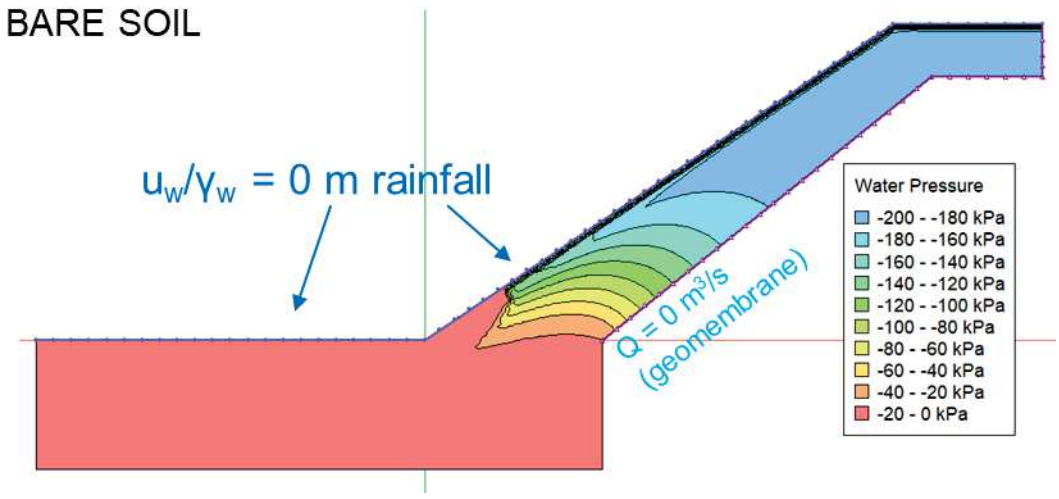

a

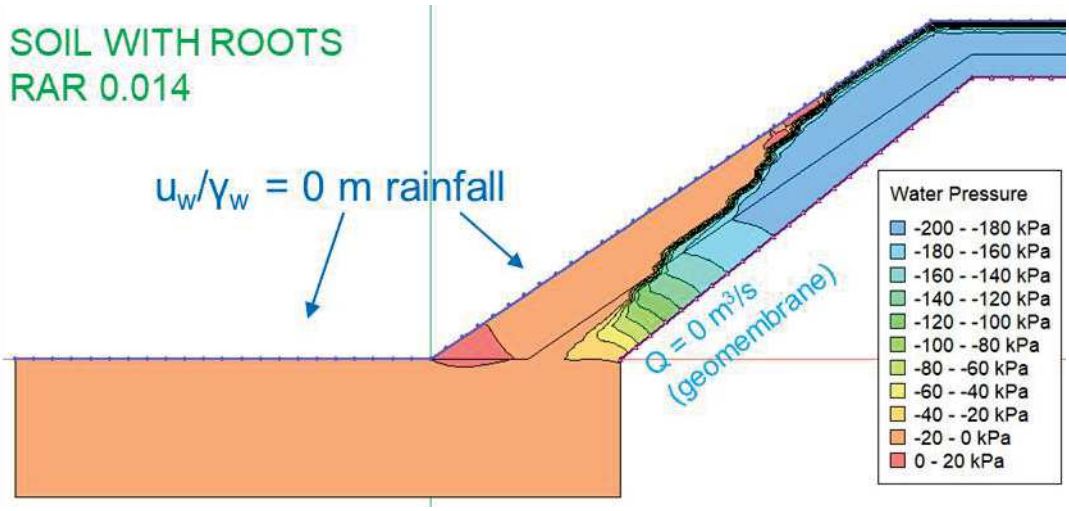

b

Figure 60 Comparison between: a) bare slope and b) vegetated slope with a high roots quantity after the same rainfall period.

The minimum value of the slope safety factor was evaluated at different hydraulic states, starting from the partially saturated one and until failure occurred within the bare soil (Figure 61).

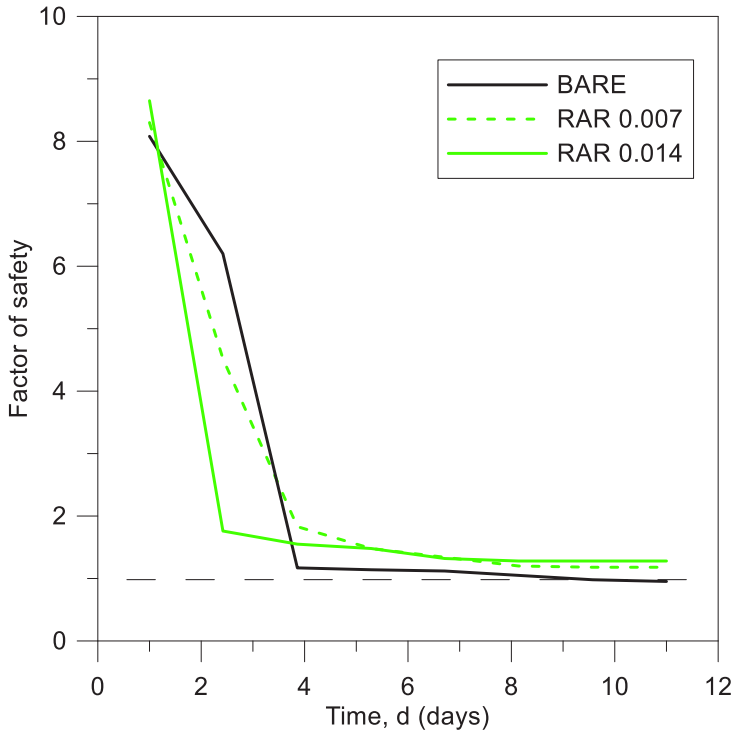

Figure 61 Evolution of the minimum safety factor for bare and vegetated slopes, during a rainfall

By comparing results of bare and root-permeated soil slope it was possible to trace the quicker drop in the value of the safety factor in the case of vegetated soil. This was due to the quicker evolution of interstitial pressure generated by the highest permeability of the vegetated slopes. As a result, the safety factor for the vegetated soil was, in an early stage of the rainfall event, lower than that for bare soil. Finally, vegetated slopes remained at a safety factor higher than the unity even when the slopes were under hydraulic stationary conditions. The bare slope finally was below this value.

Roots were proven to be mechanically beneficial for a slope, but more attention has to be paid to their hydraulic negative effects on slope stability.

6. Conclusions

Along the thesis, a complete geotechnical characterization of a partially saturated compacted silty sand with roots was carried out. Moreover, some techniques coming from agronomic engineering were used to geometrically and mechanically characterize the plant roots carefully retrieved from tested soil samples. Experimental results allowed achieving an important advance in the state-of-the-art knowledge of the following aspects: a) combined effects of suction and roots on soil hydro-mechanical response, b) relationship between effects produced by roots on soil at the microscale and behaviour observed at the macroscopic level, and c) implementation of the main roots features within constitutive laws for partially saturated soils, to predict vegetated hydraulic soil response.

In the following Sections, a more detailed explanation will be given on the conclusions drawn from each specific topic dealt with in the different Chapters of the thesis.

6.1 Preparation and testing protocol of samples

A protocol has been followed and systematically adopted both to generate plant growth within compacted large-size samples and to test bare and vegetated soil starting from the same initial conditions. Soil samples for experiments, in this Thesis, were always compacted at the same state and maximum vertical stress (e, w, s, $\sigma_{v,max}$) to facilitate the comparison of different laboratory tests, as well as to represent the initial conditions of a large-scale on-site experiment (instrumented vegetated embankment). After compaction, plants were left to grow in the soil, paying particular attention to seeding density and plant spacing: these parameters are influencing roots competition and development and are, at the same time, representative of the number of seeds used on-site for the plant cover of the above-mentioned large-scale experiment (Oorthuis et al. (2018)). The soil was then wetted to favour roots development, and then tested following a drying path to the target initial state. Advanced techniques were also used to characterize roots geometrical and mechanical properties, allowing to better interpret experimental geomechanical results.

6.2 Roots effects on soil micro-structure

Two advanced and complementary techniques (mercury intrusion porosimetry and X-ray micro-tomography) were adopted to quantitatively analyse the effects produced by the growth of different amounts of roots on the pore size distributions of the soil. Two main phenomena have been observed: clogging of small pores (pore size approx.: 2 μm) due to root hairs and mucilage, and pore size and volume enlargement (fissuring, pore size approx.: 200 μm) induced by roots growth and physiology. The evolution of these phenomena was followed at different hydraulic states. It was observed that, for the same number of roots, the volume of fissures tends to increase for the drier conditions. This volume increase was formalised and linked to roots volume by implementing this plant trait in a well-established equation for partially saturated double-porosity soil.

6.3 Geotechnical characterization of a vegetated soil

A complete geotechnical characterization of the vegetated lightly compacted soil has been carried out. Different plants growing periods were considered for preparing and running experiments. Roots enhanced soil water permeability while decreased retention properties: results appeared to be linked to the number of roots found in the tested samples, but they were hardly explainable, at the phenomenological scale. However, they were consistent with the observations gathered at soil micro-scale: fissures and interfaces generated by roots contributed to enhance soil permeability and to decrease suction generated by capillary effects. More complex chemical interactions, linked to roots mucilage and reduction of water surface tension in the rhizosphere contributed to develop, in the vegetated soil, suctions smaller than those measured in the bare soil, at the same water content. Large size equipment (triaxial cells, oedometer, direct shear box, tensile test prototype) were used to study the changes in soil mechanical response generated by roots. It was observed that roots were enhancing soil yielding stress, thanks to different roots failure mechanisms: pull-out and breakage. The former more likely to happen within a moist soil, the latter within a dry soil. These different mechanisms were responsible for different soil stress-strain response, depending on soil hydraulic state. Soil structure had an influence on soil mechanical behaviour too: fissures generated by roots contributed to produce larger compression volumetric strains in soil during the

shearing stage. Moreover, the partial loss of contact between soil and roots, generated by fissures, reduced the reinforcing capacity of the roots themselves (loss of the frictional component developing during roots pull-out and exploitation of the mere roots tensile strength). This last roots/suction coupled effect has influenced particularly the results of direct tensile tests, from which apparent cohesion was estimated using Mohr-Coulomb's failure criterion. Roots produced a greater beneficial effect, in terms of cohesion, when the soil was moist. After drying, roots reinforcement has been slightly counterbalanced by the negative effect produced due to fissures opening.

6.4 Constitutive model to predict a vegetated soil retention curve

Information gathered at soil microscale was used to adapt a well-established model, to predict the change in fissures volume as a function of root length density and suction changes. Constitutive expressions were incorporated into a model developed in literature to predict retention curve for double-porosity soils. The resulting framework was validated with the retention curves obtained in the Thesis, for different samples and different roots quantities. Statistical analyses confirmed the good quality of the model in predicting results obtained at the macroscopic level. It is believed that the model predicting fissures may be easily extendible to other plant species since it is depending on a root trait (root length density), which is indicating the quantity of soil-roots interfaces generated. These interfaces are supposed to have a direct effect on fissure volume in soil.

6.5 Simulation of the HM response of a vegetated slope submitted to water content changes

Data coming from the hydro-mechanical characterization carried out in the thesis was used to simulate the response of bare and vegetated slopes during a wetting event. Responses of soil after different plants growing times were also simulated. In vegetated soil, especially in the one with the higher roots normalized volume, a drastic drop in the slope safety factor was observed at the first stages of the hydraulic event. In the same period, the minimum safety factor of the bare slope remained higher. At complete saturation, bare slope failed (FS<1) while vegetated soil remained safe. This response

was generated by the complex hydro-mechanical behaviour that roots generated in the soil, as observed in the laboratory. The increase of permeability produced by roots, facilitated and accelerated the increase of pore water pressures within the slope and, consequently, the decrease of soil effective stresses and shear strength. Engineers and scientists must be aware of these possible responses when designing earthworks and investigating roots reinforcement.

6.6 Applications to engineering problems

In view of the potential use of plants in an engineering project and as ground improvement technique, from this thesis work, it can be deduced that:

- Although plants create a certain mechanical reinforcement on the ground, roots may cause fissures – mainly on drying – that reduce the whole reinforcement efficiency and affect the hydraulic behaviour of soil, with negative effects on the development of pore water pressures.
- it is advisable to achieve higher levels of compaction in the soil of the work, such as to increase the value of energy needed by roots to create fissures in the matrix; nevertheless, the pore size of the compacted material should be adequate for the development of roots (macro-pores within a size range of 200-300 μm) .
- It is advisable the use of plant species which develop fine and thin roots, with diameters that generally remain constant in size throughout their life and development. This aspect, coupled with a good compaction level, may induce roots to mainly “steal voids” either than creating fissures.
- The process of occupying/clogging voids by roots and their mucilage should be then “engineered” to maximize roots reinforcement potential while not degrading soil hydraulic properties too much.
- Special maintenance is recommended for works already covered by vegetation: a geometrical and mechanical characterization of the involved plant roots is fundamental to interpret the overall soil hydro-mechanical behaviour. In the case that pore water pressure and/or settlements observed

in the structure are higher than expected, it is reasonable to attribute these effects to root growth and to act accordingly.

6.7 Thesis contribution

The results of the investigation will contribute to increase the available experimental data of partially saturated soils characterization, both for the bare and the vegetated conditions. Specifically, the results highlighted the main positive and negative aspects of the use of plants in geotechnical engineering works. The thesis will be used as a basis for future lines of research in the development of hydro-mechanical constitutive models and the modelling of compacted soils with different quantities and types of roots.
Results may be useful in the assessment of slopes stability with vegetated soil subjected to ground-atmosphere interactions, in projects involving the use of materials in which root develop (road and canal embankments, flood protection embankments), as well as in the choice of adequate parameters to assign to vegetated partitions in regional-scale early warning systems for landslides.
Finally, the thesis provides a systematic methodology to perform a complete hydro-mechanical geotechnical characterization of a soil with roots.

6.8 Future lines of research

Some points still missing to fully characterize roots effects on the hydro-mechanical behaviour of compacted silty soils are:

- the effects of different initial compaction maximum stress and state on roots development and consequent changes of soil response: higher or lower water content, higher or lower initial dry density.
- the effects of different hydro-mechanical paths on soil shear strength and plant physiology: drying and wetting cycles, different mechanical impedance on roots development.
- the effects of different plants on soil hydro-mechanical response: volume of fissures generated, hydraulic conductivity, shear strength response, volume change behaviour.

- assessing the anisotropy of soil hydro-mechanical response due to roots growth and structural changes generated.
- simulating the coupled hydro-mechanical behaviour of vegetated soil during laboratory/field experiments using advanced techniques (DEM/FEM analyses) and including roots stress-strain behaviour.

7. Résumé détaillé en français

Cette thèse a reçu le soutien de la Commission européenne via le projet Marie Skłodowska-Curie Innovative Training Networks (ITN-ETN) TERRE "Training Engineers and Researchers to Rethink geotechnical Engineering for a low carbon future" (H2020-MSCA-ITN-2015-675762).
De plus elle a fait l'objet d'une collaboration avec le projet national espagnol SMUCPHY (Slope Mass-Wasting Under Climate Change).
La thèse a été menée conjointement dans deux centres de recherche : CIMNE (International Center of Numerical Methods in Engineering) à Barcelone, Espagne, et CIRAD (Recherche Agronomique pour le Développement) à Montpellier, France.

7.1 Contexte

Le réchauffement de la planète et l'approche de nombreux pays en matière de développement durable sur le plan environnemental posent de nouveaux défis aux ingénieurs. Dans le domaine de l'ingénierie géotechnique, par exemple, les changements climatiques contribuent à l'augmentation des glissements de terrain et des phénomènes d'érosion, qui résultent de précipitations isolées et très intenses suivies de longues périodes de sécheresse (Alonso et al. (2003) ; Alvioli et al. (2018) ; Cui et al. (2013) ; Vardon (2014). Ces phénomènes entraînent chaque année des pertes socio-économiques importantes. Des solutions géotechniques écologiquement durables consistent à contrecarrer ces phénomènes par des actions de revégétalisation ou de gestion raisonnée des écosystèmes existants. En effet les plantes, et en particulier via leurs racines, affectent le comportement hydromécanique global des sols avec dans la plupart des cas un impact positif sur leur stabilité.
La plupart des ouvrages en terre artificiels existants sont végétalisés. Dans certains cas les plantes y poussent spontanément, dans d'autres cas elles y sont semées par des entreprises spécialisées (Naturalea ; Prati armati ®). Cependant, il n'existe pas de

réglementation spécifique qui guide les sociétés de conseil et les entrepreneurs dans le processus de construction, d'entretien et de prévision de la réponse globale de l'ouvrage lors de l'interaction avec l'atmosphère et la végétation. Par conséquent, les effets (positifs et négatifs) de la végétation sont souvent négligés au stade de la conception de ces travaux car ils sont difficiles à prévoir. En ce sens, la recherche scientifique est nécessaire pour comprendre et quantifier ces effets, proposer des protocoles et des méthodologies avancées, et produire des bases de données et des modèles qui permettent de caractériser et d'interpréter les effets des racines sur les propriétés géotechniques du sol. Ces connaissances et outils sont nécessaires à la conception des ouvrages, en particulier pour en caractériser les états limites ultimes et les états limites de fonctionnement.

De nombreuses études expérimentales sur les interactions sol-racine s'accordent sur le fait que les plantes améliorent les propriétés mécaniques du sol (par exemple, la résistance au cisaillement). Néanmoins, les protocoles observés dans la littérature pour préparer et tester les échantillons sont souvent profondément différents, difficiles à comparer et amenant des conclusions contradictoires.

7.2 But et objectifs

Dans ce cadre, le but général de la thèse est d'introduire les caractéristiques mécaniques et morphologiques des racines dans des lois de comportement de sols partiellement saturés et d'implémenter ces lois dans des simulateurs numériques pour prédire le comportement de sols végétalisés lors d'événements pluvieux.

Les objectifs spécifiques sont les suivants :

- Comprendre et quantifier les effets des plantes sur le comportement mécanique des sols : résistance au cisaillement et à la traction, changement de volume ;
- Évaluer le comportement hydraulique du sol en prenant en compte la présence de racines : propriétés de rétention et perméabilité ;
- Étudier les causes microscopiques du changement de comportement du sol généré par les racines des plantes ;
- Déterminer les caractéristiques morphologiques et mécaniques des racines des plantes étudiées qui affectent les processus hydro-mécaniques ci-dessus.

7.3 Matériaux et compactage du sol

Le sol pour cette étude a été prélevé dans le delta du fleuve Llobregat (Barcelone, Espagne). Il a été classé comme sable limoneux selon l'USCS. Sa distribution granulométrique est présentée dans la Figure 62. Le matériau a été tamisé à 9,5 mm (ASTM E11 (2017)) pour respecter les rapports entre le diamètre de l'échantillon et la taille maximale des grains indiqués dans les normes ASTM (ASTM D2435-M (2011) ; ASTM D7181 (2011)).

Le sol a été compacté statiquement dans des pots cylindriques en PVC (de différentes tailles, selon le type d'essai) au moyen d'une presse hydraulique, à une vitesse de déplacement égale à 0,5 mm/min. L'état initial est le point A de la Figure 63. Après compactage, le sol a été ensemencé avec du *Cynodon dactilon* (espacement des plantes = 30 mm, densité d'ensemencement = 34 g/m^2), une graminée, communément appelée Chiendent, déjà étudiée par plusieurs auteurs à des fins géotechniques (Chen et al. (2015) ; Leung, Garg, Coo, et al. (2015) ; Garg et al. (2015) ; Fraccica et al. (2019)). Tous les pots ont été arrosés jusqu'à une teneur en eau de w = 21% et une succion s = 5 kPa, contrôlée et surveillée par un tensiomètre à pointe céramique (T5x, UMS, München, Allemagne), pour permettre le développement des plantes (point B de la Figure 63). La variation potentielle du volume du sol lors du mouillage a été vérifiée par un pied à coulisse (précision 0,02 mm). Cette variation s'est avérée être négligeable. Lorsque les racines ont atteint la partie inférieure des pots (de 3 à 8 mois, selon la taille du spécimen), les spécimens ont été soumis à un séchage à l'air, dans une pièce à température et humidité relative contrôlées (T = 20 ± 1° C, RH = 50%). Les mesures ont été effectuées en atteignant les points intermédiaires entre B et C de la Figure 63. Des échantillons de sol nu ont été préparés selon la même procédure.

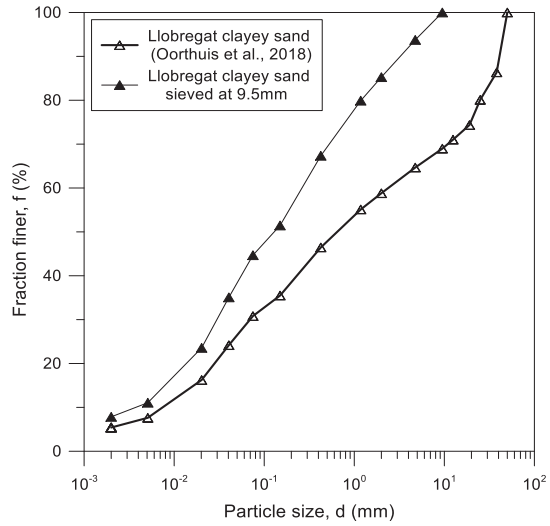

*Figure 62 : distribution de la taille des particules pour le sol testé dans la présente étude (sable limoneux du Llobregat tamisé) (*Oorthuis et al. (2018)*).*

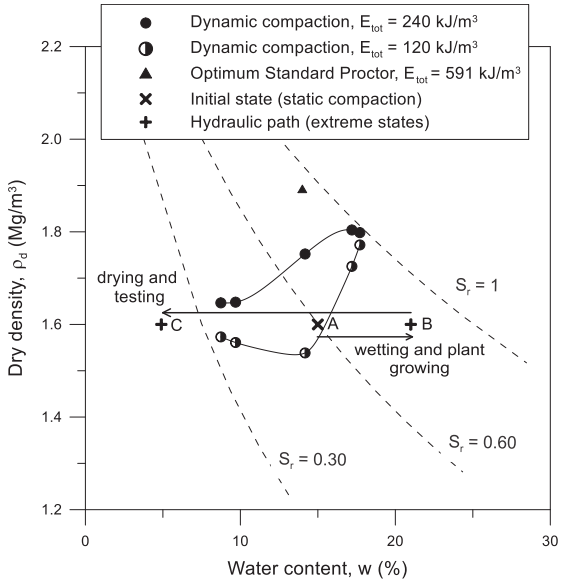

Figure 63 : État initial de compactage pour les échantillons testés (point A), et courbes de compactage à faible énergie. Parcours hydraulique suivi après compactage : mouillage (de A vers B), croissance et séchage des plantes (de B vers C) avant le test.

7.4 Comportement hydraulique du sol avec les racines

De nombreuses recherches ont concerné l'effet des plantes sur les propriétés hydrauliques des sols. Smethurst et al. (2012) ont constaté une augmentation de la perméabilité des remblais argileux végétalisés ; Ng et al. (2014) ont montré que les sols

argileux compactés à différentes densités ont des comportements de rétention d'eau contrastés en présence de racines tandis que Pagano et al. (2019) n'ont pas observé d'effets pertinents des plantes dans un sol limoneux à haute porosité. En effet, la densité, les contraintes maximales subies par la matrice et la teneur en eau imposent des contraintes sur le diamètre, le volume et la longueur des racines et sur leur capacité à ouvrir des fissures et/ou à boucher les pores (Kolb et al. (2017)). Vergani et Graf (2016) ont montré que la végétation augmentait généralement la perméabilité saturée pendant toute la durée du stade de croissance (de 1 à 8 mois). Ng et al. (2016) ont proposé un modèle dépendant d'un paramètre géométrique des racines (rapport de volume des racines R_v) pour considérer l'obstruction des pores et ses conséquences hydrauliques sur le sol tandis que Ni et al. (2019) ont analysé l'impact de la croissance et de la décomposition des plantes sur le comportement hydraulique global du sol. Ng et al. (2019) ont observé que l'espacement des plantes peut également affecter la croissance des racines et le comportement hydraulique du sol. Toutes ces observations mettent en évidence des résultats contradictoires. En outre, les caractéristiques macroscopiques des sols végétalisés (rétention d'eau, perméabilité) sont rarement liées aux interactions sol-racine à l'échelle microscopique qui, de plus, n'ont été décrites que de manière qualitative. La présente étude vise à étudier conjointement les effets chimico-hydro-mécaniques des racines sur le sol à différentes échelles et l'influence que les états hydro-mécaniques du sol (changements de porosité et de succion) ont sur la microstructure et l'enracinement des plantes.

7.4.1 Caractéristiques des racines affectant le comportement hydraulique

Le volume des racines est, pour cette étude, un paramètre fondamental pour comprendre le comportement hydro-mécanique d'un sol végétalisé, dans lequel la taille et le volume des pores jouent un rôle majeur. Il a donc été nécessaire d'évaluer ce trait structurel des racines par des techniques destructrices (picnométrie et WinRhizo) et non destructrices (microtomographie à rayons X), pendant et après d'autres essais géotechniques. La Figure 64 présente une comparaison des valeurs de volume des racines obtenues par les trois techniques, montrant de bonnes corrélations statistiques entre les mesures.

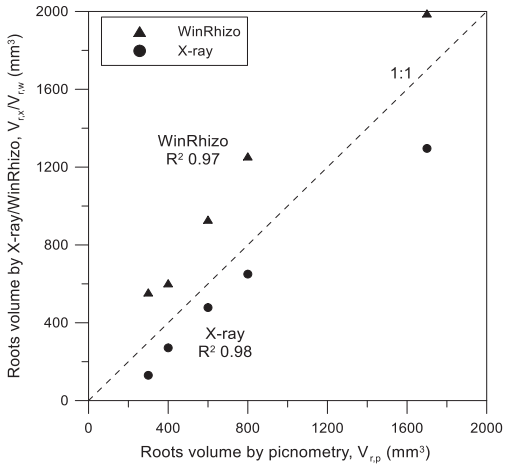

Figure 64 Comparaison des valeurs du volume des racines obtenues à partir de microtomographie rayon X, WinRhizo et picnométrie.

7.4.2 Comportement hydraulique à la macro-échelle

Trois échantillons de sol contenant des racines et un échantillon de référence (sol nu) ont été utilisés pour déterminer les courbes de rétention d'eau. La succion matricielle et la succion totale ont été évaluées respectivement par un tensiomètre de laboratoire à pointe céramique (T5x, UMS, München, Allemagne), jusqu'à 0,20 MPa, et un hygromètre (WP4, Decagon Devices, Pullman, WA, USA), à partir de 0,50 MPa. Après chaque phase de séchage, qui a duré 30 minutes, des échantillons de sol ont été placés pendant 24 heures dans des dessiccateurs en verre à l'intérieur d'une pièce à température et humidité relative contrôlées (T = 20±1°C, HR = 50%), à la lumière naturelle, pour permettre un équilibrage de la succion et de la teneur en eau. Les spécimens avec racines ont été laissés dans l'obscurité pendant au moins 2 heures pour provoquer la fermeture des stomates (Snyder et al. (2003)) et pour arrêter complètement le processus de transpiration de la plante (Howard et al. (2009)). La transpiration induit des gradients hydrauliques au sein de la matrice (Aylmore (1993)). Après cette période, le tensiomètre a été placé dans les spécimens jusqu'à une profondeur égale à leur demi-hauteur (35 mm). Une comparaison des mesures obtenues et des courbes de séchage modélisées pour des échantillons nus et végétalisés est présentée à la Figure 65. La valeur du ratio du volume des racines dans les pots est indiquée dans le graphique. Il a été observé que la valeur d'entrée dans l'air et la capacité de rétention du sol végétal ont diminué. De plus, ce phénomène est accentué dans les spécimens contenant une plus grande quantité

de racines. Enfin, toutes les mesures de rétention convergent vers une succion proche de 3 MPa.

Ce type de comportement a été observé par Ng et al. (2014), pour un sol légèrement compacté ensemencé avec la même plante que celle utilisée dans notre étude.

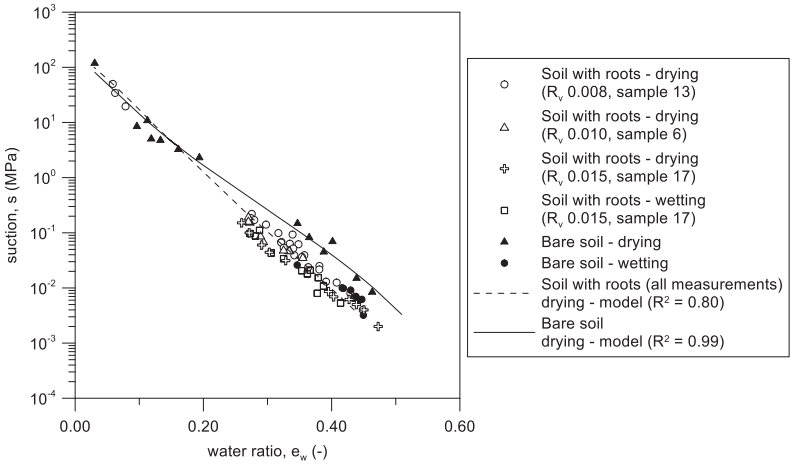

Figure 65 : principales courbes de séchage pour les sols nus et comportant des racines. Mesures effectuées avec le tensiomètre T5x et le psychromètre WP4.

Un échantillon de sol nu et un échantillon contenant des racines ont été testés dans de grandes cellules oedométriques (ASTM D2435-M (2011), 150 mm de diamètre, 70 mm de hauteur). Un échantillon avec racines a également été testé dans un perméamètre (ASTM D5084 (2003)) pour évaluer la perméabilité du sol saturé avant et après la croissance des plantes. Les plantes ont été laissées pendant 3 mois dans l'équipement. Les résultats ont montré qu'à l'échelle macro la croissance des racines augmentait la perméabilité du sol à l'eau. Dans tous les cas, la perméabilité des sols végétalisés tend à se rapprocher des valeurs du sol nu à mesure que la porosité du sol diminue.

7.5 Observations à la micro-échelle

Les racines affectent la structure du sol en raison de différents processus tels que l'obstruction chimique et physique des pores et la fissuration du sol due à leur croissance et à leur développement. Les domaines concernés par ces phénomènes correspondent bien aux domaines de porosité qui peuvent être étudiés par les deux techniques utilisées : la porosimétrie par intrusion de mercure et la microtomographie à rayons X.

La microtomographie a donné un premier aperçu qualitatif du phénomène qui se produit. La reconstruction 3D des racines et des pores dans l'échantillon de sol a mis en évidence que les racines sont souvent entourées de fissures. Les caractéristiques des pores ont été quantifiées à l'aide du traitement d'image. La porosimétrie par intrusion de mercure a permis d'étudier la taille des pores de 7 nm à 400 µm, ce qui n'était pas possible à observer avec la microtomographie.

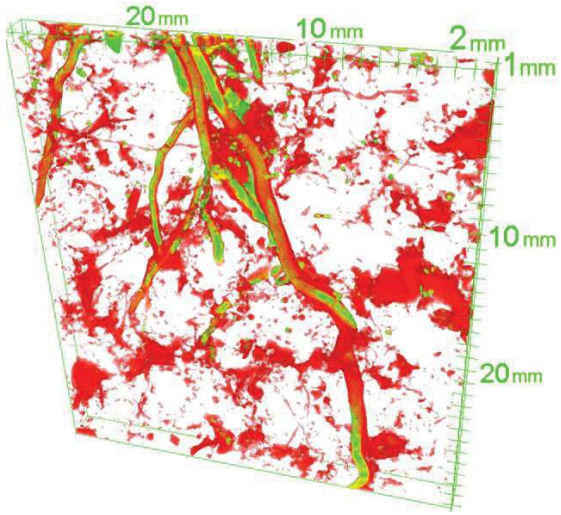

Figure 66 : plan 2D extrait d'une représentation 3D des racines (jaune) et des pores (rouge)

7.5.1 Effets des racines sur la distribution de la taille des pores

Les résultats de la microtomographie et de la porosimétrie par intrusion de mercure ont été réunis afin de construire les distributions de taille des pores caractéristiques du sol nu et du sol végétalisé. Comme on peut le voir sur la Figure 67, la plupart des pores du sol végétal entre 5 et 100 µm apparaissent réduits en volume par rapport au sol nu. Ceci est dû à un effet combiné de colmatage chimique et physique, par exemple lié à la production de mucilage qui augmente lors du séchage (Watt et al. (1994)). Les porosités supérieures à 100 µm mettent plutôt en évidence des densités de taille de pores et des pics de diamètre de pores plus élevés, dus aux fissures générées par les racines.

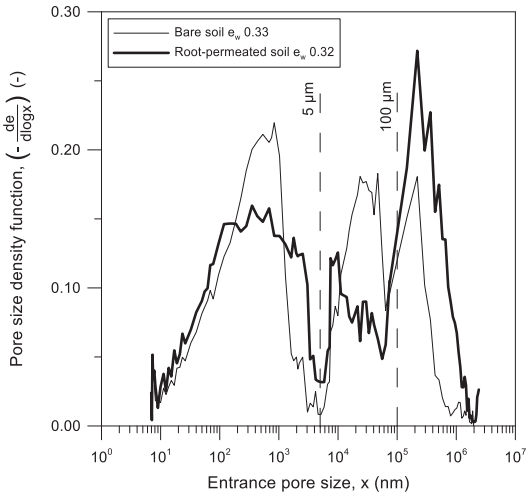

Figure 67 : fonctions de densité de la taille des pores pour un sol nu et un sol végétalisé

7.6 Prévision du comportement hydraulique du sol à partir d'observations microscopiques

Les distributions de la taille des pores ont été utilisées pour évaluer les courbes de rétention d'eau du sol. Pour la partie de la courbe obtenue par le MIP, la succion a été calculée à partir des valeurs de pression de mercure obtenues pour chaque étape d'intrusion, selon Romero et al. (1999), en supposant que le processus d'intrusion de mercure soit similaire à l'intrusion d'air, pendant un trajet de séchage. Pour la partie de la courbe obtenue par microtomographie aux rayons X, la succion a été déduite par l'équation de Young-Laplace, en supposant que la succion n'est générée que par les effets capillaires dans cette gamme de grandes porosités. Le degré de saturation de la phase gazeuse a été calculé comme le rapport entre le taux de vide cumulé à un diamètre de pore donné et le taux total (Romero et al. (1999)). La phase aqueuse a été calculée à partir du degré de saturation de la phase gazeuse, puis convertie en rapport d'eau (Romero et al. (1999)). Les résultats ont été tracés conjointement avec les mesures de rétention du sol (Figure 68).

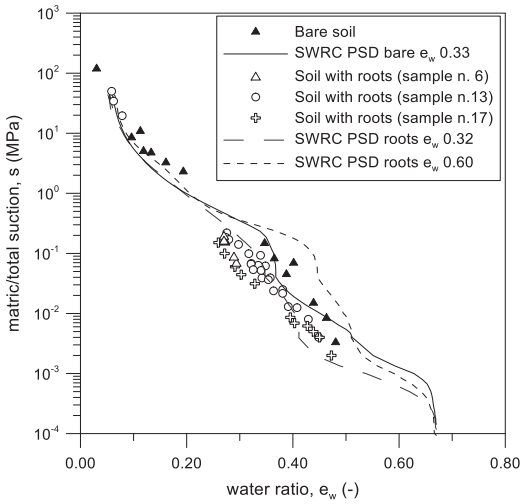

Figure 68 : SWRC du sol nu et d'échantillons comportant des racines, mesuré par tensiomètre et psychromètre et calculé à partir de la distribution de la taille des pores

7.7 Comportement mécanique du sol avec des racines

7.7.1 Essais de compression triaxiale

Des essais de compression triaxiale ont été réalisés sur des sols avec et sans racines, à l'aide d'un équipement permettant de tester de grands échantillons (Φ 200 mm et h 400 mm). Les échantillons de sol ont d'abord été laissés au séchage jusqu'à la teneur en eau souhaitée, puis emballés dans un film plastique pendant 24 heures pour permettre l'égalisation de la teneur en eau et de la succion. Avant la compression triaxiale, les échantillons ont été soumis à une consolidation isotrope. Le confinement était imposé par la pression de l'air, contrôlée par un transducteur de pression. L'étape de consolidation était considérée comme terminée lorsque la vitesse de déformation volumétrique observée dans l'échantillon était inférieure à 0,1 %/jour. Une compression triaxiale drainée a été effectuée avec contrôle du déplacement (taux de déplacement = 0,016 mm/min) et à teneur en eau constante. Les déplacements axiaux et radiaux dans le sol ont été mesurés par un LVDT vertical et huit LVDT horizontaux.

7.7.2 Essais de traction directe

Un nouveau prototype expérimental a été conçu pour cette thèse afin de déterminer la résistance à la traction du sol. Il est constitué de deux cylindres indépendants en ABS

reliés par un pont (pièces orange sur la figure 69), qui est retiré après compactage pour démarrer l'expérience. Les cylindres sont fixés sur des rails de glissement avec un frottement calibré et minimisé. L'un d'eux est relié à un moteur et l'autre, à un capteur de force.

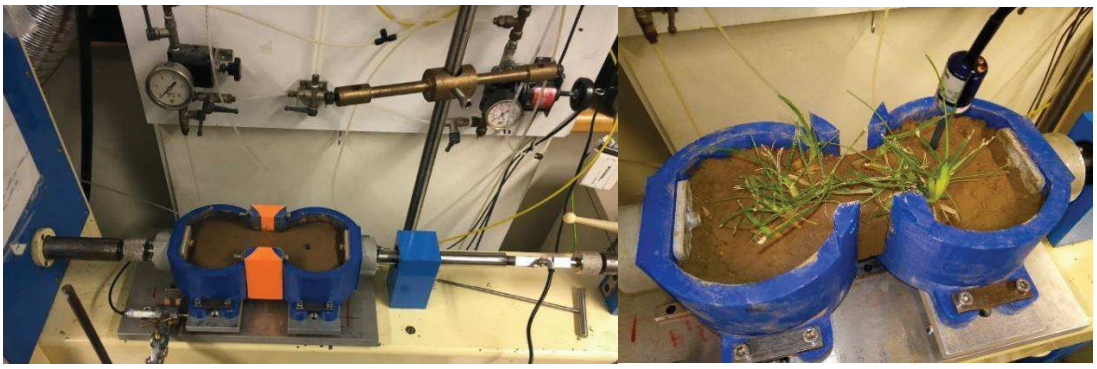

Figure 69 : équipement d'essai de traction dans sa configuration initiale, avant le test. A) : à gauche le moteur à déplacement contrôlé et le LVDT horizontal, à droite le capteur de force. B) dispositif avec sol végétalisé, après enlèvement des supports de pont.

7.7.3 Loi de comportement du complexe sol-racines

Les résultats provenant des essais de compression triaxiale et de traction directe seront interprétés selon le critère de rupture pour les sols partiellement saturés formulé par Cárdenas (2018) :

$$\tau_f = c'_0 + (\sigma - u_a)tan\varphi' + \frac{s}{a + bs} \quad (33)$$

et par Alonso et al. (2010) :

$$\tau_f = c'_0 + (\sigma - u_a)tan\varphi' + S_r^e s\ tan\varphi' \quad (34)$$

où la cohésion apparente en fonction de la succion devient :

$$c'(s) = c'_0 + S_r^e s\ tan\varphi' \quad (35)$$

dans lequel le degré de saturation effectif est $S_r^e = (S_r)^\alpha$ avec α comme paramètre matériel.

Une adaptation au modèle proposé par Wu et al. (1979) a été adoptée pour interpréter et modéliser le comportement des sols végétalisés :

$$c'_{0,roots} \approx \gamma * \sigma_{t,roots,aver.} * RAR \quad (36)$$

où γ est un paramètre dépendant du type de plante, $\sigma_{t,roots,aver.}$ est la résistance moyenne à la traction des racines et RAR est le rapport de la surface des racines (A_{roots}/A_{soil}). Ce

dernier paramètre est utilisé dans la littérature pour quantifier la quantité de racines dans la matrice du sol.

7.7.4 Résultats des essais de compression triaxiale

La Figure 70 montre les enveloppes de rupture obtenues en analysant les résultats des tests de compression triaxiale. Elles ont été calibrées par la méthode des moindres carrés pour l'angle de frottement et la cohésion à succion nulle c'(0).

L'évolution de la cohésion apparente calculée avec les deux lois est illustrée à la Figure 71. Dans la légende de la figure, les paramètres calibrés pour les deux lois sont indiqués. La cohésion calibrée à succion nulle était c'(0) = 0 kPa dans le sol nu alors que des valeurs de cohésion plus élevées (c'(0) = 9-10 kPa) ont été calibrées pour le sol végétalisé.

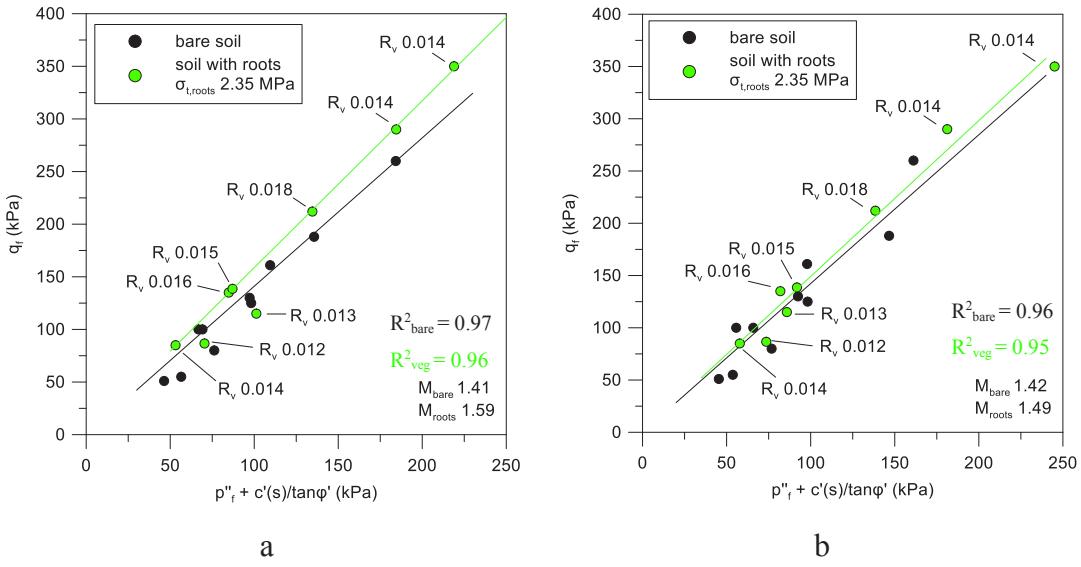

Figure 70 : enveloppes de rupture calculées pour les sols avec et sans racines avec deux lois d'évolution de la cohésion différentes : a) modèle hyperbolique de Cárdenas (2018) et b) (Alonso et al., 2010).

7.7.5 Résultats des essais de traction directe

Les résultats des essais de traction des sols végétalisés ont été analysés à deux étapes de croissance (1 et 3 mois respectivement). A 1 mois, les échantillons ont présenté un RAR moyen de 0,001±0,0001 alors qu'à 3 mois le RAR moyen était de 0,007±0,002.

Afin de comparer ces résultats avec ceux obtenus dans les essais de compression triaxiale, la cohésion apparente a été calculée à partir des valeurs de résistance à la traction, à l'aide de la formule :

$$c'(s) = \sigma_t(s) tan\varphi' \quad (37)$$

dérivée du critère de rupture de Mohr-Coulomb (Coulomb (1776) ; Mohr (1900)). L'angle de frottement utilisé a été calibré par les essais de compression triaxiale.

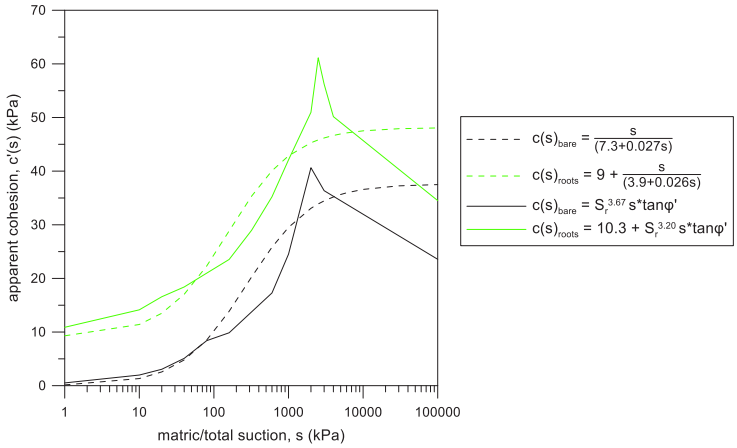

Figure 71 : évolution de la cohésion apparente calculée par des essais de compression triaxiale dans un sol avec et sans racines, et avec deux lois d'évolution de la cohésion en fonction de la succion et du degré de saturation.

Connaissant les valeurs moyennes de la teneur en eau et de la porosité dans les différents tests, il a été possible de calculer le degré de saturation de chaque échantillon. Pour chaque test avec un sol végétalisé, le rapport de surface des racines (RAR) et la résistance moyenne à la traction des racines étaient également connus ($\sigma_{t,roots,aver.}$ = 4,8MPa pour les échantillons avec RAR = 0,001 et $\sigma_{t,roots,aver.}$ = 3,5MPa pour les échantillons avec RAR = 0,007). Ainsi, seules les valeurs α, γ et les valeurs d'*a* et *b* indiquées dans les équations 33 et 36 ont été calibrées pour les sols végétalisés par la méthode des moindres carrés. Pour le sol nu, la valeur de c_0 a également été calibrée, mais la valeur obtenue était proche de zéro.

Pour la loi proposée par Alonso et al. (2010), les valeurs de α calibrées étaient comprises entre 3,3 et 4,01. Ces valeurs sont conformes à celles observées dans la littérature (Alonso et al. (2010)) pour des sols ayant des caractéristiques physiques similaires à celles du sol étudié (sols argileux). Les valeurs calibrées de γ étaient d'environ 0,30 et bien en dessous de la valeur de 1,2 prédite par Wu et al. (1979). Cela indique que γ

pourrait dépendre de plusieurs facteurs tels que le type de plante, la géométrie des racines, le type de sol, sa teneur en eau.

Les deux modèles constitutifs utilisés ont donné de bonnes corrélations avec, pour la loi donnée par Alonso et al. (2010), $R^2 = 0,97$ (sol nu), $R^2 = 0,93$ (sol végétalisé, RAR ≈ 0,001), $R^2 = 0,93$ (sol végétalisé, RAR ≈ 0,007)), et pour la loi de Cárdenas (2018) $R^2 = 0,99$ (sol nu), $R^2 = 0,99$ (sol végétalisé, RAR ≈ 0,001), $R^2 = 0,94$ (sol végétalisé, RAR ≈ 0,007)). L'utilisation du modèle donné par Alonso et al. (2010) est préférable car il inclut des informations provenant des effets que les racines induisent sur le comportement de rétention (degré de saturation et succion). Ce modèle est donc plus complet même s'il est plus complexe.

7.8 Conclusions et perspectives

Une caractérisation géotechnique complète de sols végétalisés a été réalisée. Différentes périodes de croissance des plantes ont été prises en compte pour la préparation et la réalisation des expériences. Dans les conditions de cette étude, les racines augmentent la perméabilité à l'eau du sol tout en diminuant ses propriétés de rétention. Les résultats semblent être liés au nombre de racines présentes dans les échantillons testés, mais ils sont difficilement explicables à l'échelle phénoménologique. Ils étaient cependant cohérents avec les observations recueillies à la micro-échelle du sol. Ces dernières ont mis en évidence que les fissures et les interfaces générées par les racines contribuent à rehausser la perméabilité du sol et à diminuer la succion générée par les effets capillaires. Des interactions chimiques plus complexes, liées au mucilage des racines et à la réduction de la tension superficielle de l'eau dans la rhizosphère, ont contribué à développer, dans le sol végétalisé, des succions plus faibles que celles mesurées dans le sol nu, à teneur en eau égale. Des équipements de grande taille (cellules triaxiales, œdomètre, caisse de cisaillement direct, prototype de test de traction) ont été utilisés pour étudier les changements de la réponse mécanique du sol générés par les racines. Il a été observé que les racines amélioraient la résistance du sol, grâce à différents mécanismes de rupture des racines : arrachement et rupture. Le premier est plus susceptible de se produire dans un sol humide, le second dans un sol sec.

Les outils fournis par la thèse sont :

- Une loi constitutive capable de prédire le comportement hydraulique du sol en fonction du volume des racines. Cette loi est potentiellement utile pour les agronomes ;
- Une loi constitutive capable de prédire le comportement mécanique du sol en fonction de la surface des racines, de leur résistance à la traction et de leurs effets sur la réponse hydraulique. Cet outil est potentiellement utile pour les ingénieurs qui veulent prédire la résistance au cisaillement de sols végétalisés.

Les perspectives de ces recherches sont :

- Prendre en compte l'interaction sol-végétation-atmosphère dans la modélisation ;
- Évaluer l'anisotropie des caractéristiques hydromécaniques du sol due à la présence de racines ;
- Évaluer l'influence de l'état initial de compactage du sol sur le développement des racines ;
- Évaluer l'influence des cycles d'assèchement et d'humidification sur le comportement d'un sol végétalisé ;
- Mettre à l'échelle des tests de laboratoire aux conditions *in situ* en utilisant les caractéristiques des racines (rapport de volume des racines, longueur, diamètres) ;
- Réaliser des analyses numériques couplées hydro-mécaniques avec des méthodes aux éléments finis ou discrets incluant l'hydraulique du sol et des racines et le comportement en contrainte-déformation pour des applications réelles (pentes, effondrements, atténuation de l'érosion, prévention du rétrécissement...).

References

Albrecht, B. and Benson, C.H. (2001) 'Effect of Desiccation on Compacted Natural Clays', *J. Geotech. Geoenvironmental Eng.* 127, 67–75

Alonso, E.E., Gens, A. and Delahaye, C.H. (2003) 'Influence of rainfall on the deformation and stability of a slope in overconsolidated clays: a case study', *Hydrogeol. J.* 11, 174–92

Alonso, E.E., Gens, A. and Josa, A. (1990) 'A constitutive model for partially saturated soils', *Géotechnique* 40, 405–30

Alonso, E.E., Pereira, J.M., Vaunat, J. and Olivella, S. (2010) 'A microstructurally based effective stress for unsaturated soils', *Géotechnique* 60, 913–25

Alvarado de Menéndez, C.E. (2017) 'Comportamiento hidro-mecánico de agregados gruesos', Universitat Politècnica de Catalunya - PhD Thesis

Alvioli, M. et al. (2018) 'Implications of climate change on landslide hazard in Central Italy', *Sci. Total Environ.* 630, 1528–43

Andò, E.C.G. (2013) 'Experimental investigation of microstructural changes in deforming granular media using x-ray tomography Experimental investigation of micro- structural changes in deforming granular media using x-ray tomography',

Anselmucci, F. et al. (2019) 'Root-reinforced sand: kinematic response of the soil', in A. Tarantino and E. Ibraim (eds), *IS-Glasgow* (Glasgow) 12011

Arganda-Carreras, I., Kaynig, V., Rueden, C. and et al. (2017) 'Trainable Weka Segmentation: a machine learning tool for microscopy pixel classification', *Bioinformatics* 33,

ASTM D2216 (2019) 'Standard Test Methods for Laboratory Determination of Water (Moisture) Content of Soil and Rock by Mass' [Online] Available at: www.astm.org

ASTM D2435-M (2011) 'Standard test method for one-dimensional consolidation properties of soils' [Online] Available at: www.astm.org

ASTM D4751 (2020) 'Standard Tests Methods for Determining Apparent Opening Size of a Geotextile' [Online] Available at: www.astm.org

ASTM D5084 (2003) 'Standard Test Methods for Measurement of Hydraulic Conductivity of Saturated Porous Materials Using a Flexible Wall Permeamenter'

[Online] Available at: www.astm.org

ASTM D7181 (2011) ‘Method for Consolidated Drained Triaxial Compression Test for Soils’ [Online] Available at: www.astm.org

ASTM D7263 (2018) ‘Standard Test Method fo Laboratory Determination of Density (Unit Weigth) of Soil Specimens.’ [Online] Available at: www.astm.org

ASTM E11 (2017) ‘Standard Specification for Woven Wire Test Sieve Cloth and Test Sieves’ [Online] Available at: www.astm.org

Aylmore, L.A.G. (1993) ‘Use of Computer-Assisted Tomography in Studying Water Movement Around Plant Roots’, *Adv. Agron.* 49, 1–54

Beckett, C., Fourie, A. and Toll, D. (2016) ‘Water repellent soils: the case for unsaturated soil mechanics’, in P. Delage, Y.J. Cui, J.M. Pereira and A.M. Tang (eds), *E-UNSAT 2016* (Paris, France) 11011

Berger, M.J. et al. (2010) ‘XCOM: Photon Cross Sections Database’ [Online] Available at: www.nist.gov/pml/xcom-photon-cross-sections-database

Bishop, A.W. (1954) ‘The use of Pore Pressure Coefficients in Practice’, *Geotechnique* 4, 148–52

Boldrin, D., Leung, A.K. and Bengough, A.G. (2018) ‘Effects of root dehydration on biomechanical properties of woody roots of Ulex europaeus’, *Plant Soil* 431, 347–69

Borken, W. and Matzner, E. (2009) ‘Reappraisal of drying and wetting effects on C and N mineralization and fluxes in soils’, *Glob. Chang. Biol.* 15, 808–24

Cao, R., Jia, X., Huang, L., Zhu, Y., Wu, L. and Shao, M. (2018) ‘Deep soil water storage varies with vegetation type and rainfall amount in the Loess Plateau of’, 1–12

Cárdenas, O.E. (2018) ‘Estudio del comportamiento de colapso en arenas arcillosas bajo un estado generalizado de tensiones’, Universitat Politècnica de Catalunya, PhD thesis.

Carminati, A. et al. (2010) ‘Dynamics of soil water content in the rhizosphere’, *Plant Soil* 332, 163–76

Carminati, A., Benard, P., Ahmed, M.A. and Zarebanadkouki, M. (2017) ‘Liquid bridges at the root-soil interface’, *Plant Soil* 417, 1–15

Carminati, A., Vetterlein, D., Koebernick, N., Blaser, S., Weller, U. and Vogel, H.J.

(2013) ‘Do roots mind the gap ?’, *Plant Soil* 367, 651–61

Chen, F., Zhang, J., Zhang, M. and Wang, J. (2015) ‘Effect of Cynodon dactylon community on the conservation and reinforcement of riparian shallow soil in the Three Gorges Reservoir area’, *Ecol. Process.* 4, 3

Coppin, N.J. and Richards, I.G. (1990) *Use of Vegetation in Civil Engineering, Butterworths, London* (London)

Cordero, J.A., Useche, G., Prat, P.C., Ledesma, A. and Santamarina, J.C. (2017) ‘Soil desiccation cracks as a suction – contraction process’, 272–78

Coulomb, C.A. (1776) ‘Sur une application des regles maximis et minimis a quelques problems de statique, relatives a l’architecture’, *Acad. Sci. Paris Mem. Math. Phys* 7, 343–82

Cui, Y., Ta, A.N., Hemmati, S., Tang, A.M. and Gatmiri, B. (2013) ‘Experimental and numerical investigation of soil-atmosphere interaction’, 165, 20–28

Cui, Y.J. and Delage, P. (1996) ‘Yielding and plastic behaviour of an unsaturated compacted silt’, *Géotechnique* 46, 291–311

Dieudonné, A.-C., Levasseur, S., Charlier, R., Della Vecchia, G. and Jommi, C. (2013) ‘A water retention model for compacted clayey soils’, *3rd Int. Symp. Comput. Geomech. (ComGeo III)* 23–31

Divya, P. V, Viswanadham, B.V.S. and Gourc, J.P. (2014) ‘Evaluation of Tensile Strength-Strain Characteristics of Fiber-Reinforced Soil through Laboratory Tests’, *J. Mater. Civ. Eng.* 26, 14–23

Dougherty, B. (2007) ‘Computing Local Thickness of 3D Structures with ImageJ’ [Online] Available at: http://www.optinav.info/LocalThicknessEd.pdf

Fraccica, A., Romero, E. and Fourcaud, T. (2019) ‘Multi-scale effects on the hydraulic behaviour of a root-permeated and compacted soil’, in A. Tarantino and E. Ibraim (eds), *IS-Glasgow* (Glasgow) 12014

Fredlund, D.G. and Rahardjo, H. (1993) *Soil Mechanics for Unsaturated Soils*

Fredlund, D.G. and Xing, A. (1994) ‘Equations for the soil-water characteristic curve’, *Can. Geotech. J.* 31, 521–32

Garg, A., Coo, J.L. and Ng, C.W.W. (2015) ‘Field study on influence of root characteristics on soil suction distribution in slopes vegetated with Cynodon dactylon and Schefflera heptaphylla’, *Earth Surf. Process. Landforms* 40, 1631–

Garrigues, E., Doussan, C. and Pierret, A. (2006) ‘Water uptake by plant roots : I – Formation and propagation of a water extraction front in mature root systems as evidenced by 2D light transmission imaging’, *Plant Soil* 283, 83–98

van Genuchten, M.T. (1980) ‘A Closed-form Equation for Predicting the Hydraulic Conductivity of Unsaturated Soils’, *Soil Sci. Soc. Am. J.* 44, 892–98

Geoslope (2019) ‘Geoslope International Ltd., Calgary, Alberta, Canada’ [Online] Available at: www.geoslope.com

Ghestem, M., Veylon, G., Bernard, A., Vanel, Q. and Stokes, A. (2014) ‘Influence of plant root system morphology and architectural traits on soil shear resistance’, *Plant Soil* 377, 43–61

Gonzalez-Ollauri, A. and Mickovski, S. (2017) ‘Plant-soil reinforcement response under different soil hydrological regimes’, *Geoderma* 285, 141–50

Grierson, C. and Schiefelbein, J. (2002) ‘Root Hairs’, *Arab. B.* 1, 60–82

Hinsinger, P., Bengough, A.G., Vetterlein, D. and Young, I.M. (2009) ‘Rhizosphere: biophysics, biogeochemistry and ecological relevance’, *Plant Soil* 321, 117–52

Howard, A.R., Van Iersel, M.W., Richards, J.H. and Donovan, L.A. (2009) ‘Night-time transpiration can decrease hydraulic redistribution’, *Plant, Cell Environ.* 32, 1060–70

Interstate Plastics Inc., . (2019) ‘Interstate Plastics, Inc.’ [Online] Available at: interstateplastics.com

Ji, X. (2019) ‘GDS Triaxial Test on the Reinforcement Effects of Bermudagrass Root-soil Complex’, in *IOP Conference Series: Earth and Environmental Science* 304 032106

Jommi, C. (2000) ‘Remarks on the constitutive modelling of unsaturated soils’, in A. Tarantino and C. Mancuso (eds), *Experimental Evidence and Theoretical Approaches in Unsaturated Soils* 139–53

Jones, H.G. (2007) ‘Monitoring plant and soil water status: established and novel methods revisited and their relevance to studies of drought tolerance’, *J. Exp. Bot.* 58, 119–30

Karup, D., Moldrup, P., Tuller, M., Arthur, E. and de Jonge, L.W. (2017) ‘Prediction of the soil water retention curve for structured soil from saturation to oven-

dryness', *Eur. J. Soil Sci.* 68, 57–65

Koebernick, N. et al. (2017) 'High-resolution synchrotron imaging shows that root hairs influence rhizosphere soil structure formation', *New Phytol.* 216, 124–35

Kolb, E., Hartmann, C. and Genet, P. (2012) 'Radial force development during root growth measured by photoelasticity', *Plant Soil* 360, 19–35

Kolb, E., Legué, V. and Bogeat-Triboulot, M.B. (2017) 'Physical Root-Soil Interactions', *Phys. Biol.* 14, 1–40

Lakshmikantha, M.R., Prat, P.C. and Ledesma, A. (2012) 'Experimental evidence of size effect in soil cracking', 284, 264–84

Lamont, B. (1983) 'Root hair dimensions and surface/volume/weight ratios of roots with the aid of scanning electron microscopy', *Plant Soil* 74, 149–52

Legland, D., Arganda-Carreras, I. and Andrey, P. (2016) 'MorphoLibJ: integrated library and plugins for mathematical morphology with ImageJ', *Bioinformatics* 32, 3532–34

Leung, A.K., Garg, A., Coo, J.L., Ng, C.W.W. and Hau, B.C.H. (2015) 'Effects of the roots of Cynodon dactylon and Schefflera heptaphylla on water infiltration rate and soil hydraulic conductivity', *Hydrol. Process.* 29, 3342–54

Leung, A.K., Garg, A. and Ng, C.W.W. (2015) 'Effects of plant roots on soil-water retention and induced suction in vegetated soil', *Eng. Geol.* 193, 183–97

Liu, X.P., Zhang, W.J., Wang, X.Y., Cai, Y.J. and Chang, J.G. (2015) 'Root – soil air gap and resistance to water flow at the soil – root interface of Robinia pseudoacacia', *Tree Physiol.* 35, 1343–55

Manzoni, S., Schimel, J.P. and Porporato, A. (2012) 'Responses of soil microbial communities to water stress: results from a meta-analysis', *Ecology* 93, 930–38

Mickovski, S., Hallett, P.D., Bransby, M.F., Davies, M.C.R., Sonnenberg, R. and Bengough, A.G. (2009) 'Mechanical Reinforcement of Soil by Willow Roots: Impacts of Root Properties and Root Failure Mechanism', *Soil Sci. Soc. Am. J.* 73, 1276–85

Mickovski, S.B., Bengough, A.G., Bransby, M.F., Davies, M.C.R., Hallett, P.D. and Sonnenberg, R. (2007) 'Material stiffness , branching pattern and soil matric potential affect the pullout resistance of model root systems', *Eur. J. Soil Sci.* 58, 1471–81

Milleret, R., Le Bayon, R.C., Lamy, F., Gobat, J.M. and Boivin, P. (2009) 'Impact of roots, mycorrhizas and earthworms on soil physical properties as assessed by shrinkage analysis', *J. Hydrol.* 373, 499–507

Mohr, O. (1900) 'Welche Umstande bedingen die Elastizitatsgrenze und den Bruch eines Materials?', *Zeit des Ver Deut Ing* 44, 1524–30

Moradi, A.B. et al. (2011) 'Three-dimensional visualization and quantification of water content in the rhizosphere', *New Phytol.* 192, 653–63

Münch, B. and Lorenz, H. (2008) 'Contradicting Geometrical Concepts in Pore Size Analysis Attained with Electron Microscopy and Mercury Intrusion', *J. Am. Ceram. Soc.* 91, 4059–67

Murray, I. and Tarantino, A. (2019) 'Mechanisms of failure in saturated and unsaturated clayey geomaterials subjected to (total) tensile stress', *Geotechnique* 69, 701–12

Nam, S., Gutierrez, M., Diplas, P., Petrie, J., Wayllace, A., Lu, N. and Jorge, J. (2009) 'Comparison of testing techniques and models for establishing the SWCC of riverbank soils', *Eng. Geol.* 110, 1–10

Naturalea 'Naturalea' [Online] Available at: www.naturalea.eu

Ng, C.W.W., Leung, A.K. and Woon, K.X. (2014) 'Effects of soil density on grass-induced suction distributions in compacted soil subjected to rainfall', *Can. Geotech. J.* 51, 311–21

Ng, C.W.W., Ni, J.J. and Leung, A.K. (2019) 'The effects of plant growth and spacing on soil hydrological changes: A field study', *Géotechnique* Ahead of p,

Ng, C.W.W., Ni, J.J., Leung, A.K. and Wang, Z.J. (2016) 'A new and simple water retention model for root-permeated soils', *Géotechnique Lett.* 6, 106–11

Ni, J.J., Leung, A.K. and Ng, C.W.W. (2019) 'Modelling effects of root growth and decay on soil water retention and permeability', *Can. Geotech. J.* 56, 1049–55

Ohu, J.O., Raghavan, G.S.V., Prasher, S. and Mehuys, G. (1987) 'Prediction of water retention characteristics from soil compaction data and organic matter content', *J. Agric. Eng. Res.* 38, 27–35

Oorthuis, R., Hürlimann, M., Fraccica, A., Lloret, A., Moya, J., Puig-Polo, C. and Vaunat, J. (2018) 'Monitoring of a full-scale embankment experiment regarding soil-vegetation-atmosphere interactions', *Water (Switzerland)* 10, 688

Pagano, L., Reder, A. and Rianna, G. (2019) 'The effects of vegetation on the

hydrological response of silty volcanic covers', *Can. Geotech. J.* 56, 1261–77

Pang, W., Crow, W.T., Luc, J.E., McSorley, R., Giblin-Davis, R.M., Kenworthy, K.E. and Kruse, J. (2011) 'Comparison of Water Displacement and WinRHIZO Software for Plant Root Parameter Assessment', *Plant Dis.* 95, 1308–10

Pollen, N. (2007) 'Temporal and spatial variability in root reinforcement of streambanks: Accounting for soil shear strength and moisture', *Catena* 69, 197–205

Pornaro, C., Macolino, S., Menegon, A. and Richardson, M. (2017) 'WinRHIZO Technology for Measuring Morphological Traits of Bermudagrass Stolons', *Agron. J.* 109, 3007–10

Prati armati ® 'Prati armati ®' [Online] Available at: www.pratiarmati.it

Preti, F. and Giadrossich, F. (2009) 'Root reinforcement and slope bioengineering stabilization by Spanish Broom (Spartium junceum L.)', *Hydrol. Earth Syst. Sci.* 13, 1713–26

Prieto, I., Armas, C. and Pugnaire, F.I. (2012) 'Water release through plant roots: new insights into its consequences at the plant and ecosystem level', *New Phytol.* 193,

Read, D.B. et al. (2003) 'Plant roots release phospholipid surfactants that modify the physical and chemical properties of soil', *New Phytol.* 157, 315–26

Romero, E. (1999) 'Characterisation and thermo-hydro-mechanical behaviour of unsaturated boom clay: an experimental study', Universitat Politècnica de Catalunya - PhD Thesis

----- (2013) 'A microstructural insight into compacted clayey soils and their hydraulic properties', *Eng. Geol.* 165, 3–19

Romero, E., Gens, A. and Lloret, A. (1999) 'Water permeability , water retention and microstructure of unsaturated compacted Boom clay', *Eng. Geol.* 54, 117–27

Romero, E. and Vaunat, J. (2000) 'Retention curves of deformable clays', in A. Tarantino and C. Mancuso (eds), *International Workshop on Unsaturated Soils: Experimental Evidence and Theoretical Approaches in Unsaturated Soils* 91–106

Romero, E., Della Vecchia, G. and Jommi, C. (2011) 'An insight into the water retention properties of compacted clayey soils', *Géotechnique* 61, 313–28

Rose, L. (2017) 'Pitfalls in Root Trait Calculations : How Ignoring Diameter Heterogeneity Can Lead to Overestimation of Functional Traits', *Front. Plant Sci.*

8, 898

Sánchez, M., Wang, D., Briaud, J.L. and Douglas, C. (2014) 'Typical geomechanical problems associated with railroads on shrink-swell soils', *Transp. Geotech.* 1, 257–74

Sauli, G., Cornelini, P. and Preti, F. (2005) *Manuale Di Ingegneria Naturalistica, Volume 3, Sistemazione dei versanti. Regione Lazio, Roma*

Schindelin, J. et al. (2012) 'Fiji: an open-source platform for biological-image analysis', *Nat. Methods* 9, 676–82

Scholl, P., Leitner, D., Kammerer, G., Loiskandl, W., Kaul, H.P. and Bodner, G. (2014) 'Root induced changes of effective 1D hydraulic properties in a soil column', *Plant Soil* 381, 193–213

Schwarz, M., Cohen, D. and Or, D. (2010) 'Root - soil mechanical interactions during pullout and failure of root bundles', *J. Geophys. Res.* 115, F04035

Singh, B. and Schulze, D.G. (2015) 'Soil Minerals and Plant Nutrition', *Nat. Educ. Knowl.* 6, 1

Skempton, A.W. (1954) 'The pore pressure coefficients A and B', *Geotechnique* 4, 143–47

Smethurst, J.A., Clarke, D. and Powrie, W. (2012) 'Factors controlling the seasonal variation in soil water content and pore water pressures within a lightly vegetated clay slope', *Géotechnique* 62, 429–46

Snyder, K., Richards, J.H. and Donovan, L.A. (2003) 'Night-time conductance in C3 and C4 species: do plants lose water at night ?', *J. Exp. Bot.* 54, 861–65

Soriano, I., Ibraim, E., Andò, E., Diambra, A., Laurencin, T., Moro, P. and Viggiani, G. (2017) '3D fibre architecture of fibre-reinforced sand', *Granul. Matter* 19, 75

Terzaghi, K. (1936) 'The shearing resistance of saturated soils', in *First ICSMFE* 54–56

Tinker, P.B. and Nye, P.H. (2000) *Solute movement in the rhizosphere* (2nd edn) (New York, NY, USA: Oxford University Press)

Trabelsi, H., Chebbi, M., Guiras, H., Jamei, M. and Romero, E. (2018) 'Stabilization of clayey soil using fiber reinforcement', in *The 7th International Conference on Unsaturated Soils, UNSAT2018* (Hong Kong: The Hong Kong University of Science and Technology (HKUST)) 545–50

Vanapalli, S.K., Fredlund, D.G., Pufahl, D.E. and Clifton, A.W. (1996) 'Model for the prediction of shear strength with respect to soil suction', *Can. Geotech. J.* 33, 379–92

Vardon, P.J. (2014) 'Climatic influence on geotechnical infrastructure: a review', *J. Environ. Geotech.* 2, 166–74

Vergani, C. and Graf, F. (2016) 'Soil permeability, aggregate stability and root growth: a pot experiment from a soil bioengineering perspective', *Ecohydrology* 9, 830–42

Veylon, G., Ghestem, M., Stokes, A. and Bernard, A. (2015) 'Quantification of mechanical and hydric components of soil reinforcement by plant roots', *Can. Geotech. J.* 52, 1839–49

Wang, C., Zhao, C.Y., Xu, Z.L., Wang, Y. and Peng, H.H. (2013) 'Effect of vegetation on soil water retention and storage in a semi-arid alpine forest catchment', *J. Arid Land* 5, 207–19

Wang, M.B. and Zhang, Q. (2009) 'Issues in using the WinRHIZO system to determine physical characteristics of plant fine roots', *Acta Ecol. Sin.* 29, 136–38

Watt, M., McCully, M.E. and Canny, M.J. (1994) 'Formation and stabilization of rhizosheaths of Zea mays L.', *Plant Physiol.* 106, 179–86

Watt, M., Silk, W.K. and Passioura, J.B. (2006) 'Rates of Root and Organism Growth, Soil Conditions, and Temporal and Spatial Development of the Rhizosphere', *Ann. Bot.* 97, 839–55

Weng, Z., Wang, J., Senthil, T. and Wu, L. (2016) 'Mechanical and thermal properties of ABS / montmorillonite nanocomposites for fused deposition modeling 3D printing', *Mater. Des.* 102, 276–83

Wood, D.M., Diambra, A. and Ibraim, E. (2016) 'Fibres and soils: a route towards modelling of root-soil systems', *Soils Found.* 56, 765–78

Wu, T.H., McKinnell III, W.P. and Swanston, D.N. (1979) 'Strength of tree roots and landslides on Prince of Wales Island, Alaska', *Can. Geotech. J.* 16, 19–33

Wulfsohn, D. and Nyengaard, J.R. (1999) 'Simple stereological procedure to estimate the number and dimensions of root hairs', *Plant Soil* 209, 129–36

Yildiz, A., Graf, F., Rickli, C. and Springman, S.M. (2018) 'Determination of the shearing behaviour of root-permeated soils with a large-scale direct shear apparatus', *Catena* 166, 98–113

Zhang, C.B., Chen, L.H., Liu, Y.P., Ji, X.D. and Liu, X.P. (2010) ‘Triaxial compression test of soil-root composites to evaluate influence of roots on soil shear strength’, *Ecol. Eng.* 36, 19–26